Dipartimento di Ingegneria Civile Ambientale Meccanica

Corso di Laurea Magistrale
in Ingegneria per l'ambiente e il territorio

MODELLING HYDRODYNAMICS AND ICE FORMATION IN A PUMP-STORAGE SYSTEM BETWEEN TWO NORWEGIAN RESERVOIRS

Relatore
Prof. MARCO TOFFOLON

Laureanda
GAIA DONINI

Correlatori
ATLE HARBY
ANA ADEVA BUSTOS

Anno Accademico 2021/2022

ABSTRACT

Pumped-storage systems are expected to be used more in the future to provide an energy balancing system from renewable sources. In particular, Norway, due to its high availability of reservoirs and traditional hydropower plants already in operation, aims to provide this service to the European countries. However, the upgrade of traditional hydropower plants into pumped-storage hydropower plants could impact the thermal equilibrium of the two reservoirs connected.

In this study are detected the effects on the water temperature due to the upgrade of the Rosskrepp power plant, which connects Rosskreppfjorden, the upper reservoir, to Øyarvatn, the lower reservoir. In order to assess the impacts due to the adding of the pump, four scenarios were simulated with CE-QUAL-W2, a two-dimensional laterally averaged hydrodynamic model.

The four scenarios, two with conventional hydropower plants and two with pumped-storage, are obtained from an optimal price-based scheduling model in reference to two selected price years. The latter differ in the range of variation of the energy price, one more variable and the other more constant. As a consequence, two different amounts of water volumes are pumped in the Rosskrepp power plant.

The greater the amount of water pumped, the more severe the effects on the two reservoirs compared to a conventional hydroelectric power plant. In particular, the area closest to the inlet/outlet results to be the most affected. There the stratification is intended to become more unstable, worsening especially in the upper reservoir, Rosskreppfjorden. The lower reservoir, Øyarvatn, which is already affected by the operation of conventional hydropower plant, reports an increase in the frequency of water level fluctuations.

With a high energy price, as during winter period, the pumping mode does not operate. Therefore, ice cover is not further altered. However, the turbined water alone has a strong impact in the lower reservoir, in the area closest to the outlet, the ice formation does not occur every year.

In summary, with the implementation of the pumped-storage system, the thermal stratification is expected to weaken closer to the intake/outlet and water levels are expected to be more variable.

CONTENTS

1 INTRODUCTION

Norway, with its large number of lakes and power plants, has the potential to increase energy storage for Europe. The production of energy from renewable sources has increased in the last years in European countries and at the same time also the necessity to implement the storage capacity. However, renewable energies, due to their discontinuous and hardly controllable production, need storage in order to be exploited.

To resolve this increasing demand, an interesting choice could be to convert conventional hydroelectric power plant into pumped-storage system. The latter stores energy as potential energy pumping water from a lower to an upper reservoir. In fact, when energy demand is low, and therefore also the prices, this system operates as pump bringing water from down reservoir to the upper one. In the opposite situation, when energy demand is high and therefore also the prices, this system operates as turbine generating energy.

Although this system has an evident benefit from an energy point of view, simulating its hydrodynamics becomes relevant to detect the effects of these kind of systems on the environment. As a result of the implementation of the pump to a conventional hydropower plant, the water flow will no longer be directed only downstream. Consequently, water from two reservoirs, with different properties in terms of temperature but also biological and chemical constituents, is continuously mixed affecting both of them.

The study case examined in this study is located in Norway, where the relevance of ice needs particular attention considering that a pumped-storage system will increase the water level fluctuations in the two reservoirs. This phenomenon can adversely affect the ice stability and consequently its duration and extension. For these reasons, it is necessary to detect carefully the impacts due to this system because lots of features can concur to its outcomes.

First, the bathymetry of the lake, especially in the proximity of the intake/outlet, is important. In fact, a long and narrow shape of the lake can enhance mixing and so negatively affecting the stratification (Bermudez *et al.*, 2018). In addition, the area closest to the system is the most mixed considering that hydroelectric operations generate 25 times more turbulent kinetic energy (TKE) than the natural TKE from wind (Müller *et al.*, 2018).

Not only the lake's characteristics but also technical choices can play a role on hydro-

dynamic conditions. Kobler *et al.* (2018) find out that if the withdrawal depth is located in the hypolimnion the impact on thermal distribution is minor.

Finally, weather conditions are fundamental in driving fluxes across lake-atmosphere surface boundary and in determining lake dynamics, its stratification and ice-cover. The latter in Norwegian lakes is a crucial component to consider. Its formation is strictly connected to the amount of negative degree days to which the lake is exposed and this quantity increases with the depth (Franssen and Scherrer, 2008). In fact, deep-water temperature and oxygen content are relevant in determine the ice season (Leppäranta, 2014). Furthermore, the presence of wind postpones the freeze-up date (Toffolon *et al.*, 2021). Once the ice is present, it modify heat exchange, momentum and material between atmosphere and lake (Leppäranta, 1993). Moreover, snowfall can affect ice-cover increasing it thanks to ice-snow formation, but also limiting it due to its insulator capacity; the intensity of the phenomenon is related to the rate of snowfall (Leppäranta, 1993).

This thesis is focused on modeling the hydrodynamics of two Norwegian reservoirs connected by a pumped-storage system, Rosskreppfjorden and Oyarvatn, in order to quantify its impacts on thermal distribution and ice cover. The model used to achieve this purpose is CE-QUAL-W2, a two-dimensional water quality and hydrodynamic model averaged along the transverse direction.

This work is a small part of a big project under development, called *HydroConnect - Impacts of connecting Norwegian hydropower to continental Europe and UK*, carried out by SINTEF Energi. This project involves a multidisciplinary research whose goal is to investigate the economical, technical and environmental aspects to better understand how Norwegian hydropower can provide large-scale balancing services to Europe. In more detail, the project analyses the effects on CO_2 emissions, power prices and environmental conditions. Regarding the latter theme, the University of Trento is involved in the project to support the quantification of the impacts of future hydropower operations on the environment, and this thesis provides an initial analysis on reservoirs thermal alteration.

2 STUDY CASE

2.1 Sira-Kvina system

The study case refers to only a first small part of a bigger system of lakes connected, called Sira-Kvina, used for hydropower production, *Figure* 2.1.1.

Roskrepp is the smallest power plant in the Sira-Kvina power company (Sira-Kvina, 2022) with a drop height of 83 meters and a Francis turbine with a rated capacity of 50 MW. The production occurs mainly in the winter period when the power price is high. The reservoir is then filled by snow melting and precipitation throughout the summer and autumn.

The water that starts in the Roskreppfjorden must go through five power stations before it flows into the sea at Åna-Sira with a total hydraulic head of 900 metres.

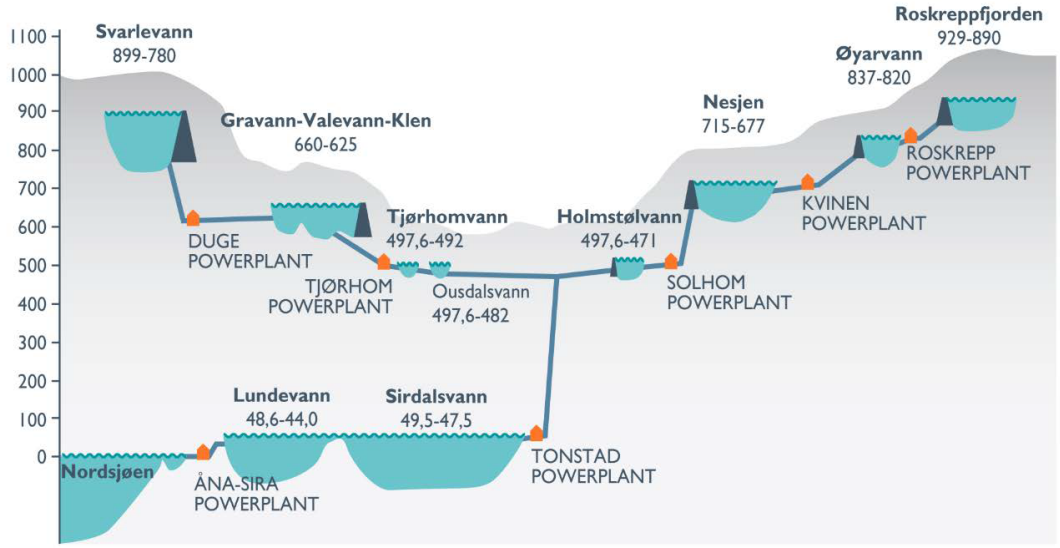

Figure 2.1.1: Sira-Kvina hydropower system and reservoir - *SINTEF*

2.2 Rosskreppfjorden and Øyarvatn reservoirs

The two lakes analysed, Rosskreppfjorden and Øyarvatn, are located in the southern part of Norway. Both of the lakes are situated in Sirdal and Valle municipalities in Agder county, Norway.

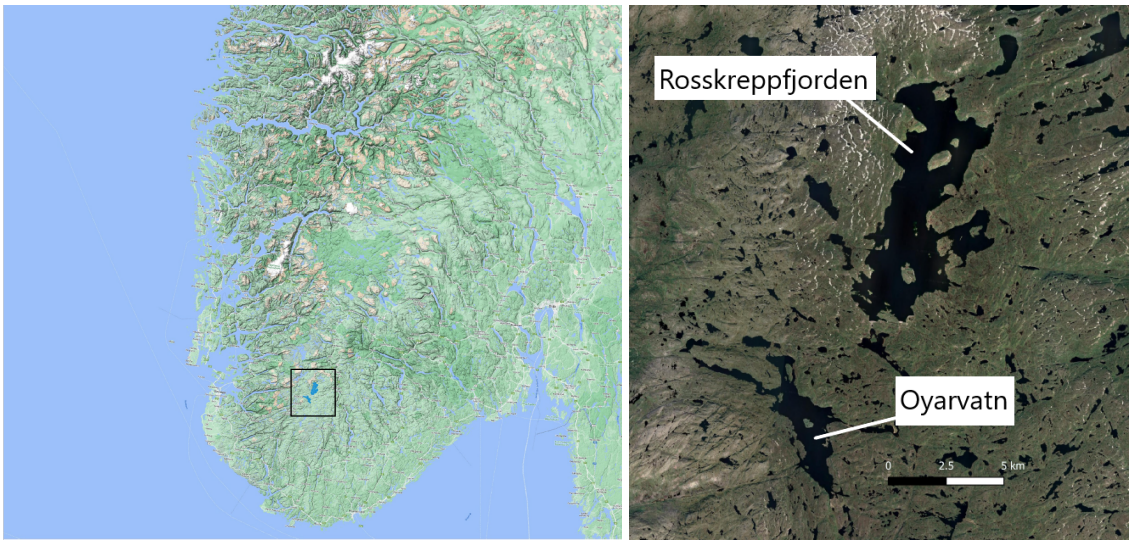

(a) (b)

Figure 2.2.1: Position of Rosskreppfjorden and Øyarvatn

They have a narrow and long shape with irregular shores and small islands in the middle. Rosskreppfjorden, the upper reservoir, is the biggest one with a water volume around six times the lower reservoir, Øyarvatn. The latter is smaller but deeper, it is 60 meters deep, while the upper reservoir is about 35 meters deep.

In $Table$ 2.1 are summarized the main dimensions and regulating level and production for the lakes. In fact, both reservoirs currently are used for hydropower production with a conventional hydroelectric power plant. Regarding the degree of regulation of the two reservoirs, the NVE (*Norwegian Water Resources and Energy Directorate*) defines the permitted water level that must be in a range between the lowest regulated water level (LRV) and the highest regulated water level (HRV).

Parameter	Rosskreppfjorden	Øyarvatn
Length	11 km	7 km
Width	3 km	1.5 km
Bottom elevation	876.29 $m\ a.s.l.$	766.92 $m\ a.s.l.$
Area	29.82 km^2	8.02 km^2
Catchment area	271.49 km^2	401.21 km^2
Regulation volume capacity	684 Mm^3	104 Mm^3
LRV	890 $m\ a.s.l.$	820 $m\ a.s.l.$
HRV	929 $m\ a.s.l.$	837 $m\ a.s.l.$
Energy capacity	137 GWh	30 GWh

Table 2.1: Roskreppfjorden and Øyarvatn characteristics [Sira-Kvina (2022)]

In the area analysed, the hydrographic network is extensively developed. There are plenty of tributaries distributed all around the perimeter of the lakes that convey their flows into them.

Figure 2.2.2: Hydrographic network [NEVINA (2022)]

The outlets are regulated with dams, a zoom in that area is more visible in $Figure$ 2.2.3.

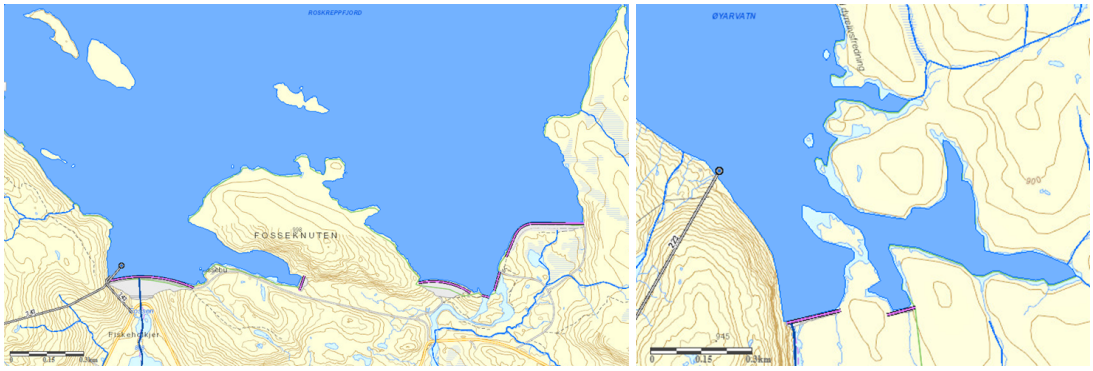

(a) (b)

Figure 2.2.3: Zoom on the dams, highlighted in pink, located at the outlet of Rosskreppfjorden (a) and Øyarvatn (b) [NEVINA (2022)]

(a) (b)

Figure 2.2.4: Rosskreppfjorden dam

3 MORPHOLOGICAL, HYDROLOGICAL AND METEOROLOGICAL CHARACTERISATION

Before starting work at the modelling process, a data collection and analysis was performed. In particular, it was necessary to acquire information on both morphological and meteorological aspects of the site of interest in order to reconstruct the bathymetry of the two reservoirs and the meteorological forcings acting on them. In addition, natural inflows and outflows for each reservoir and their temperature are also essential boundary condition to know.

Different data from different sources were considered and compered in order to choose the best option among the possible ones.

Although the data reconstruction aims to be as realistic as possible, it is important here to point out that the uncertainties and the absence of data may affect the correctness of the results obtained. Only by increasing the measurements available can the accuracy of the outcome be improved.

3.1 Bathymetry

In order to reconstruct the bathymetry a DEM (*Digital Elevation Model*) was built starting from all data available. These data refers to:

- water level obtained from satellite pictures;
- DEM 1 meter resolution for the shore (Kartverkets, 2022);
- ADCP (*Acoustic Doppler Current Profiler*) measurements taken in the two lakes, $Figure$ 3.1.1.

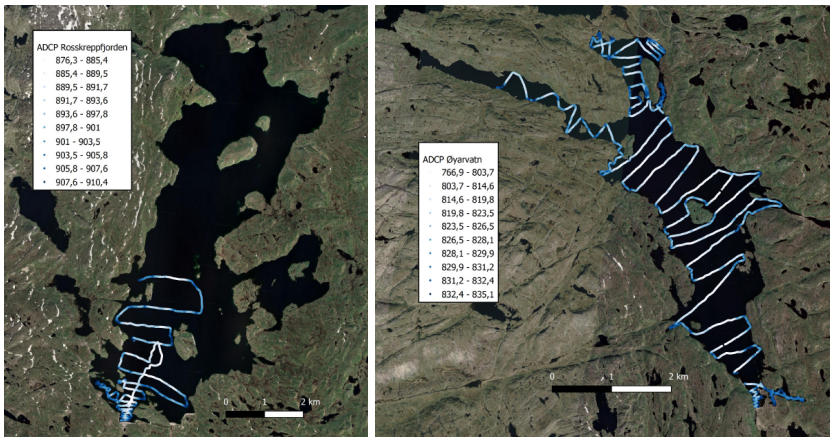

(a) (b)

Figure 3.1.1: ADCP measurements in Rosskreppfjorden (a) and Øyarvatn (b)

Regarding Rosskreppfjorden, more elaboration was required due to the lack of ADCP data in the upper part of the lake. In fact, an historical map from year 1958 ($Figure$ 3.1.2) was used to extract contours for the internal part of the actual lake which was at that time dry. Also, the talweg has been extrapolated from the same map and the elevation assigned has been interpolated between known external points.

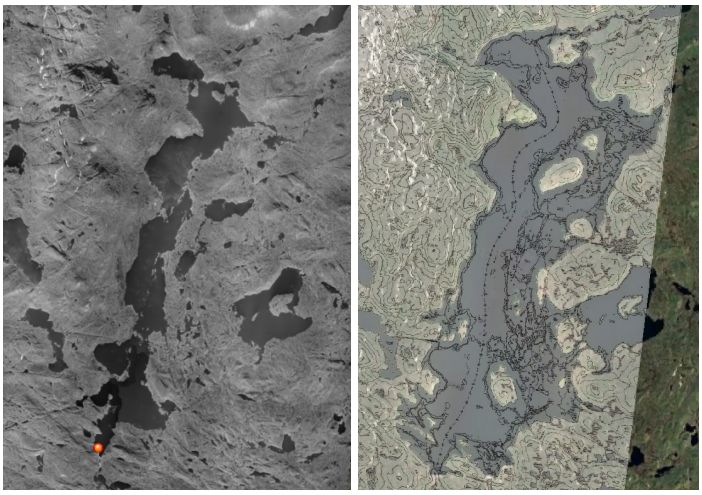

(a) (b)

Figure 3.1.2: Orthophoto of Rosskreppfjorden (NiB, 2022) (a) in year 1958 and its contour lines overlapping the actual situation (Kartverkets, 2022) (b)

Once all data available was converted in points, an interpolation using $GQIS$ 3.22.6 was done to obtain the DEM. In order to choose the best interpolation method a statistical analysis was made, selecting randomly 10 % of all the points available and using them as test points, as reported in some articles (Meng *et al.*, 2013; Erdede and Bektas,

2020). In fact, the comparison among the methods was done comparing the elevation of those known points with the elevation obtained at the same location with the different interpolation methods.

The interpolation methods were selected so that it is possible to achieve a quick method calibration which does not require many input parameters. In particular, in this case the interpolation method used are:

- TIN: Triangular interpolation
- IDW: Inverse Distance Weighting
- B-spline interpolation
- RST: spline interpolation

For each of them maximum (Max), minimum (Min) and mean values ($Mean$) and standard deviation (SD) computed at the test points position were compared with their real values. In addition, also the root mean square error ($RMSE$), the maximum difference between predict and actual value (Δ_{max}) and the mean absolute error (MAE) were analysed.

The same procedure is applied for both the lakes.

3.1.1 Rosskreppfjorden

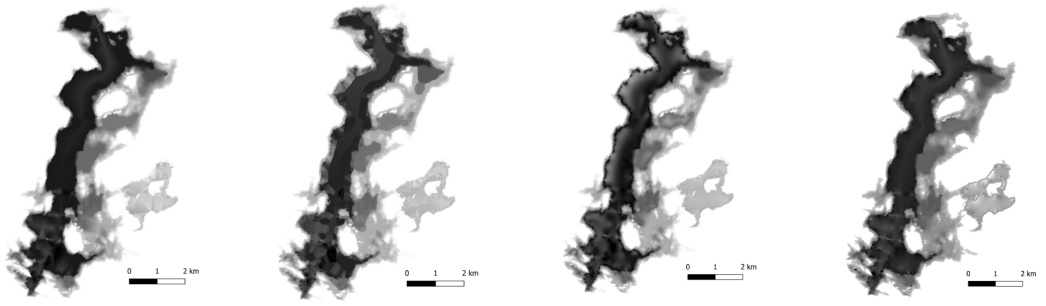

(a) (b) (c) (d)

Figure 3.1.3: Comparison among different interpolation methods for Rosskreppfjorden: TIN (a), IDW (b), Bspline (c) and RST (d)

The amount of test points among which the statistic is done is 20'899, corresponding to the 10 % of the total points available.

Interpolation method	*Max*	*Min*	*Mean*	*SD*	*RMSE*	Δ_{max}	*MAE*
TIN	930.00	877.08	918.79	7.631	3.763	26.43	2.284
IDW	930.00	877.03	917.28	7.159	2.547	32.93	1.460
$Bspline$	931.82	876.79	917.32	7.253	2.375	27.52	1.466
RST	935.40	874.36	917.11	7.486	2.625	29.74	1.460
Test points	930.00	877.04	917.28	7.633			

Table 3.1: Comparison between different interpolation methods for the DEM of Rosskreppfjorden using 20'899 randomly sampled points. The best result for each statistic is highlighted in light blue. All the values are expressed in meters

Referring to the statistical results obtained, $Table$ 3.1, TIN interpolation reproduces data distribution well but with the highest errors, both RMSE and MAE. IDW keeps the maximum, minimum and mean value, but it records the highest value difference between points. Finally both Bspline and spline interpolation give maximum and minimum elevation out of the range of the real test points but maintaining low errors.

The considerations made are not sufficient to identify the best method. Moreover, due to the irregular spatial pattern distribution of the points and the test points proximity, different cross sections, especially far from measurements, were compered.

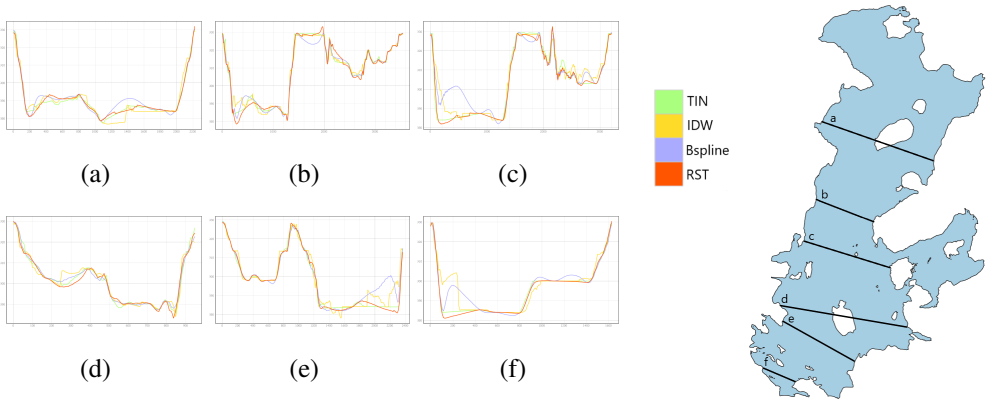

Figure 3.1.4: Cross sections selected in Rosskreppfjorden

As a result of this analysis, RST interpolation has been used to obtain the DEM from which the bathymetry has been extrapolated.

3.1.2 Øyarvatn

The same analysis done for Rosskreppfjorden has been made for Øyarvatn, in this case the statistic refers to 8'086 test points.

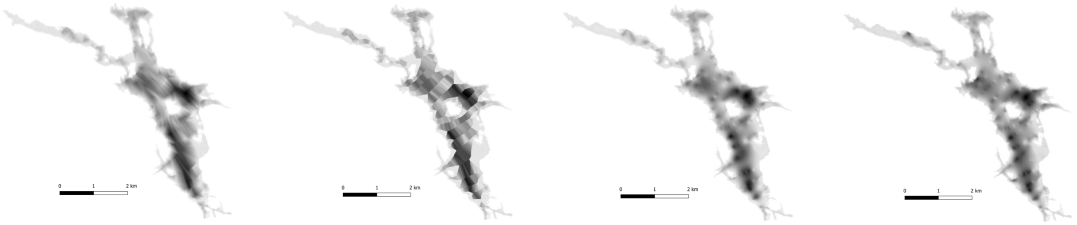

(a) (b) (c) (d)

Figure 3.1.5: Comparison among different interpolation methods for Øyarvatn: TIN (a), IDW (b), Bspline (c) and RST (d)

Interpolation method	*Max*	*Min*	*Mean*	*SD*	*RMSE*	Δ_{max}	*MAE*
TIN	840.00	787.91	833.24	4.960	1.527	12.01	1.078
IDW	840.00	787.50	832.54	4.707	1.126	10.84	0.782
$Bspline$	840.00	787.91	833.24	4.960	1.527	12.01	1.078
RST	840.21	787.88	832.28	4.707	1.325	10.21	0.973
Test points	840.00	787.39	832.55	4.843			

Table 3.2: Comparison among different interpolation methods for the DEM of Øyarvatn using 8'086 randomly sampled points

For Øyarvatn, where the data were distributed more omogeneously, IDW seems to be the best method. However, also in this case a visual comparison at selected cross sections was made to check the interpolation efficiency especially far from the measurements.

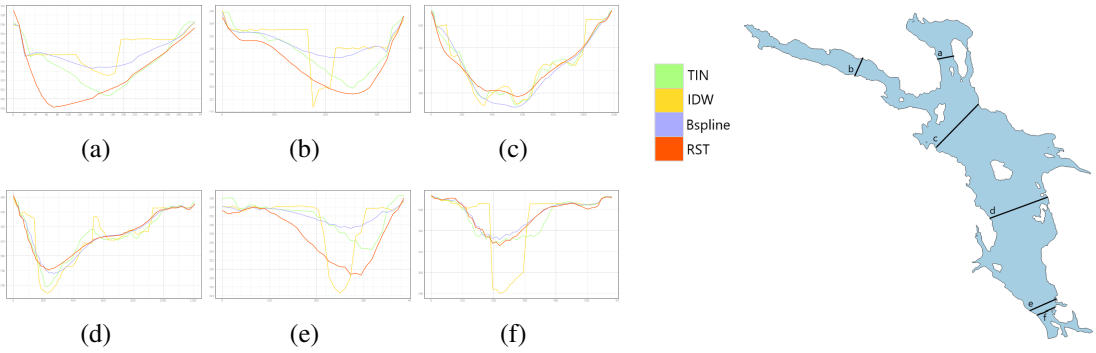

(a) (b) (c) (d) (e) (f)

Figure 3.1.6: Cross sections selected in Øyarvatn

In the end, based on the results obtained, and mainly on visual considerations, the RST method has been used to create the DEM for both the lakes.

3.2 Weather data

The meteorological information were collected by two different sources: OpenWeather and MET Nordic dataset. Both of them process different data sources in order to reconstruct spacial distribution of them. Therefore, they provide the requested data by giving as input a specific point. In order to choose the best weather data set, a comparison was conducted with the nearest meteorological stations with similar altitude: Blåsjo and Sirdal. All the data analysed refer to the period January 2014 - August 2022 with an hourly timestep and for the location corresponding to source considered, shown in $Figure$ 3.2.1.

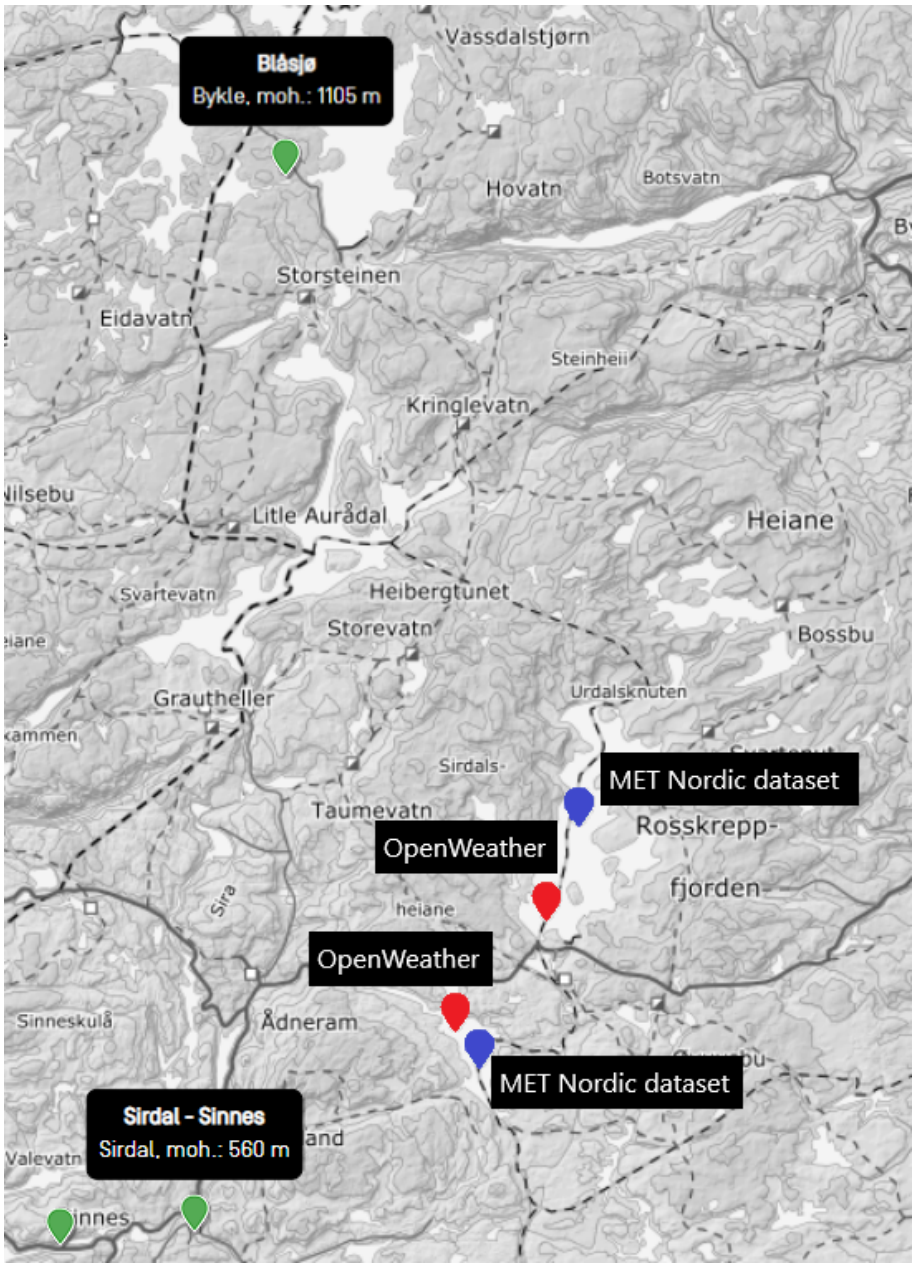

Figure 3.2.1: Location of weather data

3.2.1 OpenWeather

OpenWeather (OpenWeather, 2022) is an online service that provides weather data globally from different sources: national meteorological agencies, weather stations, weather satellites and others. The data resolution is 500 meters and the data available regard: air temperature, dew point temperature, relative humidity, air pressure, cloud cover, wind speed and direction and precipitation both rainfall and snowfall. For each parameter maximum, mean and minimum daily value and the duration curve for both reservoirs are analysed.

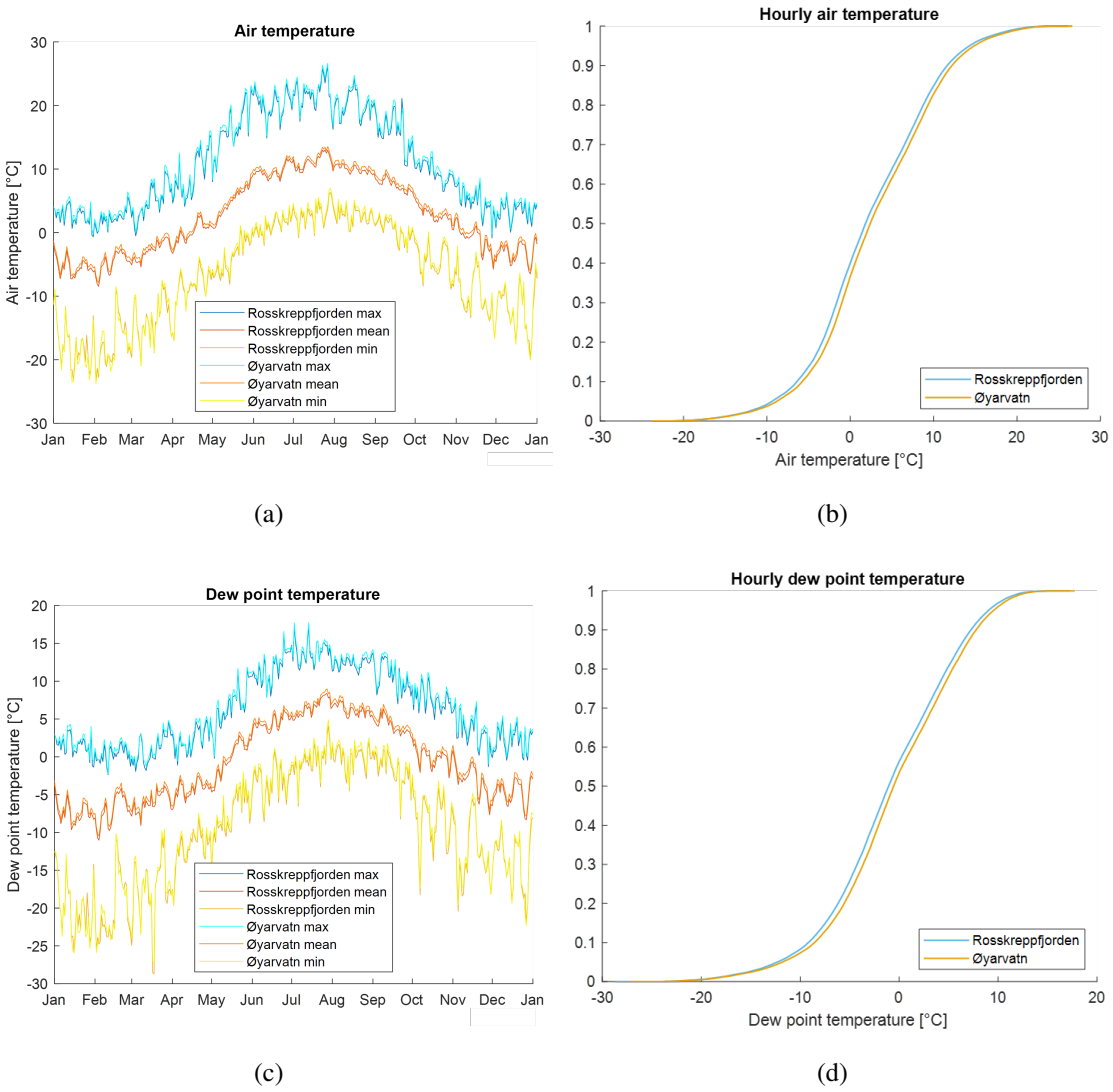

(a) (b)

(c) (d)

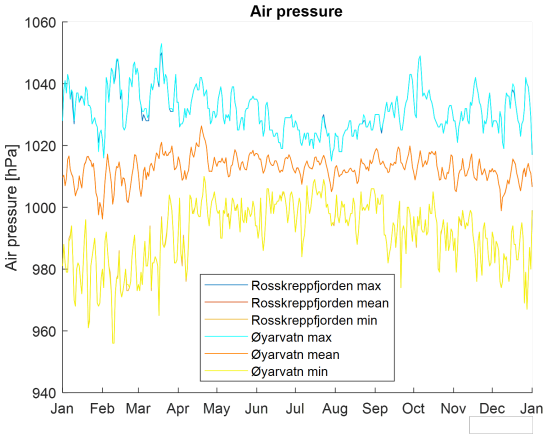
Air pressure
Air pressure [hPa]
1060
1040
1020
1000
980
960
940
Jan Feb Mar Apr May Jun Jul Aug Sep Oct Nov Dec Jan
Rosskreppfjorden max
Rosskreppfjorden mean
Rosskreppfjorden min
Øyarvatn max
Øyarvatn mean
Øyarvatn min

(e)

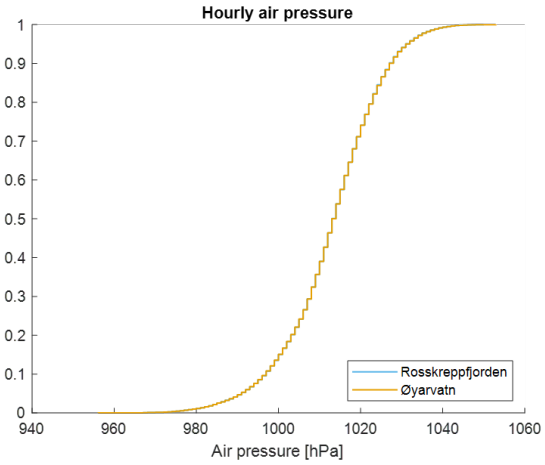
Hourly air pressure
1
0.9
0.8
0.7
0.6
0.5
0.4
0.3
0.2
0.1
0
940 960 980 1000 1020 1040 1060
Air pressure [hPa]
Rosskreppfjorden
Øyarvatn

(f)

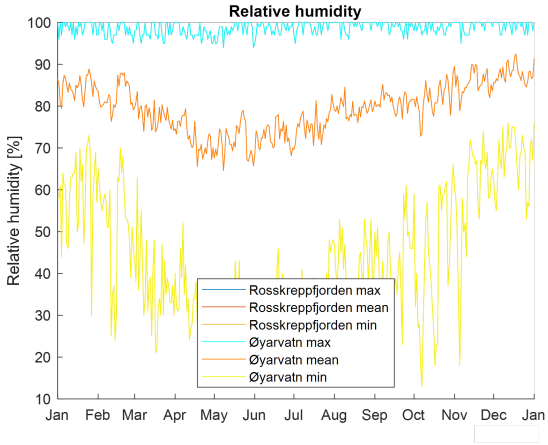
Relative humidity
Relative humidity [%]
100
90
80
70
60
50
40
30
20
10
Jan Feb Mar Apr May Jun Jul Aug Sep Oct Nov Dec Jan
Rosskreppfjorden max
Rosskreppfjorden mean
Rosskreppfjorden min
Øyarvatn max
Øyarvatn mean
Øyarvatn min

(g)

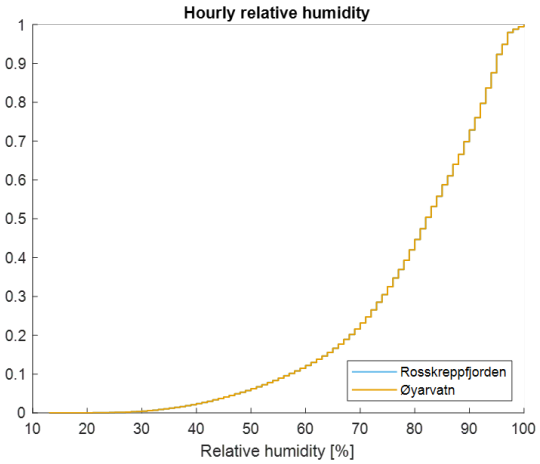
Hourly relative humidity
1
0.9
0.8
0.7
0.6
0.5
0.4
0.3
0.2
0.1
0
10 20 30 40 50 60 70 80 90 100
Relative humidity [%]
Rosskreppfjorden
Øyarvatn

(h)

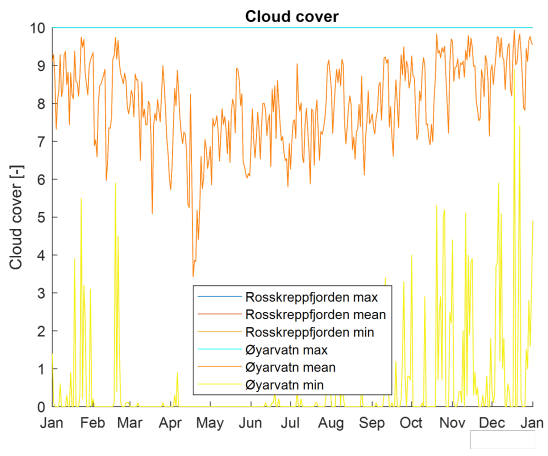
Cloud cover
Cloud cover [-]
10
9
8
7
6
5
4
3
2
1
0
Jan Feb Mar Apr May Jun Jul Aug Sep Oct Nov Dec Jan
Rosskreppfjorden max
Rosskreppfjorden mean
Rosskreppfjorden min
Øyarvatn max
Øyarvatn mean
Øyarvatn min

(i)

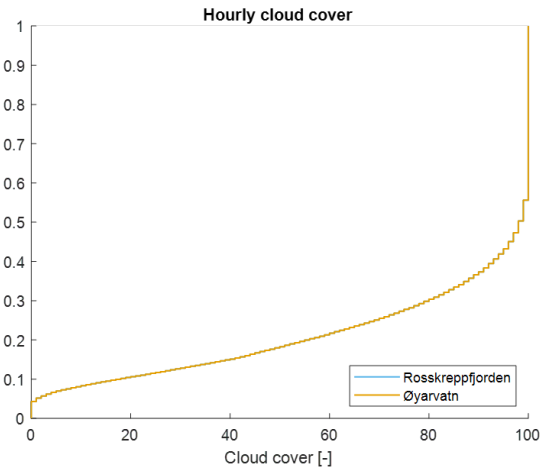
Hourly cloud cover
1
0.9
0.8
0.7
0.6
0.5
0.4
0.3
0.2
0.1
0
0 20 40 60 80 100
Cloud cover [-]
Rosskreppfjorden
Øyarvatn

(j)

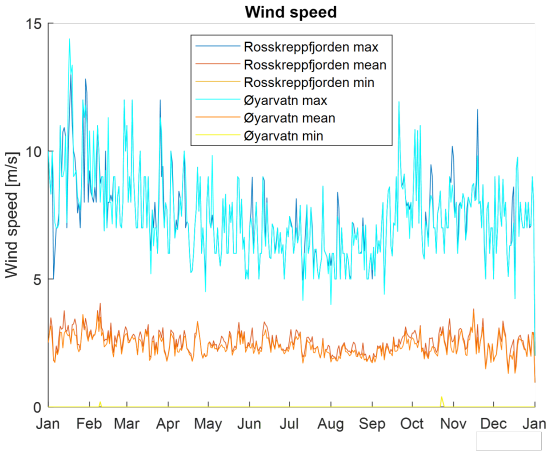
Wind speed
Wind speed [m/s]
Rosskreppfjorden max
Rosskreppfjorden mean
Rosskreppfjorden min
Øyarvatn max
Øyarvatn mean
Øyarvatn min
Jan Feb Mar Apr May Jun Jul Aug Sep Oct Nov Dec Jan

(k)

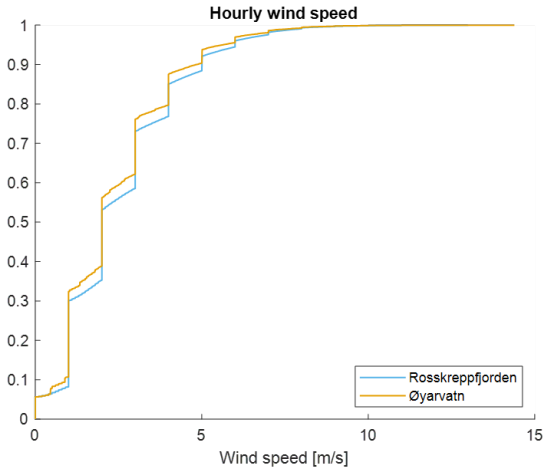
Hourly wind speed
Rosskreppfjorden
Øyarvatn
Wind speed [m/s]

(l)

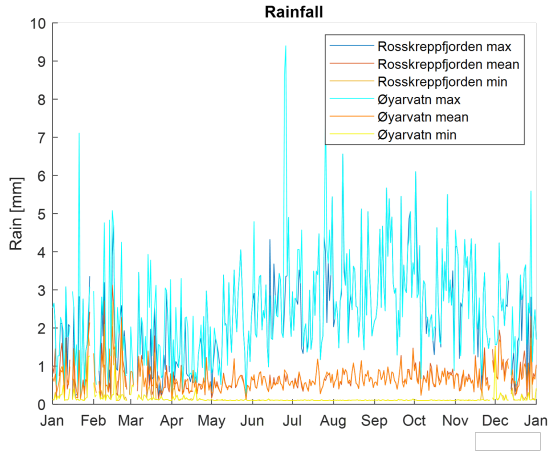
Rainfall
Rain [mm]
Rosskreppfjorden max
Rosskreppfjorden mean
Rosskreppfjorden min
Øyarvatn max
Øyarvatn mean
Øyarvatn min
Jan Feb Mar Apr May Jun Jul Aug Sep Oct Nov Dec Jan

(m)

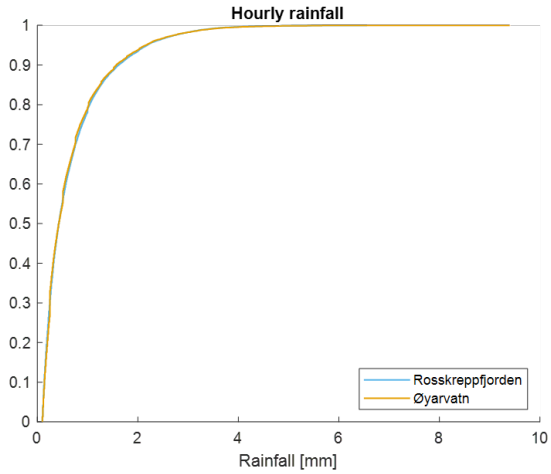
Hourly rainfall
Rosskreppfjorden
Øyarvatn
Rainfall [mm]

(n)

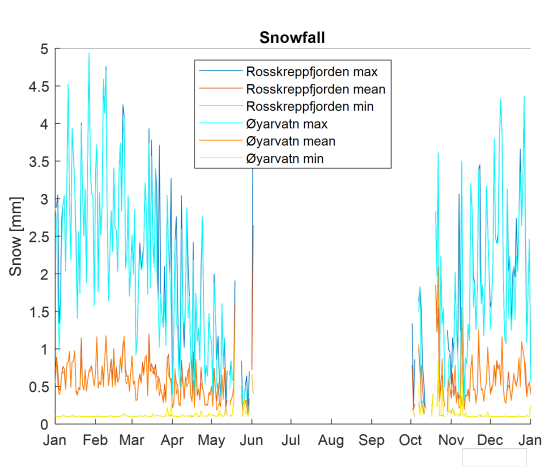
Snowfall
Snow [mm]
Rosskreppfjorden max
Rosskreppfjorden mean
Rosskreppfjorden min
Øyarvatn max
Øyarvatn mean
Øyarvatn min
Jan Feb Mar Apr May Jun Jul Aug Sep Oct Nov Dec Jan

(o)

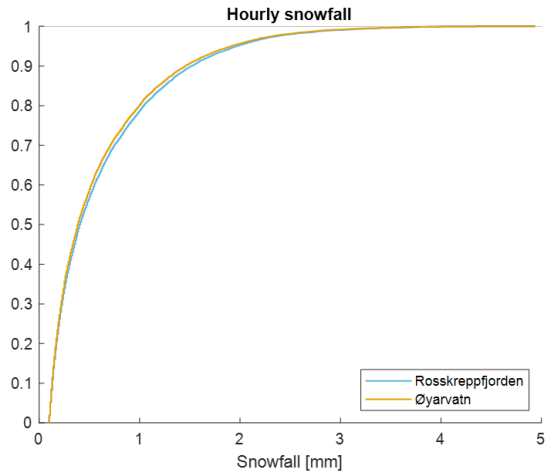
Hourly snowfall
Rosskreppfjorden
Øyarvatn
Snowfall [mm]

(p)

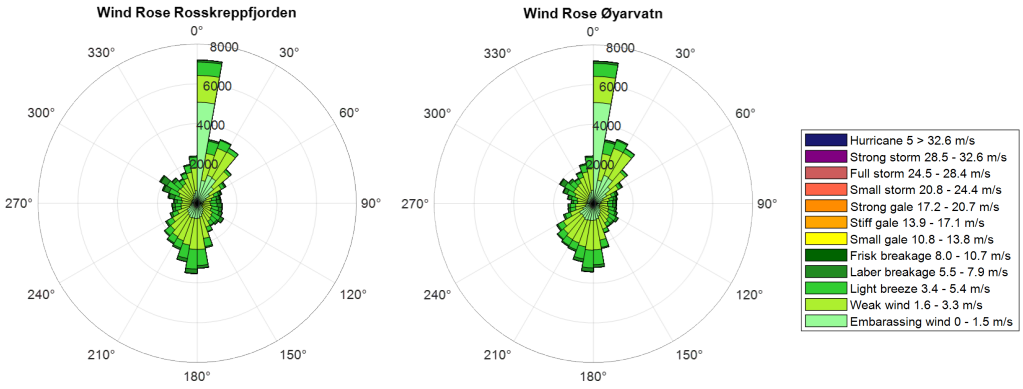

(q) (r)

Figure 3.2.2: OpenWeather meteorological data for both Rosskreppfjorden and Øyarvatn. For each parameter maximum, mean and minimum value and hourly duration curve are shown. The wind rose legend refers to the one used by *Norsk Klimaservicecenter* (Klima, 2022)

Both reservoirs show a similar trend in all the parameters. Rosskreppfjorden, the upper reservoir, records lower temperature and an higher rate of snowfall.

3.2.2 MET Nordic dataset

The second source considered is *MET Norway* (MET, 2022). In particular, the MET Nordic dataset, which is a post-processed product with 1 km resolution. The data available regard: air temperature and pressure, relative humidity, wind speed and direction, cloud cover, downwelling shortwave and precipitation.

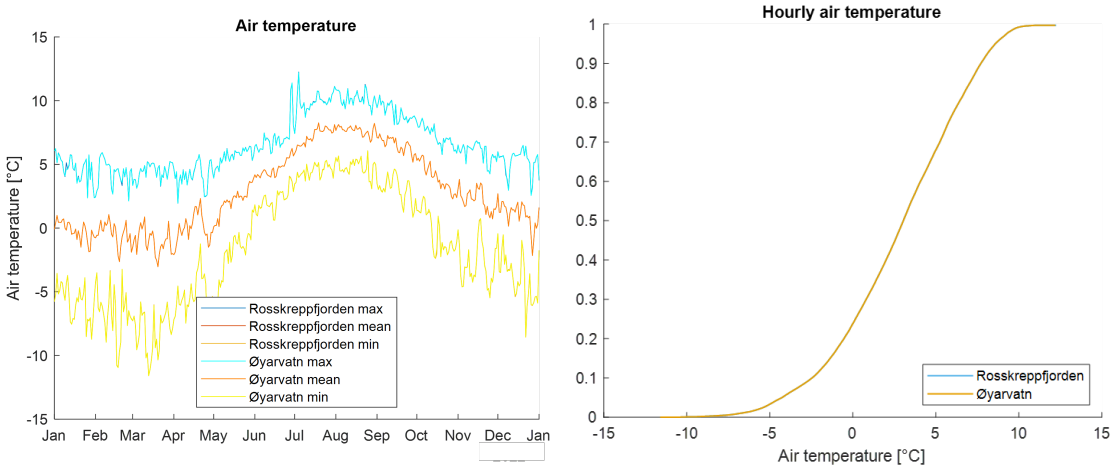

(a) (b)

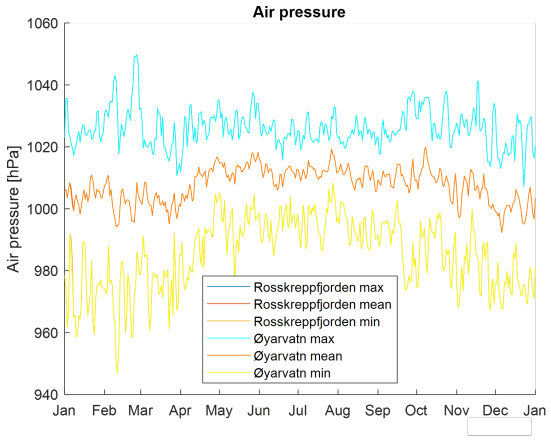
Air pressure
Air pressure [hPa]
1060
1040
1020
1000
980
960
940
Jan Feb Mar Apr May Jun Jul Aug Sep Oct Nov Dec Jan
Rosskreppfjorden max
Rosskreppfjorden mean
Rosskreppfjorden min
Øyarvatn max
Øyarvatn mean
Øyarvatn min

(c)

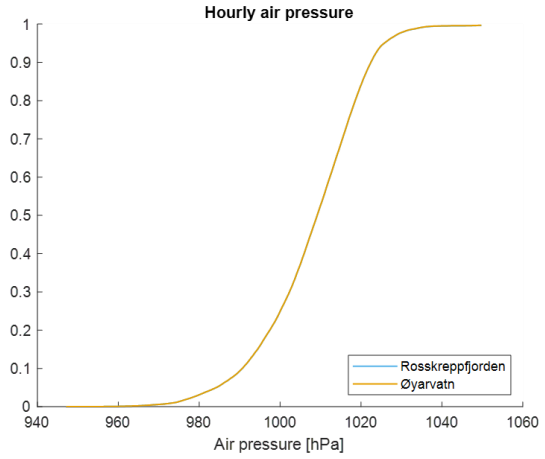
Hourly air pressure
1
0.9
0.8
0.7
0.6
0.5
0.4
0.3
0.2
0.1
0
940 960 980 1000 1020 1040 1060
Air pressure [hPa]
Rosskreppfjorden
Øyarvatn

(d)

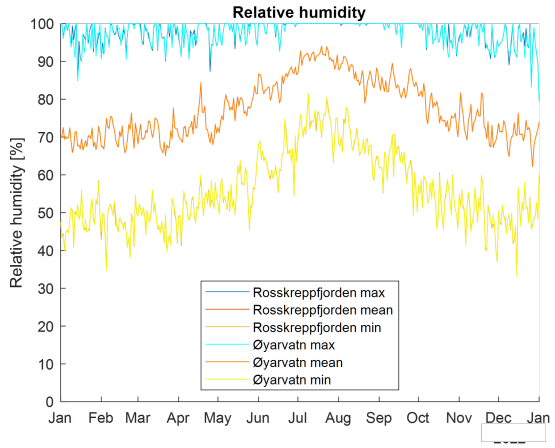
Relative humidity
Relative humidity [%]
100
90
80
70
60
50
40
30
20
10
0
Jan Feb Mar Apr May Jun Jul Aug Sep Oct Nov Dec Jan
Rosskreppfjorden max
Rosskreppfjorden mean
Rosskreppfjorden min
Øyarvatn max
Øyarvatn mean
Øyarvatn min

(e)

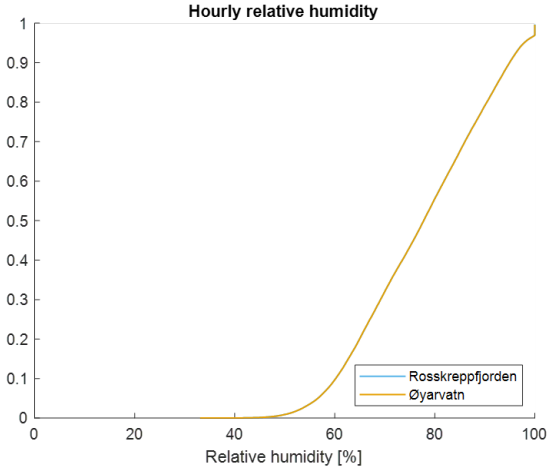
Hourly relative humidity
1
0.9
0.8
0.7
0.6
0.5
0.4
0.3
0.2
0.1
0
0 20 40 60 80 100
Relative humidity [%]
Rosskreppfjorden
Øyarvatn

(f)

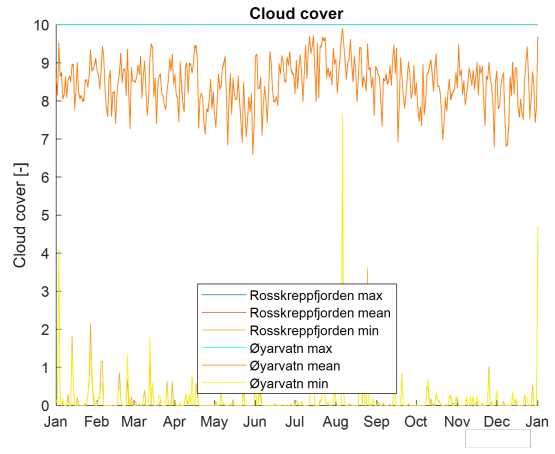
Cloud cover
Cloud cover [-]
10
9
8
7
6
5
4
3
2
1
0
Jan Feb Mar Apr May Jun Jul Aug Sep Oct Nov Dec Jan
Rosskreppfjorden max
Rosskreppfjorden mean
Rosskreppfjorden min
Øyarvatn max
Øyarvatn mean
Øyarvatn min

(g)

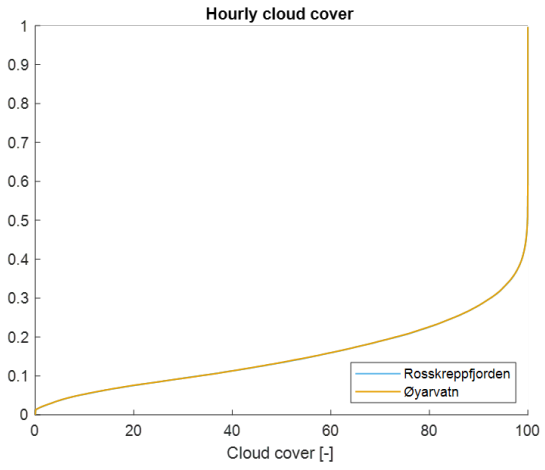
Hourly cloud cover
1
0.9
0.8
0.7
0.6
0.5
0.4
0.3
0.2
0.1
0
0 20 40 60 80 100
Cloud cover [-]
Rosskreppfjorden
Øyarvatn

(h)

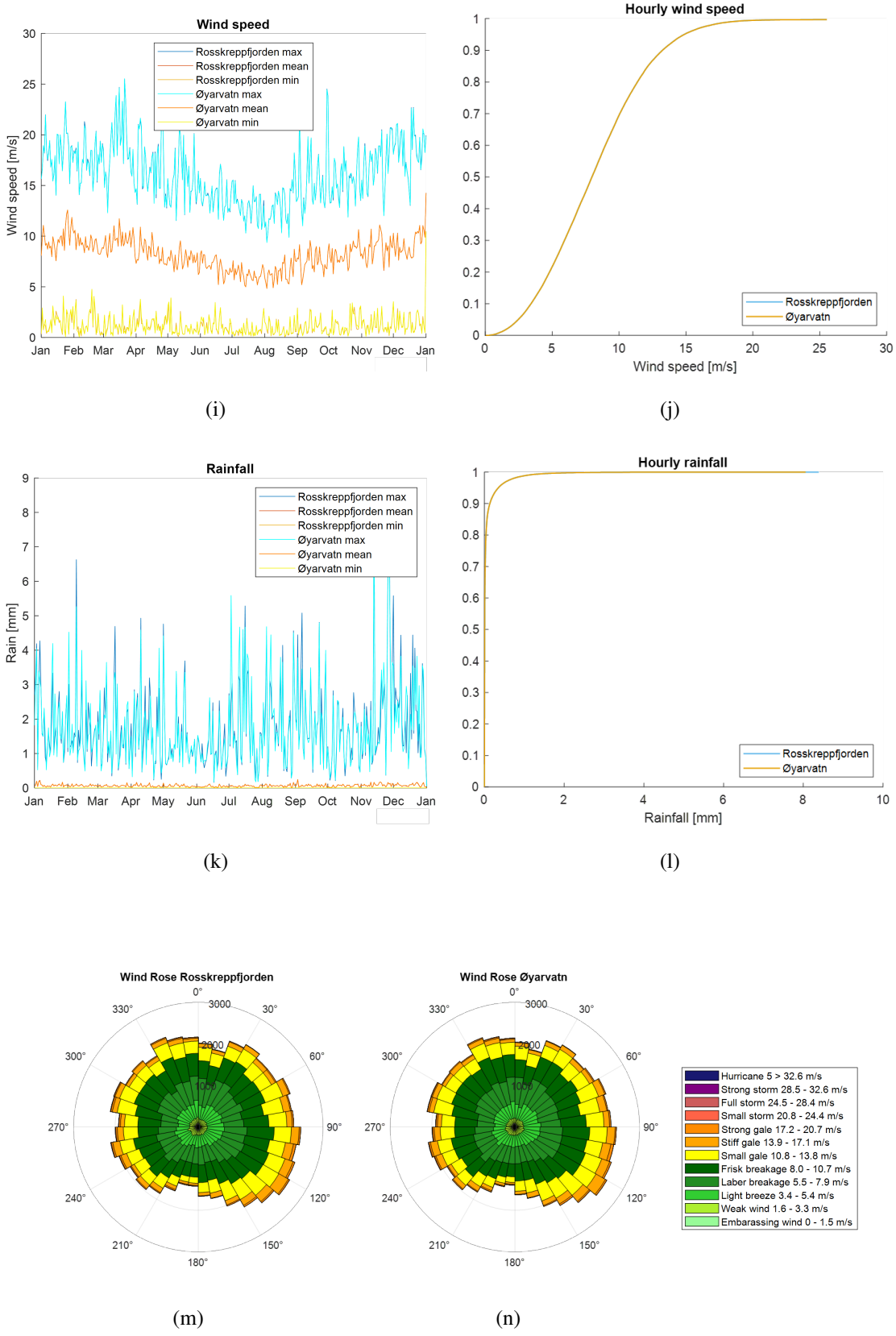

Figure 3.2.3: MET meteorological data for both Rosskreppfjorden and Øyarvatn. The wind rose legend refers to the one used by *Norsk Klimaservicecenter* (Klima, 2022)

In this data set, the difference between the two lakes is not noticeable. Moreover, the data acquired report a limited temperature range, approximately between -12 °C and + 12 °C, and a high wind speed in all the directions.

In addition, MET nordic dataset provides data on shortwave solar radiation. However, there is an error in the last year reported, 2022, in fact, in that year the intensity is higher than expected (*Figure* 3.2.4). Moreover, during winter period, between November and February, radiation is zero. This result is not consistent with the latitude of the lakes analysed therefore this parameter is not considered.

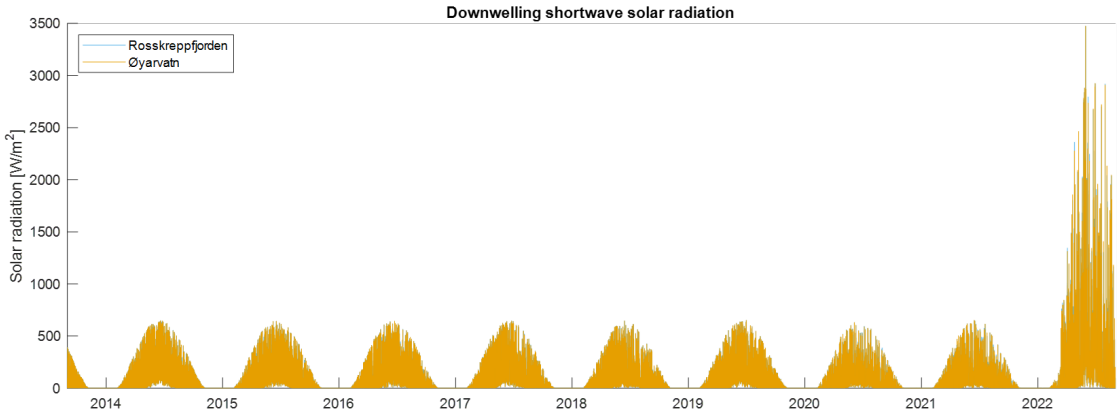

Figure 3.2.4: Downwelling shortwave solar radiation

3.2.3 Meteorological data comparison

The data from the two sources considered report different values. Therefore, in order to choose the best data set a comparison with two meteorological station is performed. It is important to note that all data refer to a defined point and is not known how they are computed and how is the spatial data distribution.

Meteorological stations

The two meteorological stations are: Blåsjo and Sirdal. The first is 1105 m a.s.l. and located about 30 km northwest the two lakes considered. This station is close to lake of the same name, the largest artificial lake in Norway with similar characteristics to the reservoirs considered. The second, Sirdal is 560 m a.s.l. and about 20 km southwest of the case study.

Data comparison

Hourly and daily duration curves of the data provided by the two stations are compared with those obtained from MET Nordic dataset and OpenWeather. The data analysed refer

to: air temperature, air pressure, relative humidity, wind speed. In addition, the wind rose of the two stations is reported.

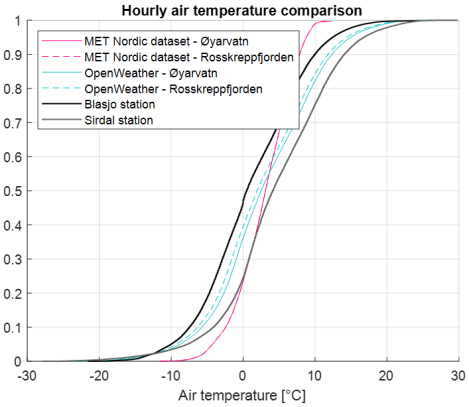

(a)

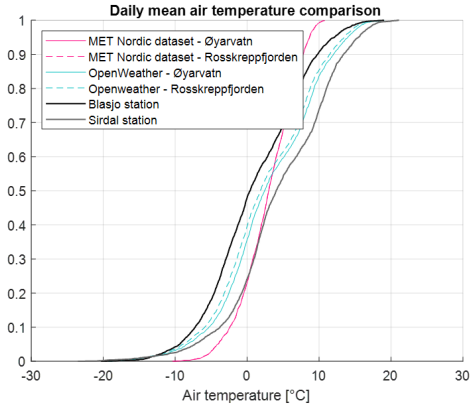

(b)

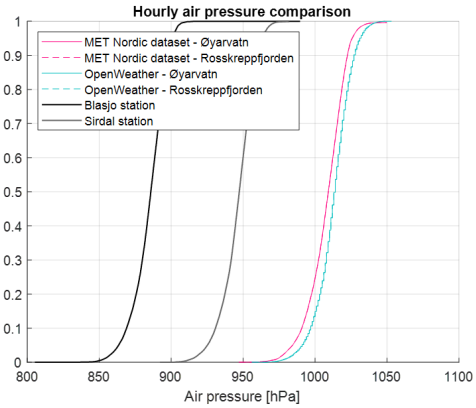

(c)

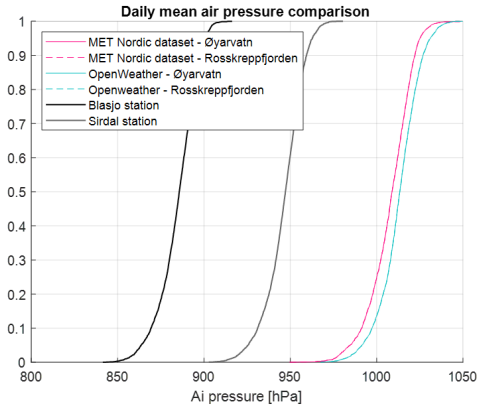

(d)

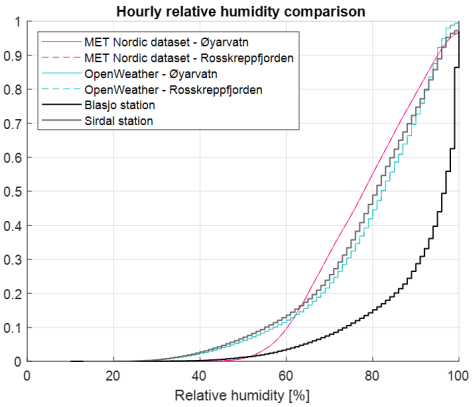

(e)

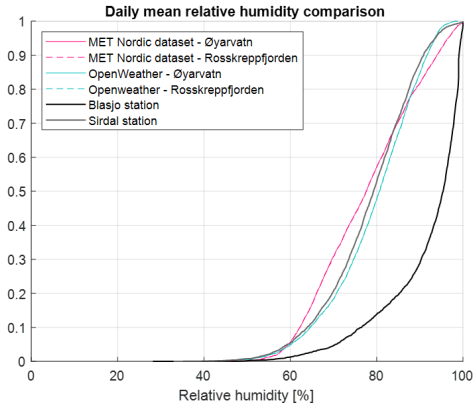

(f)

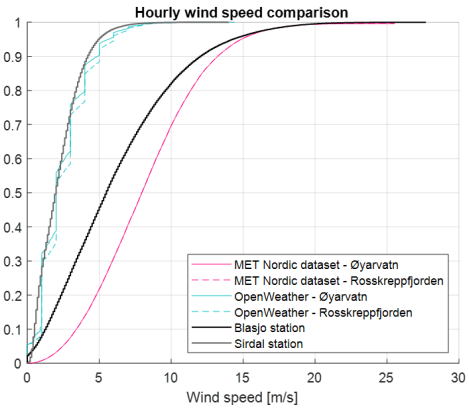

(g)

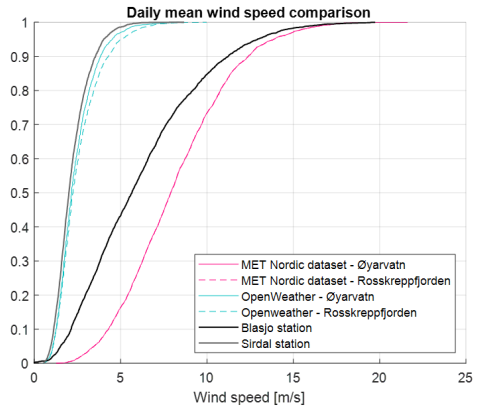

(h)

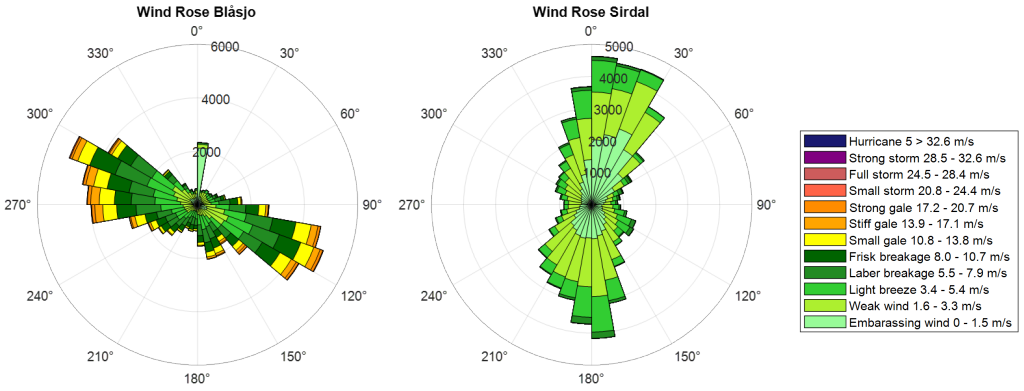

(i) (j)

Figure 3.2.5: Hourly and daily duration curves for meteorological data comparison for both Rosskreppfjorden and Øyarvatn. The wind rose legend refers to the one used by *Norsk Klimaservicecenter* (Klima, 2022)

Air temperature provided by OpenWeather is consistent according to the elevation of the stations and the lakes considered. Instead, MET data have a different distribution with a smaller range of values. Air pressure from the two sources analysed are similar but they do not follow a trend with elevation considering the two stations. Also the relative humidity from both MET and OpenWather are similar and more in accordance to Sirdal than Blåsjo. Moreover, wind speed is very different in the two data set. The wind speed provided by OpenWeather is similar to Sirdal station as its main direction north-south. MET Nordic dataset records the strongest wind speed distributed in all the directions ($Figure\ 3.2.3\ (m)\ (n)$).

MET Nordic data set reports an unrealistic air temperature range for the area considered and a strong wind speed distributed on all the directions, very different from that

measured at the meteorological stations. In addition, the radiation is inconsistent. Therefore, this dataset shows issues, probably related to the downloading process.

Consequently, considering the results obtained in this analysis and the uncertainties related to the MET data set, the meteorological data considered refer to OpenWeather.

3.3 Natural inflow and outflow

As already observed in $Figure$ 2.2.2, natural inflows are distributed all along the shore and there are no data available on them.

In order to deal with this issue they were back calculated performing a water balance on each of the two reservoirs. In addition to the natural components, there are those due to the operation of the hydropower plant. Therefore, regarding the discharges involved, the data for the spill and the discharge used for actual production were provided from the power plant with an hourly resolution as the water level in the two lakes.

First, the discharge, dQ, resulting from a variation in the water level was computed as follow:

$$dQ = \frac{A \cdot dw_l}{dt} \tag{3.3.1}$$

where A is the area associated to a specific water level, w_l, and dt is equal to 3600 s considering the hourly resolution of the data.

Secondly, the water balance is performed:

$$dQ = inflow - outflow \tag{3.3.2}$$

This balance is slightly different for the two lakes:

- Rosskreppfjorden: $inflow = dQ + Q_{turb} + Q_{R,spill}$
- Øyarvatn: $inflow = dQ + Q_{O,spill} + Q_{dmv} + Q_{kvinen} - Q_{turb}$

in which the discharges involved are:

- Q_{turb} is the discharge used for production, that flows through the tunnel from Rosskreppfjorden to Øyarvatn;
- $Q_{R,spill}$ is the spillage from Rosskreppfjorden;
- $Q_{O,spill}$ is the spillage from Øyarvatn;
- Q_{dmv} is the environmental flow;
- Q_{kvinen} is the discharge used for production in the second power plant of the Sira-Kvina system, Kvinen powerplant, that connects Øyarvatn to Nesjen.

Note that the $inflow$ obtained can be positive or negative, in the first case they were considered as natural inflow, in the opposite case as natural outflow.

In addition, in the model used, CE-QUA-W2, is specified only one outlet for each lake, consequently, natural outflows include also the spill and environmental flow when present. Moreover, it is important to specify that precipitation is already included in the balance, therefore it is not added separately in the model.

3.3.1 Inflow temperature

The temperature of the inflows is a required information by the model used. As already discussed, the inflows used do not refer to a specific tributary but include all the "natural" incomes feeding to each of the lake. Consequently, it is impossible to obtain a detail characterisation of the inflow.

However, regarding water temperature there are measurements available in Gjuvatn, a lake upstream of Rosskreppfjorden ($Figure$ 3.3.1).

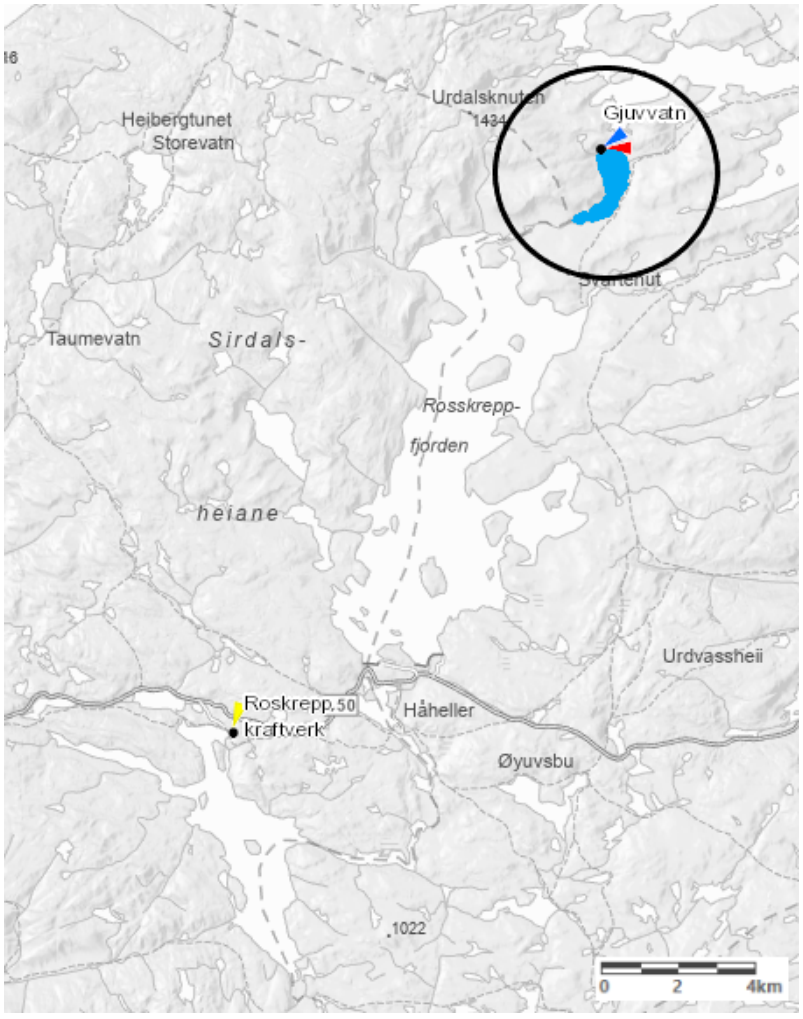

Figure 3.3.1: Location of Gjuvatn - *NVE*

These data of water temperature measured in Gjuvatn refer to the period from 23 October 2018 until 29 July 2022.

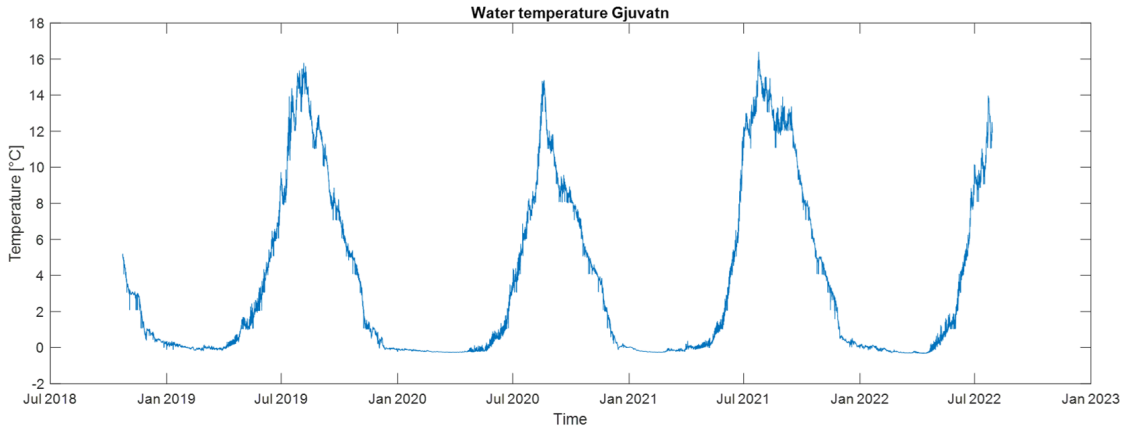

Figure 3.3.2: Water temperature in Lake Gjuvatn, period: 23/10/2018 - 29/07/2022

However, in order to simulate a more extended period, a longer time series is required. Without any other direct measurement, it is necessary to correlate the water temperature to others data. In particular, first water temperature was obtained computing the equilibrium temperature and then using the model *air2water*.

Equilibrium temperature

The equilibrium temperature is the temperature at which the net heat flux at the lake surface is zero. In shallow lakes the surface temperature is close to the equilibrium temperature (Schmid and Read, 2022). In this case the assumption done is that the fictitious river from which the natural inflows flow is shallow, and its temperature is equal to the equilibrium temperature.

The latter is obtained performing a heat balance at the water surface. The procedure used is the one proposed by Fink *et al.* (2014). The net heat flux, H_{net}, is defined as:

$$H_{net} = H_s + H_a + H_w + H_e + H_c \tag{3.3.3}$$

in which:

- H_s is the shortwave absorption;
- H_a is the longwave absorption;
- H_w is the longwave emission;
- H_e is the evaporation/condensation flux;
- H_c is the convection.

The balance is performed on a river, hence the heat flux caused by throughflow is neglected.

- Shortwave absorption

In order to compute the heat components of the flux, it is necessary to know the global radiation incident at the surface. In the absence of direct measurements, radiation is calculated referring to the same formulation used in the model CE-QUAL-W2. This last refers to the relationship proposed by the *United States Environmental Protection Agency* (EPA, 1971). The amount of reflected radiation depends on the portion of direct and diffusive shortwave radiation, hence:

$$H_s = G \cdot F_{dir} \cdot (1 - A_{dir}) + G \cdot F_{diff} \cdot (1 - A_{diff}) \tag{3.3.4}$$

in which:

- G is the global radiation incident at the lake surface;
- $F_{dir} = (1 - C) \cdot [(1 - C) + 0.5C]^{-1}$ is the fraction of direct radiation and C the cloudiness (0 clear sky - 1 complete cover);
- A_{dir} is the albedo of direct shortwave radiation, the value considered is a monthly mean value for 60 latitude reported in Table 5 by Cogley (1979);
- $F_{diff}(0.5C) \cdot [(1 - C) + 0.5C]^{-1}$ is the portion of diffusive shortwave;
- $A_{diff} = 0.066$ (Burt, 1954) is the albedo of the diffusive shortwave.

- Longwave absorption

This component represents the longwave radiation absorbed by the water body and is computed as:

$$H_a = (1 - A_L) \cdot E_a \cdot \sigma \cdot T_a^4 \tag{3.3.5}$$

in which:

- $A_L = 0.03$ (Raphael, 1962) is the albedo for the infrared radiation;
- $\sigma = 5.67 \cdot 10^{-8}\ W/(m^2 K^4)$ is the Stefan-Boltzmann constant;
- $T_a\ [K]$ is the atmosphere absolute temperature;
- $E_a = (1 + 0.17C^2) \cdot 1.24 \cdot (e_a/Ta)^{1/7}$ is the emissivity, where C is the cloudiness and $e_a\ [hPa]$ the water vapour pressure.

- Longwave emission

The longwave emission from the lake surface is calculated with the Stefan-Boltzmann law:

$$H_w = E_w \cdot \sigma \cdot T_w^4 \tag{3.3.6}$$

in which:

- $E_w = 0.972$ (Davies *et al.*, 1971) is the lake surface emissivity;
- $\sigma = 5.67 \cdot 10^{-8}\ W/(m^2K^4)$ is the Stefan-Boltzmann constant;
- $T_w\ [K]$ is the water absolute temperature.

- Evaporation and condensation

The difference between saturated (e_s) and not (e_a) water vapor pressure drives this heat transfer. In particular, when $e_s < e_a$ there is condensation.

$$H_e = -f \cdot (e_s - e_a) \tag{3.3.7}$$

in which:

- $f = 4.8{+}1.98 \cdot u_{10}{+}0.28(T_w{-}T_a)$ (Livingstone and Imboden, 1989) is an empirical function of wind speed, u_{10}, water T_w and air T_a temperature;
- $e_s = 6.11 \cdot exp\left(\frac{17.62T_w}{243.12+T_w}\right)$ (WMO, 2008) is the saturated water vapor pressure.

- Convection

This component is related to the previous one and is computed as:

$$H_c = -\gamma \cdot f \cdot (T_w - T_a) \tag{3.3.8}$$

in which $\gamma = \frac{c_p \cdot p}{0.622 L_v}$ (Livingstone and Imboden, 1989) is the psychrometric constant, where $c_p = 1005\ [J/(kg \cdot K)]$, $p\ [hPa]$ is the air pressure and $L_v = 2.47 \cdot 10^6\ [J/kg]$ is the latent heat of vaporization.

The last three components of the heat flux, H_w, H_e, H_c, are dependant on the water temperature, T_w, therefore they are implicit equations. In order to find the equilibrium temperature the zero of the $Equation\ 3.3.3$ is computed.

The heat balance is applied on both the reservoirs: Rosskreppfjorden and Øyarvatn.

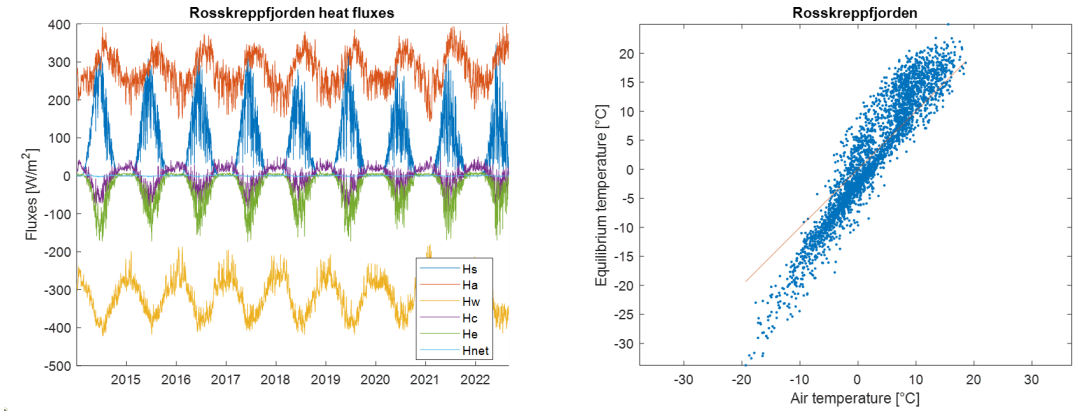

(a) (b)

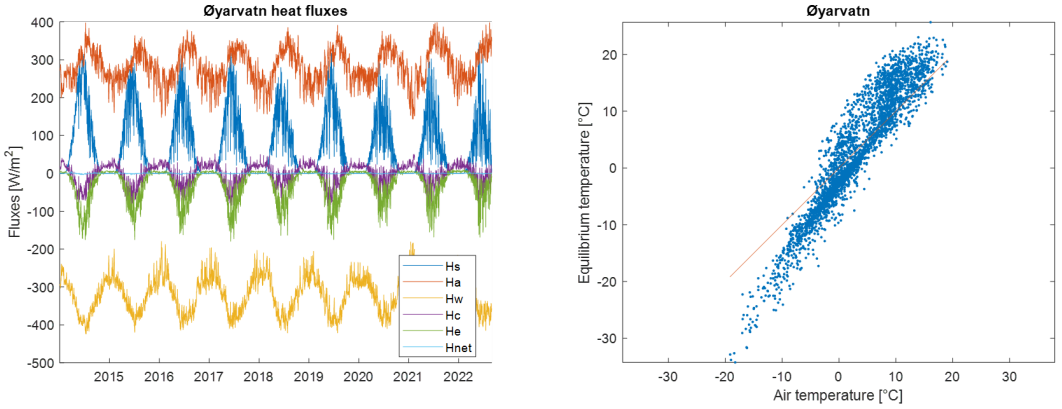

(c) (d)

Figure 3.3.3: Heat fluxes acting on the water surface in Rosskreppfjorden (a) and Øyarvatn (c) and the comparison between air temperature and the equilibrium temperature obtained (b) (d)

In order to use this temperature as the water temperature for the inflows, all negative values are set to 0.1. In *Figure* 3.3.4 are represented the results obtained. The range of values is between 0 °C and 25 °C.

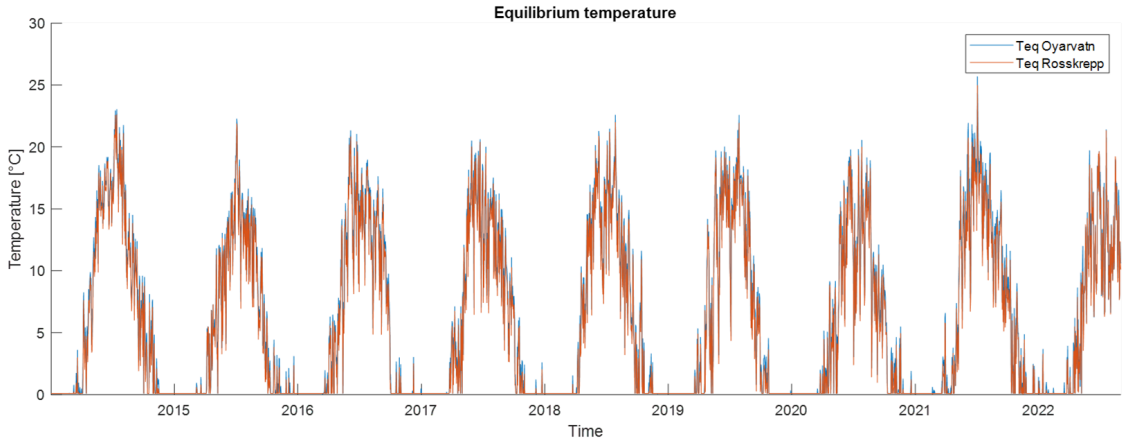

Figure 3.3.4: Inflow temperature as equilibrium temperature in Rosskreppfjorden and Øyarvatn.

The equilibrium temperature is strongly dependant on meteorological forcing. In fact, the difference between equilibrium temperature and air temperature increases decreasing equilibrium temperature and wind velocity and increasing relative humidity (Schmid *et al.*, 2014).

Air2water

Air2water is a model which relates the superficial water temperature to the air temperature alone (Piccolroaz *et al.*, 2013; Toffolon *et al.*, 2014). Specifically, this model is used to predict water temperature from year 2014 considering the water temperature measured in Gjuvatn (23/10/2018-29/07/2022) to calibrate the model. Air temperature in Rosskreppfjorden and in Øyarvatn are very similar (*Figure* 3.3.5), RMSE = 0.653 °C, therefore, the analysis is not applied to the two lakes separately.

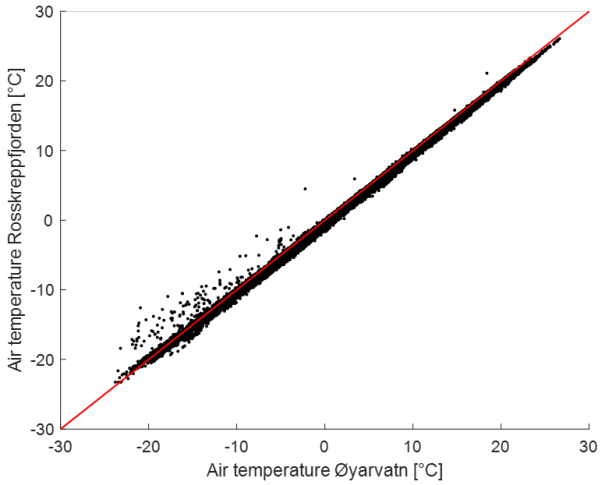

Figure 3.3.5: Comparison between air temperature in Rosskreppfjorden and Øyarvatn

The result obtained by the model shows a good correlation between measured and simulated water temperature with a RMSE = 0.926 °C.

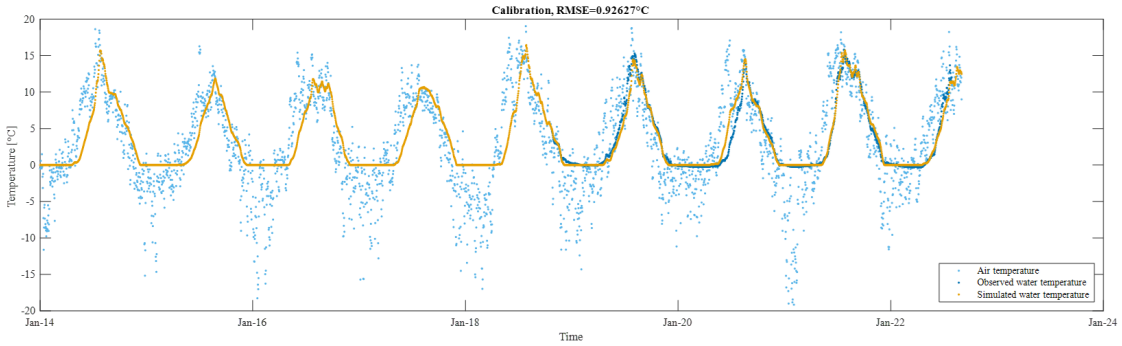

Figure 3.3.6: Result of the model air2water

3.3.2 Inflow temperature comparison

In order to select the best inflow temperature between the two methods considered, the results obtained are compared first with air temperature (*Figure* 3.3.7) and then with

the water temperature measured in Gjuvatn (*Figure* 3.3.8).

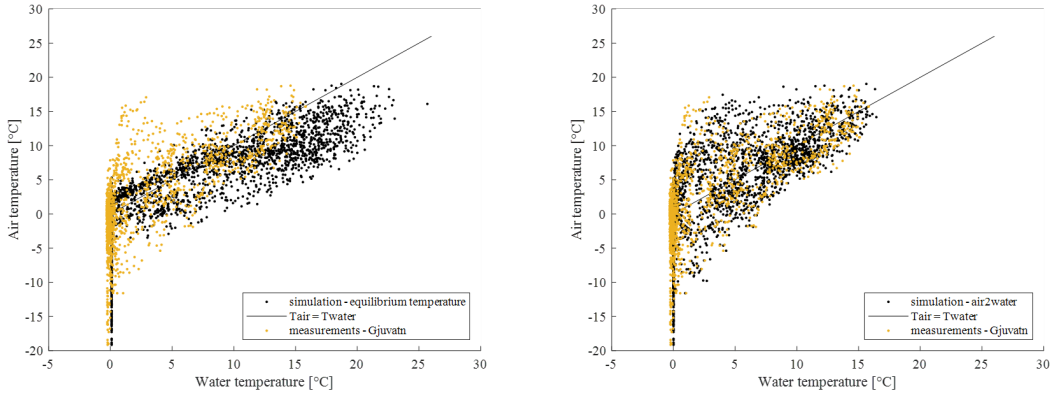

(a) (b)

Figure 3.3.7: Air temperature compared to water temperature computed with equilibrium temperature (a) and the model air2water (b)

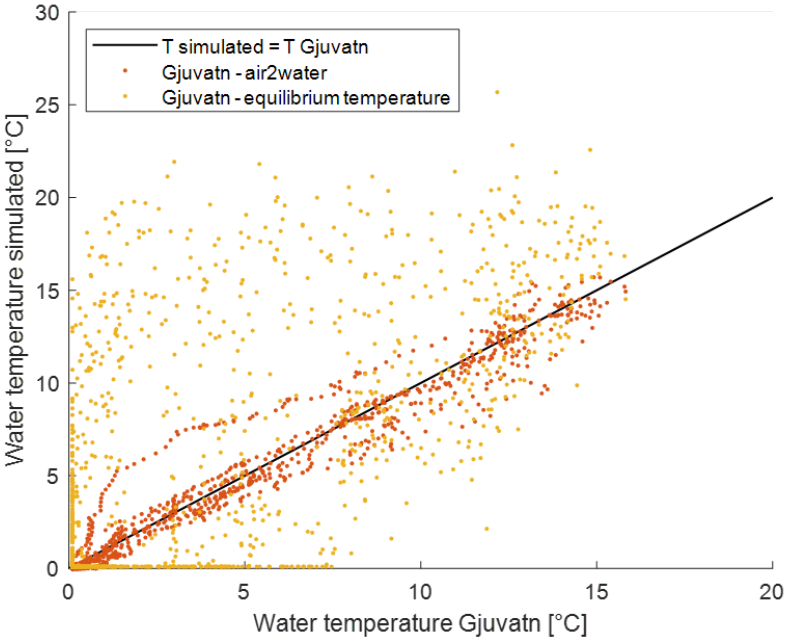

Figure 3.3.8: Comparison between water temperature measured and simulated

In *Figure* 3.3.8 is evident how water temperature from the model air2water is more closely related to the water temprature of Gjuvatn than the equilibrium temperature which is more distributed. In fact, with air2water, the RMSE is 0.92 °C while the equilibrium temperature has a RMSE of 5.25 °C.

As a result, the water temperature used for the inflows is the one obtained by the model *air2water*.

4 SETUP OF THE CE-QUAL-W2 MODEL

CE-QUAL-W2 (*Corps of Engineers QUALity Width averaged 2D*) is a software developed by the U.S. Army Corps of Engineers and the Portland State University, in this specific case the results obtained refers to the *version 4.5* (Wells, 2021).

CE-QUAL-W2 is a two-dimensional hydrodynamic and water quality model averaged along the transverse direction. For this reason, it is suitable to represent the case study due to the fact that the two reservoirs are both deep and mainly developed longitudinally. The current configuration, which refers to a standard (one-way) hydropower plant, where water is released from Rosskreppfjorden and goes to Øyarvatn, was used to calibrate the model. Once the model was calibrated, a pump, which allows to move water from Øyarvatn to Rosskreppfjorden, is implemented in the model. In the model the penstock is not simulated, hence the two lakes are directly linked. Consequently, the water volume in it and the turbine/pump effects are neglected. However, frictional losses are negligible considering that the hydraulic head is less than 100 meters.

4.1 Equations

Regarding the hydrodinamical component of the model, the equations solved are the RANS (*Reynolds Averaged Navier Stokes*) equations. In particular, they are the continuity and momentum equations along x and z directions obtained by a balance on the control volume of the fluid phase. The latter is semplified to a vertical hydrostatic pressure distribution, considering that vertical velocities are much less than horizontal velocities.

The governing equations ($Equation$ 3.1.1) are obtained by making the following assumptions:

- incompressible fluid;
- centripetal acceleration is a minor correction to gravity;
- Boussinesq approximation;

- all velocities and pressure are the sum of turbolent time averages and deviations from that average.

$$\begin{cases} \frac{\partial UB}{\partial x} + \frac{\partial WB}{\partial z} = qB \\ \frac{\partial UB}{\partial t} + \frac{\partial UUB}{\partial x} + \frac{\partial WUB}{\partial z} = gB\sin\alpha - \frac{B}{\rho}\frac{\partial P}{\partial x} + \frac{1}{\rho}\frac{\partial B\tau_{xx}}{\partial x} + \frac{1}{\rho}\frac{\partial B\tau_{xz}}{\partial x} \\ \frac{1}{\rho}\frac{\partial P}{\partial z} = g\cos\alpha \end{cases} \tag{4.1.1}$$

where:

- U is the horizontal velocity;
- W is the vertical velocity;
- B the channel width;
- P the pressure;
- τ_{xx} the turbolent shear stress acting in x-direction on the x-face of contol volume;
- τ_{xz} the turbolent shear stress acting in x-direction on the z-face of contol volume;
- ρ the density.

Density is known trough the equation of state, which relates density as a function of water temperature (T_w), concentration of total dissolved solids or salinity (Φ_{TDS}) and the concentration of inorganic suspended solids (Φ_{ISS}). As a consequence, the system has three equations and three unknown: U, W, P.

Integrating the z-momentum from the depth z to the water surface, η, it is reduced to a pressure equation. Then by combining it with the x-momentum equation, pressure is removed from unknown terms but water surface level η is added.

As a result, the free water surface equation, which is derived from the integration of the continuity equation on depth, is performed.

The governing equations can be rewritten as:

$$\begin{cases} \frac{\partial UB}{\partial x} + \frac{\partial WB}{\partial z} = qB \\ \frac{\partial UB}{\partial t} + \frac{\partial UUB}{\partial x} + \frac{\partial WUB}{\partial z} = gB\sin\alpha + g\cos\alpha B\frac{\partial\eta}{\partial x} - \frac{g\cos\alpha B}{\rho}\int_\eta^z \frac{\partial\rho}{\partial x}dz + \frac{1}{\rho}\frac{\partial B\tau_{xx}}{\partial x} + \frac{1}{\rho}\frac{\partial B\tau_{xz}}{\partial z} + qBU_x \\ \frac{1}{\rho}\frac{\partial P}{\partial z} = g\cos\alpha \\ \rho = f(T_w, \Phi_{TDS}, \Phi_{SS}) \\ B_\eta\frac{\partial\eta}{\partial t} = \frac{\partial}{\partial x}\int_\eta^h UBdz - \int_\eta^h qBdz \end{cases} \tag{4.1.2}$$

In addition, it is necessary to specify the turbolent closure scheme for vertical shear stress, τ_{xz}, defined as:

$$\frac{\tau_{xz}}{\rho} = \nu_t \frac{\partial U}{\partial z} = A_z \frac{\partial U}{\partial z} \tag{4.1.3}$$

where $\nu_t = A_z\ [m^2/s]$ is the vertical eddy viscosity, $U\ [m/s]$ the longitudinal velocity and $\rho\ [kg/m^3]$ the water density. In order to compute the vertical eddy viscosity the model allows to choose between different formulations: Nickuradse (NICK), parabolic (PARAB), W2, W2 with mixing length of Nickuradse (W2N), renormalization group (RNG), turbolent kinetic energy (TKE).

Instead the longitudinal shear stress, it is computed as:

$$\frac{\tau_{xx}}{\rho} = \nu_t \frac{\partial U}{\partial x} = A_x \frac{\partial U}{\partial x} \tag{4.1.4}$$

where $\nu_t = A_x$ is the longitudinal eddy viscosity, a constant defined in input.

4.1.1 Temperature modelling

Regarding temperature the reference equation is the ADE (*Turbolent Advection-Diffusion Equation*) averaged along the transverse direction. The same equation is valid for both constituents and temperature, in fact, concentration of heat can be written as $\rho c_p T$ where c_p is the specific heat of water and T the temperature. The general formula is:

$$\frac{\partial B\Phi}{\partial t} + \frac{\partial UB\Phi}{\partial x} + \frac{\partial WB\Phi}{\partial z} - \frac{\partial}{\partial x}\left[BD_x \frac{\partial \Phi}{\partial x}\right] - \frac{\partial}{\partial z}\left[BD_z \frac{\partial \Phi}{\partial z}\right] = q_\Phi B + S_\Phi B \tag{4.1.5}$$

where:

- $\Phi\ [g/m^3]$ is the laterally averaged constituent concentration;
- $D_x\ [m^2/s]$ longitudinal dispersion coefficient;
- $D_z\ [m^2/s]$ vertical dispersion coefficient;
- $q_\Phi\ [g/(m^3 s)]$ lateral inflow/outflow mass flow rate per unit volume;
- $S_\Phi\ [g/(m^3 s)]$ laterally averaged source/sink term.

In particular, the source/sink term for temperature is $S_T = -\frac{\partial \Phi}{\partial z}$ where Φ is the heat flux $[W/m^2]$ transmitted through the waterbody.

4.1.2 Surface heat exchange

The surface heat exchange is the flux boundary condition at the water surface. It is computed as:

$$\Phi_n = \Phi_s - \Phi_{sr} + \Phi_a - \Phi_{ar} - \Phi_{br} - \Phi_e - \Phi_c \tag{4.1.6}$$

where:

- Φ_n $[W/m^2]$ is the net surface heat flux;
- Φ_s $[W/m^2]$ is the incoming short-wave solar radiation;
- Φ_{sr} $[W/m^2]$ is the reflected short-wave solar radiation;
- Φ_a $[W/m^2]$ is the incoming long-wave atmospheric radiation;
- Φ_{ar} $[W/m^2]$ is the reflected atmospheric long-wave radiation;
- Φ_{br} $[W/m^2]$ is the back long-wave radiation;
- Φ_e $[W/m^2]$ is the evaporative heat loss;
- Φ_c $[W/m^2]$ is the conductive heat loss.

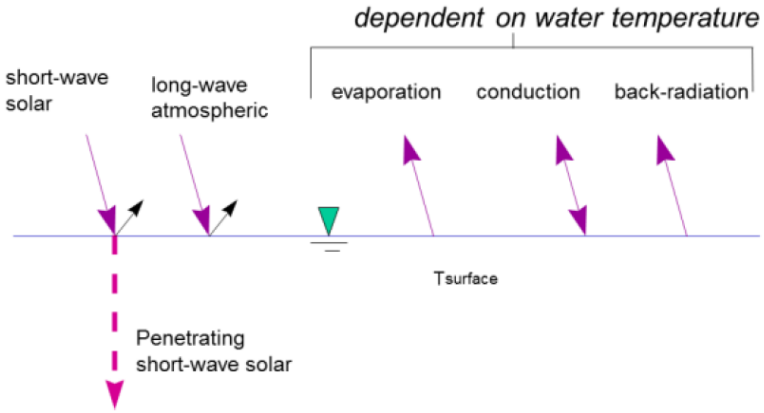

Figure 4.1.1: Surface heat exchange [Wells (2021)]

4.1.3 Ice cover

The ice cover is a crucial component to be modelled, especially for the purpose of the analysis in this thesis. It is relevant to note that ice cover is made by only one layer of black ice, hence in the model snow-ice is not included. Therefore, its presence, which affects the heat budget of the lake, is not taken into account. In particular, the heat balance for the water-ice-air system can be written as:

$$\rho_i L_f \frac{\Delta\Theta}{\Delta t} = h_{ai}(T_i - T_e) - h_{wi}(T_w - T_m) \tag{4.1.7}$$

in which:

- ρ_i $[kg/m^3]$ is the ice density;
- $L_f [J/kg]$ is the latent heat of fusion of ice;
- $\Delta\Theta/\Delta\, t [m/s]$ is the change in ice thickness (Θ) with time (t);
- h_{ai} $[W/(m^2\,{}^\circ C)]$ is the coefficient of ice-to-air heat exchange;

- h_{wi} $[W/(m^2\ ^\circ C)]$ is the coefficient of water-to-ice heat exchange through the melt layer;
- T_i $[^\circ C]$ is the ice temperature;
- T_e $[^\circ C]$ is the equilibrium temperature of ice-to-air heat exchange;
- T_w $[^\circ C]$ is the water temperature below ice;
- $T_m = 0\ ^\circ C$ is the melt temperature.

Initially, ice forms when surface water temperature is lower than the freezing point. At that point, negative water surface temperature is converted to ice thickness as:

$$\Theta_0 = \frac{-T_w \cdot \rho_w \cdot c_{P,w} \cdot h}{\rho_i \cdot L_f} \tag{4.1.8}$$

in which:

- T_w $[^\circ C]$ is the temporary negative water temperature;
- ρ_w $[kg/m^3]$ is the density of water;
- $c_{P,w}$ $[J/(kg\ ^\circ C)]$ is the coefficient of ice-to-air heat exchange;
- h $[m]$ is layer thickness;
- L_f $[J/kg]$ is the latent heat of fusion.

Consequently, an equivalent heat flux is added to the heat source and sink term for water.

Heat components and thermal gradient in the ice are all a function of the ice surface temperature, T_s. During active thawing season, the latter is constant at 0 °C and in the other periods it is computed using the upper air-ice flux boundary condition. Therefore, the approximate value for the ice surface temperature is obtained by linearizing the ice thickness across timestep:

$$T_s^n \approx \frac{\Theta^{n-1}}{K_i}[H_{sw}^n + H_{lw}^n - H_{br}(T_s^n) - H_e(T_s^n) - H_c(T_s^n)] \tag{4.1.9}$$

in which:

- $K_i[W/(m \cdot ^\circ C]$ is the thermal conductivity of ice;
- H_{sw} $[W/m^2]$ is the short wave;
- H_{lw} $[W/m^2]$ is the long wave;
- H_{br} $[W/m^2]$ is back radiation flux;
- H_e $[W/m^2]$ is the evaporative flux;
- H_c $[W/m^2]$ is the conductive flux;

The heat balance is:

$$\rho_i \cdot L_f \cdot \frac{d\Theta}{dt} = H_{sw,2} + H_{lw} - H_{br} - H_e - H_c + q_i \tag{4.1.10}$$

where q_i, the heat through ice $[W/m^2]$ is defined as:

$$q_i = K_i \frac{(T_f - T_s(t))}{\Theta(t)} \tag{4.1.11}$$

The ice melting occurs only when $T_s > T_f$, its formulation reported in the manual considers the stored energy for melting:

$$\rho_i \cdot c_{P,i} \cdot \frac{T_S}{2} \cdot \Theta(t) = \rho_i \cdot L_f \cdot \Delta\Theta \tag{4.1.12}$$

in which $c_{P,i}$ $[J/(kg \cdot °C]$ is the specific heat of ice and $\Delta\Theta$ is the amount of ice melted at the air-ice interface.

However, the ice-cover duration in spring is considerably underestimated. In fact, as already notice in previous articles, the model tends to overestimate the heating in spring and underestimate it in summer especially in the surface layer (Bonalumi *et al.*, 2012). In addition, the snow pack is omitted, hence its effect on reduction of heat conduction through ice is missing (Sadeghian *et al.*, 2015). Sadeghian *et al.* (2015), to overcome this problem, adjust the ice algorithm with two empirical coefficients to reduce heat conduction.

Kobler and Martin (2019) suggest in the *Supported material* that the issue of the fast melting is due to the incorrect representation of the short-wave radiation transfer through ice cover. In agreement with the solution proposed by these latter, it is implemented in the source code.

4.1.4 Ice melting formula variation

Ice melting starts operating when ice temperature computed is higher than zero. When it happens, the new formulation substitute the original. In the solution proposed, an additional flux, that refers to the short-wave radiation transfer through ice cover, is computed:

$$H_{sw,2} = \frac{sw}{refl} \cdot shade \cdot (1 - albedo) \cdot (1 - (1 - \beta_i) \cdot e^{-\gamma_i \cdot h_{ice}}) \tag{4.1.13}$$

in which:

- sw $[W/m^2]$ is the net short-wave solar radiation;
- $refl$ $[-]$ the reflectance (= 0.94);
- $shade$ $[-]$ is the shading coefficient;
- $albedo$ $[-]$ is is the ice albedo;

- β_i $[-]$ is the fraction of incoming solar radiation absorbed in the ice surface;
- γ_i $[1/m]$ is the ice extinction coefficient,
- h_{ice} $[m]$ is the ice thickness;

When $T_{ice} > 0$ melting starts. First, ice temperature is set equal to zero, $T_{ice} = 0$, and then the heat balance is performed:

$$\rho_i \cdot L_f \cdot \frac{d\Theta}{dt} = H_{sw,2} + H_{lw} - H_{br} - H_e - H_c \tag{4.1.14}$$

from which:

$$d\Theta = -\frac{dt}{\rho_i \cdot L_f} \cdot (H_{sw,2} + H_{lw} - H_{br} - H_e - H_c) \tag{4.1.15}$$

Note that he negative sign is due to the fact that the ice thickness is reduced.

The improvement obtained is significant. In $Figure$ 4.1.2 are reported an example for each lake analysed, where the only difference between the two simulated temperatures is in the executable file used. The melting period is underestimated by more than a month using the original formula.

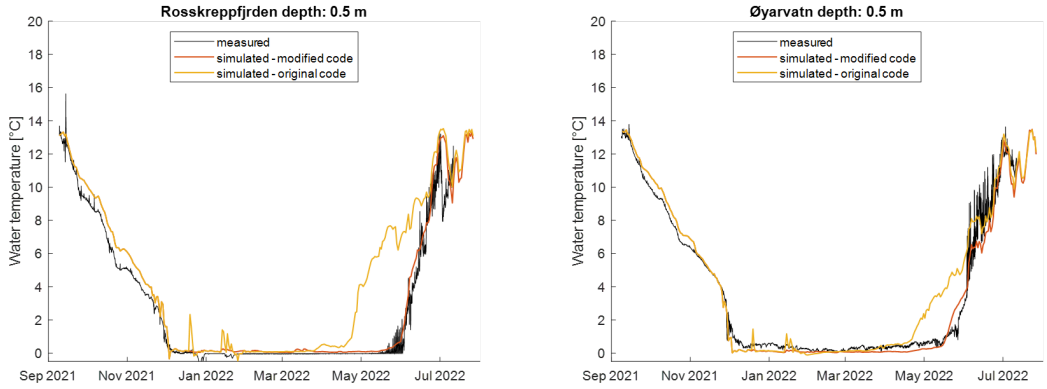

(a) (b)

Figure 4.1.2: Water temperature obtained from the original and modified formula at a depth of 0.5 m in Rosskreppfjorden (a) and Øyarvatn (b). In black are reported the measured temperatures from sensors

4.2 Input data

CE-QUAL-W2 requires bathymetry data, meteorological data, and initial and boundary conditions as input.

4.2.1 Bathymetry

CE-QUAL-W2 needs geometric data to operate. Specifically, the model refers to a two-dimensional bathymetry. In fact, it discretises the reservoirs into a grid of longitudinal segments and vertical layers with for each cell an assigned cross-sectional width determined by the bathymetry. Therefore, starting from the DEM created ($Chapter$ 3.1), the bathymetry has been extracted using the plugin *CE-QUAL-W2_Bathymetry* available on *QGIS*.

Rosskreppfiorden bathymetry consists of 33 segments, of which, excluding the boundary cells, there are 31 active segments. They have variable lengths, in the range 25-800 meters, in order to have a high resolution only in the area closest to the outlet, $Figure$ 4.2.1.

Instead, the bathymetry of Øyarvatn comprises 43 segments, including a lateral branch. In this case, there are 4 boundary cells, 2 for each branch, hence there are 39 active segments, 29 for the main branch and 10 for the lateral branch. As for the other reservoir, the segments length is not constant but varies between 20 and 800 meters, with the highest resolution close to the inlet, $Figure$ 4.2.2.

It should be noted that the numbering of segments begins at Rosskreppfjorden and continues to Øyarvatn, first to the main branch and then to the lateral one. Consequently, the active segments numbering is from 2 to 32 for Rosskreppfjorden, from 35 to 63 for Øyarvatn and from 66 to 75 for its lateral branch.

Both reservoirs have 91 layers 1 meter deep, including the two boundary cells.

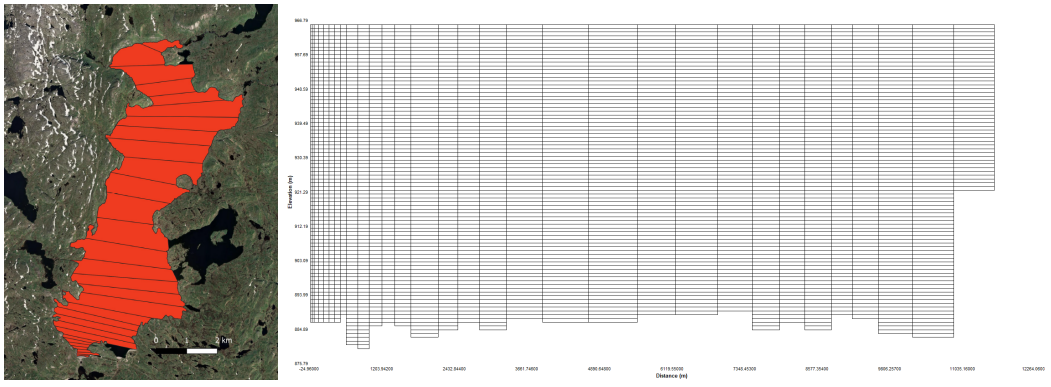

(a) (b)

Figure 4.2.1: Segments selected (a) and its referring 2D bathymetry (b) for Rosskrepp

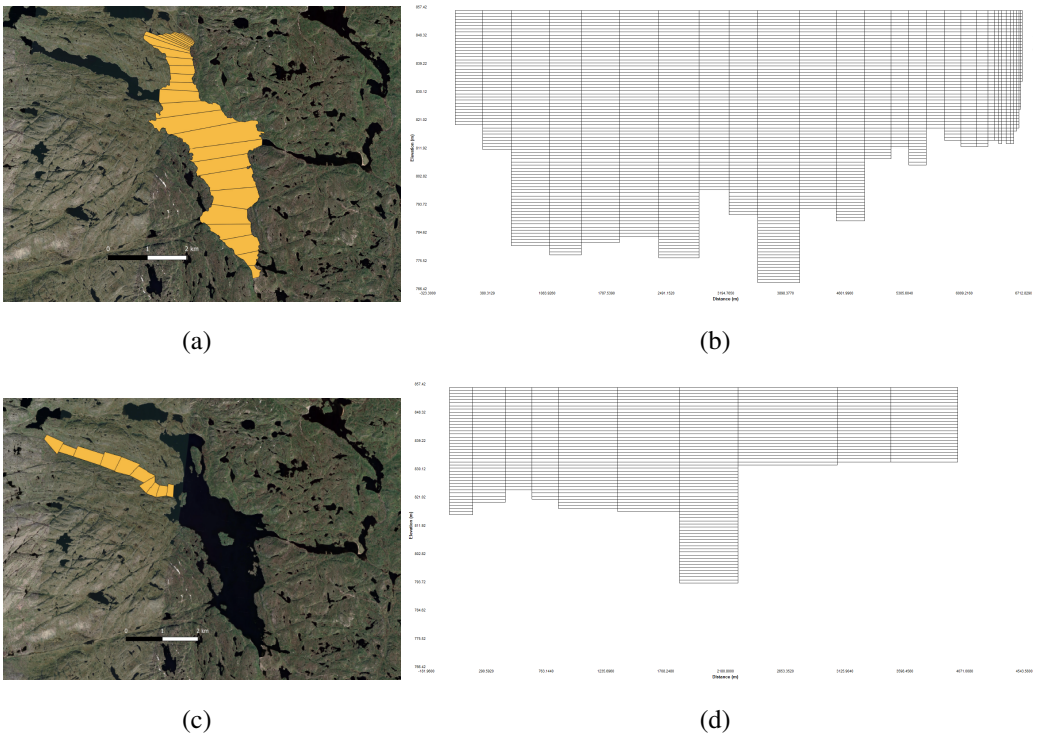

(a) (b)

(c) (d)

Figure 4.2.2: Segments selected (a) (c) and its referring 2D bathymetry (b) (d) for Øyarvatn

In addition to the computational grid, the bathymetry input file contains information related to the orientation of the segments respect to north direction, the bottom friction factor and the initial water level.

4.2.2 Meteorological data

The weather data required to the model are: air temperature, dew point temperature, wind speed and direction, cloud cover and shortwave solar radiation. All the data selected refer to those provided by $OpenWeather$. The only missing component, solar radiation, is computed from cloud cover and the theoretical formulation proposed by the *United States Environmental Protection Agency* (EPA, 1971).

Two additional file must be created. The first is a file containing the amount of shade on each bathymetry segment. The second is a file which defines the wind sheltering coefficient at each segment and for all timestep.

4.2.3 Initial conditions

The initial conditions specified regard water level, defined in the bathymetry file, the initial ice thickness and the initial temperature vertical profile. The latter can be defined

as constant or, alternatively, a different temperature value can be assigned to each layer.

4.2.4 Boundary conditions

In each branch simulated an upstream and downstream boundary condition must be defined. In particular, in this case a discharge is considered both for upstream and downstream boundaries. In the lateral branch of Øyarvatn the downstram boundary condition is the connection with the main branch, located at the segment 51.

4.3 Simulation setup

The simulation involves a connection between Rosskreppfjorden and Øyarvatn which allows to simulate the pumped and turbined discharges. In the model this connection is direct, therefore the conduct is not modelled. In addition, there are others external contributions to the water balance. In fact, there are the spillages and the natural inflows and outflows in both Rosskreppfjorden and Øyarvatn. In addition, an environmental flow must be ensured in Øyarvatn. This last is equal to 0.5 m^3/s in the period 15 June - 15 September and equal to 0.2 m^3/s in the period 16 September - 15 October.

Natural inflows enter in the first active segment of each lake. Instead, natural outflows, spillages and environmental flows exit the domain in the last active segment. The tunnel connecting the lakes is implemented in the model considering two gates. The first gate has a flow from Rosskreppfjorden to Øyarvatn, in order to simulate the turbined discharge, and the second one a flow in the opposite direction, to simulate the pumped discharge. Moreover, Øyarvatn is connected downstream to the Kvinen powerplant. In order to take into account this outlet, a withdrawal is included in the model. Finally, the lateral branch of Øyarvatn is added to the main branch at segment 51.

In $Figure$ 4.3.1 and $Figure$ 4.3.2 is illustrated the location in the bathymetry grid of each component implemented in the model.

Moreover, as already mentioned, precipitation is not added separately but it is included in the natural inflows. Regarding evapotranspiration, it is computed by the model.

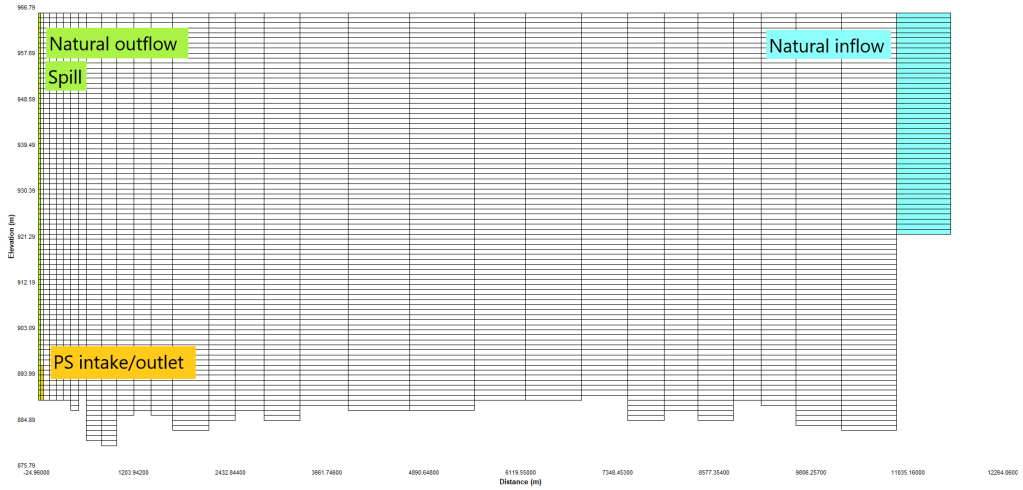

Figure 4.3.1: Rosskreppfjorden scheme

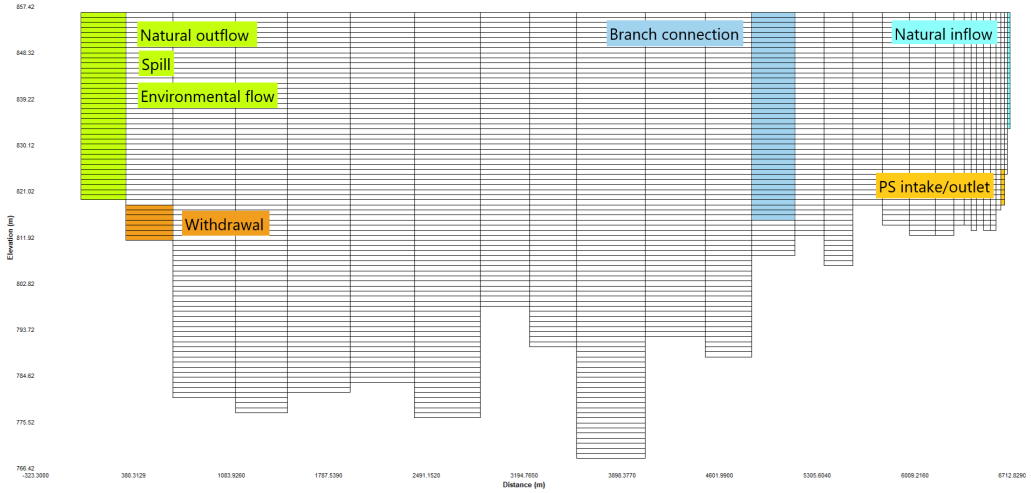

(a)

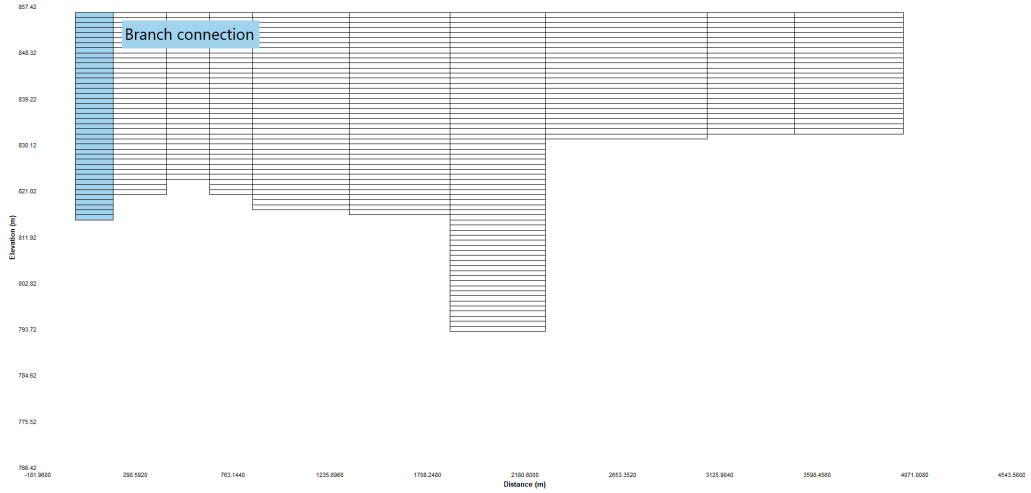

(b)

Figure 4.3.2: Øyarvatn scheme

4.4 Model calibration

The model calibration has been done referring to the current situation. In particular, it considers only the discharge turbined from Rosskreppfjorden to Øyarvatn and nothing pumped. The period considered starts on 9^{th} of September 2021, when the first fieldwork took place, and until 27^{th} of July 2022.

(a) Buoy (b) Temperature sensor

(c) Camera (d) CTD

Figure 4.4.1: Instruments used to acquire data: buoy (a) with temperature sensors (b), camera (C) and CTD (d)

In order to check the validity of the results are available vertical temperature profiles for the period starting from $8^{th} - 9^{th}$ September 2021 until 11^{th} July 2022.

The data are acquired from temperature sensors placed at different depths along a rope tied to an anchor at the bottom and a buoy at the top. In particular, three buoys are placed in the two lakes, two in Øyarvatn and one in Rosskreppfjorden ($Figure$ 4.4.2). The buoy in Øyarvatn closer to the outlet of the Rosskrepp power plant is named "Øyarvatn shallow" while the other one, in the southern part of the lake is nemed "Øyarvatn deep". It is important to note that all of them move. Moreover, during winter period Øyarvatn

shallow lost its anchor. In addition, the bouy in Rosskreppfjorden lost a weight placed along the rope added in order to keep the rope as vertical as possible. In addition, to compare the ice cover duration and extension two cameras are located in Øyarvatn, the first close to the outlet of the turbine and the second one in the center of the lake. A third camera is located in Rosskreppfjorden, however, it became useless after a storm and so it could not be used, some satellite pictures were taken into account to have some comparison.

A second fieldwork took place on the 11^{th} of July 2022 and some CTD (*Conductivity, Temperature, and Depth*) profiles were acquired on that occasion.

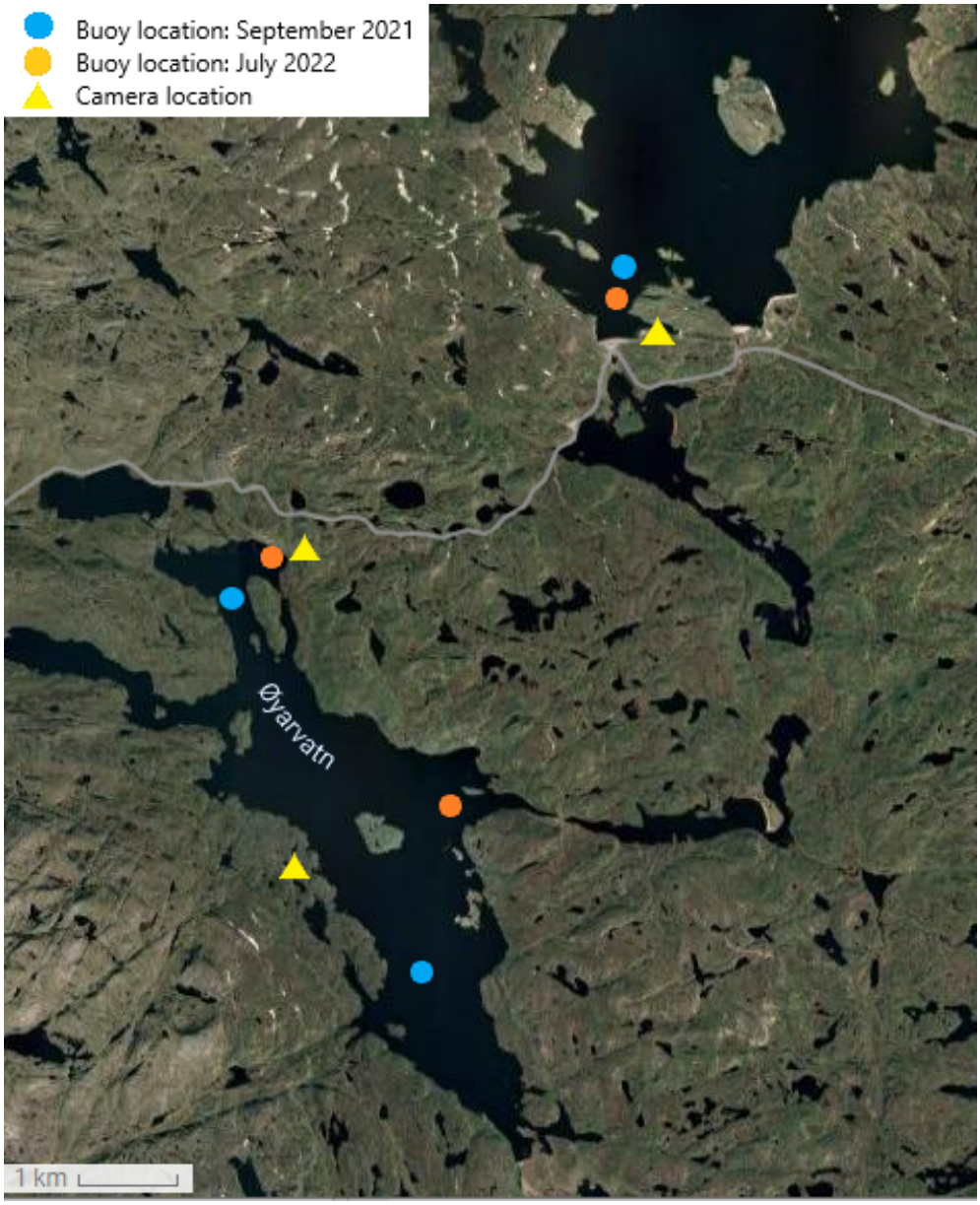

Figure 4.4.2: Map of the cameras and buoy initial and final location for the period analysed

4.4.1 Model inputs during the calibration period

The calibration period refers to the time interval 09/09/2021 14:00:00 - 27/07/2022 00:00:00. During this period water level reached low elevation in May, *Figure* 4.4.3, and its effect is noticeable in the natural inflows and outflows computed, *Figure* 4.4.5 and *Figure* 4.4.7.

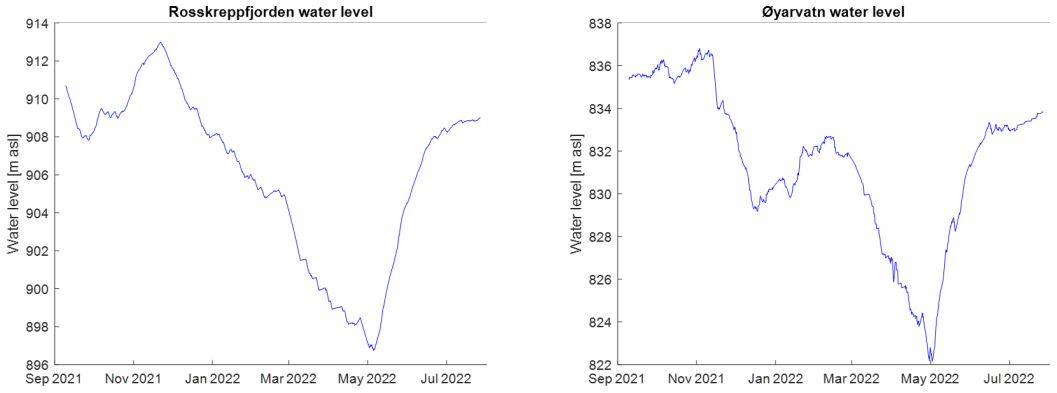

(a) (b)

Figure 4.4.3: Water level in Rosskreppfjorden (a) and Øyarvatn (b) during calibration period

All the discharges involved are reported below. In particular, in the model natural outflows include spillage and environmental flow, when present (*Figure* 4.4.4, *Figure* 4.4.6).

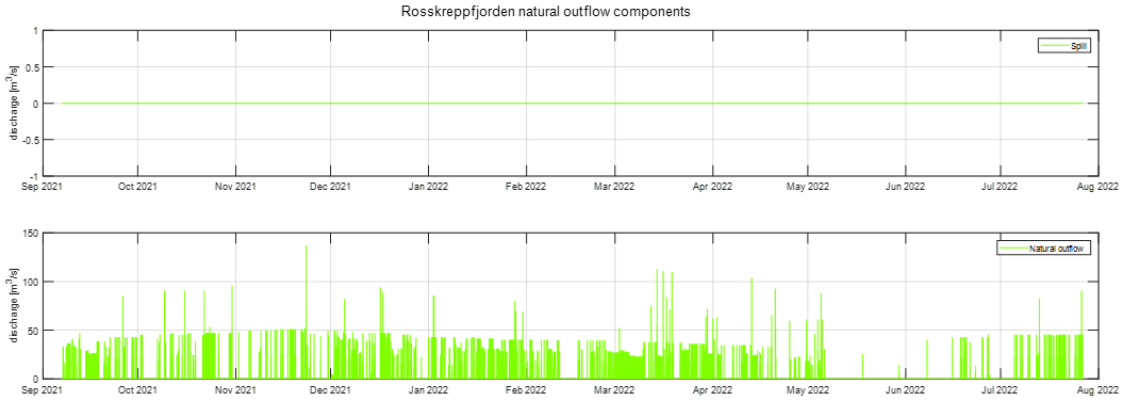

Figure 4.4.4: Natural outflow in Rosskreppfjorden

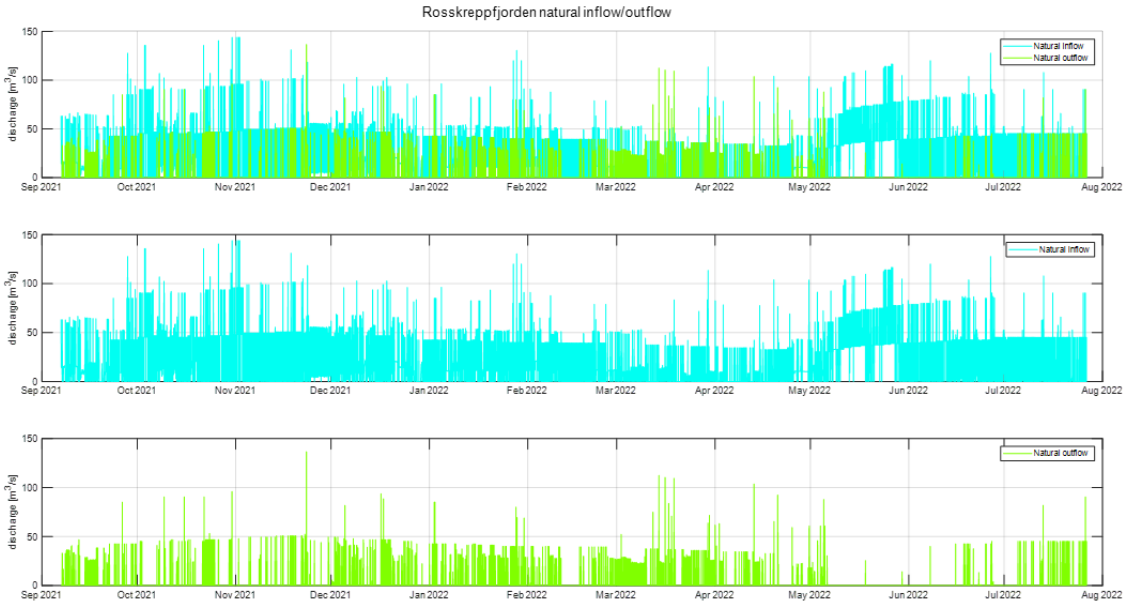

Figure 4.4.5: Natural inflow/outflow in Rosskreppfjorden

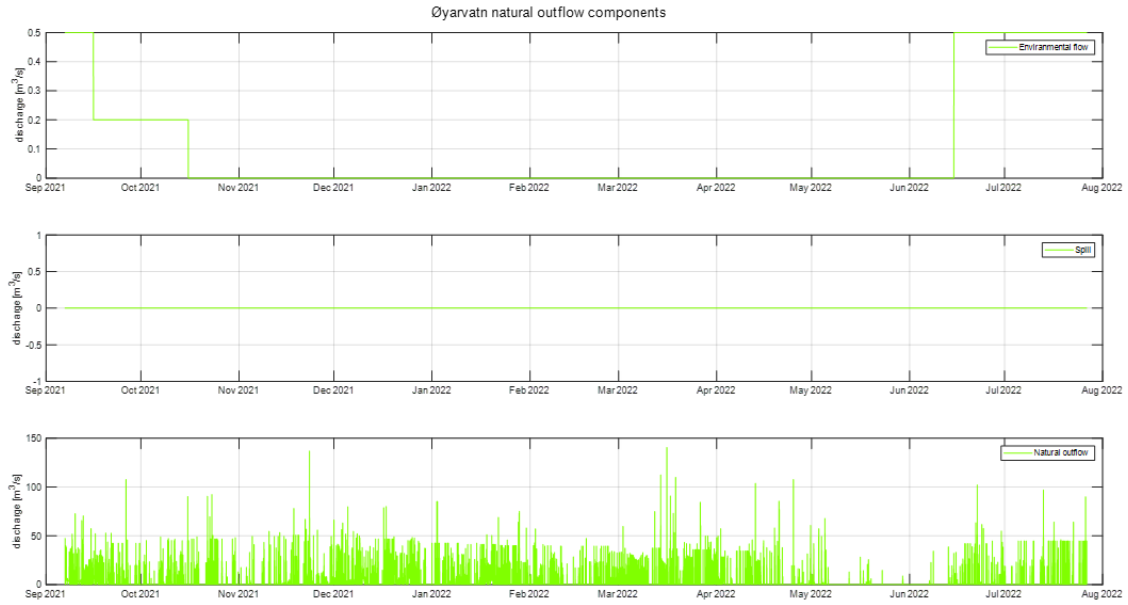

Figure 4.4.6: Natural outflow in Øyarvatn

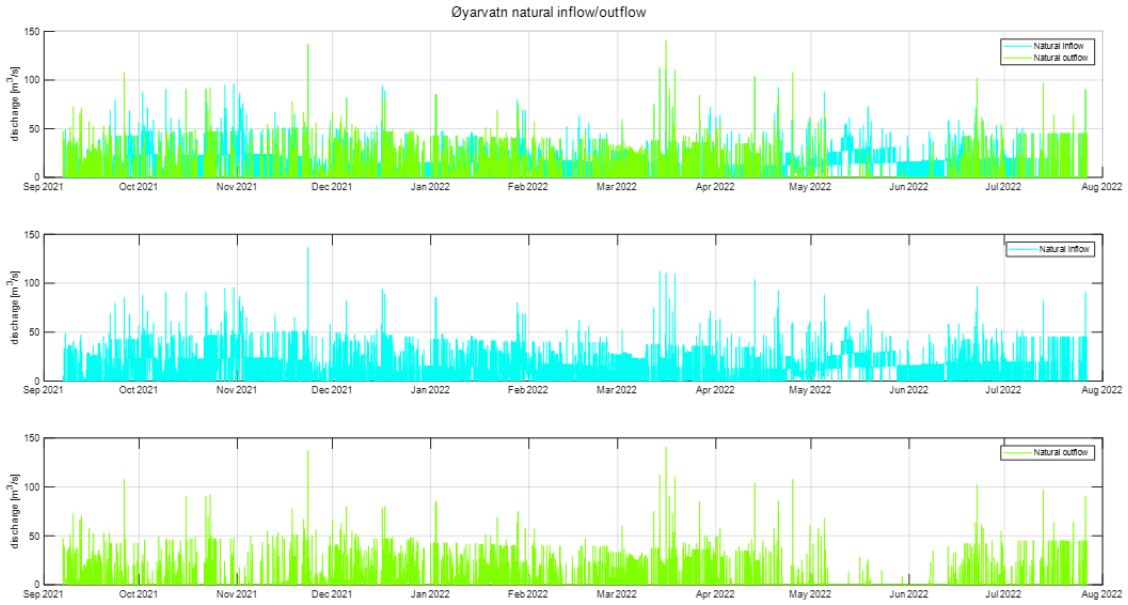

Figure 4.4.7: Natural inflow/outflow in Øyarvatn

In addition to the "natural" component, the discharges used for actual production must be included, $Figure$ 4.4.8. In particular, the withdrawal inserted in the model refers to the inlet of Kvinen power plant. Instead, in the two gates flows the discharge used for energy production in Rosskrepp power plant.

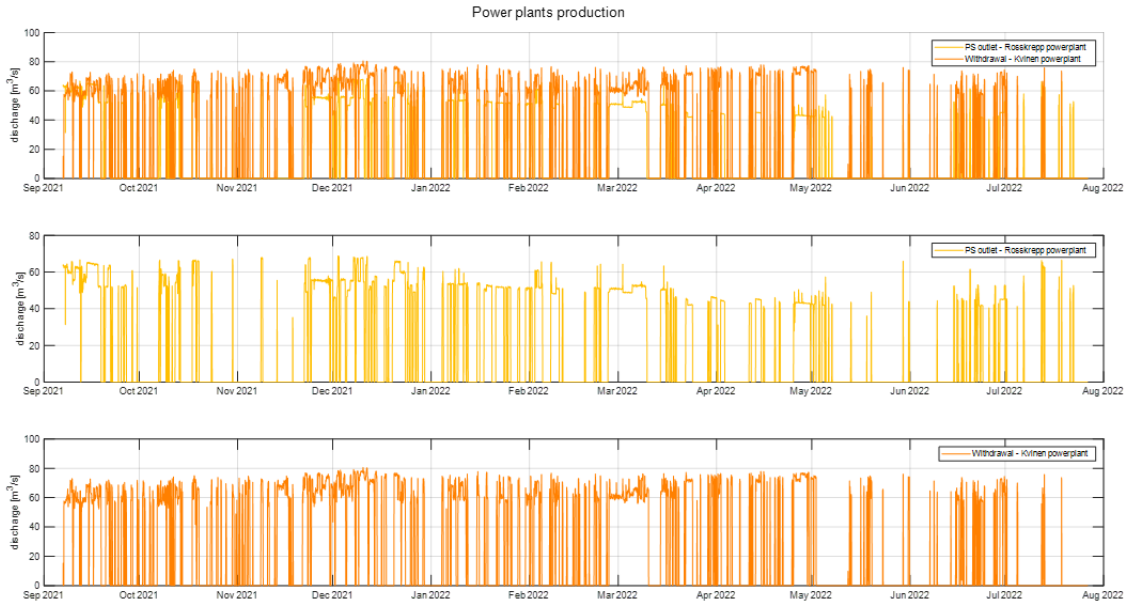

Figure 4.4.8: Current power plant production

The weather conditions acting on the system are reported in $Figure$ 4.4.9. The biggest difference between Rosskreppfjorden (in red in the Figure) and Øyarvatn (in blue in Figure) time series is in the wind speed. The latter is lower in Øyarvatn especially in the fall

and winter period.

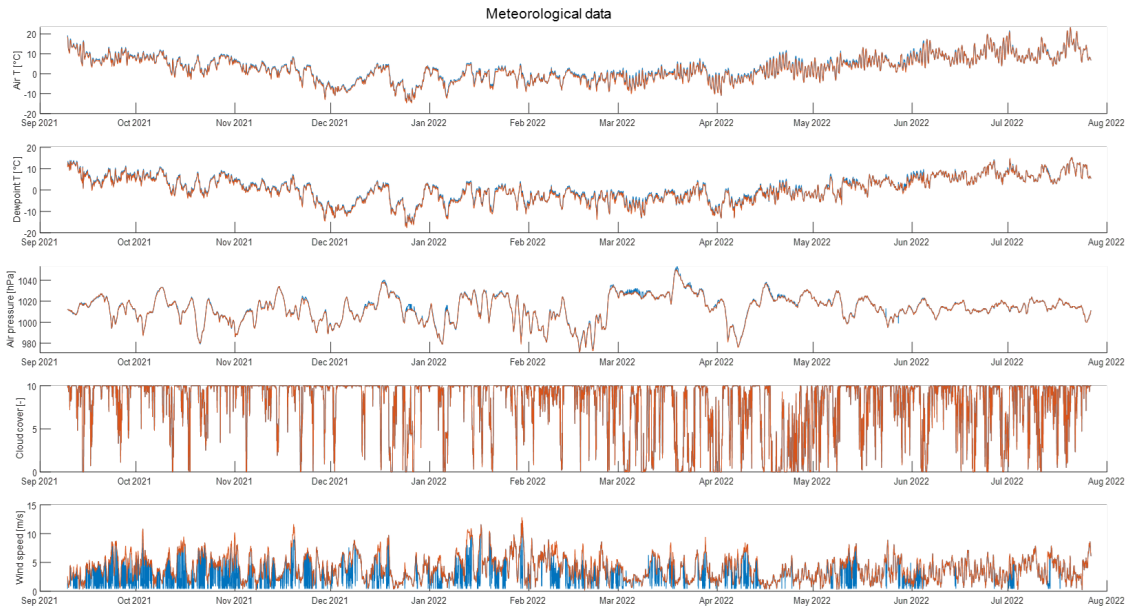

Figure 4.4.9: Meteorological data during the calibration period (OpenWeather, 2022). In red Rosskreppfjorden, in blu Øyarvatn

Regarding the initial water temperature vertical profile, it is acquired from CTD measurements, considering the deepest point available. The reference initial water level is 910.7 m a.s.l. in Rosskreppfjorden and 835.38 m a.s.l. in Øyarvatn.

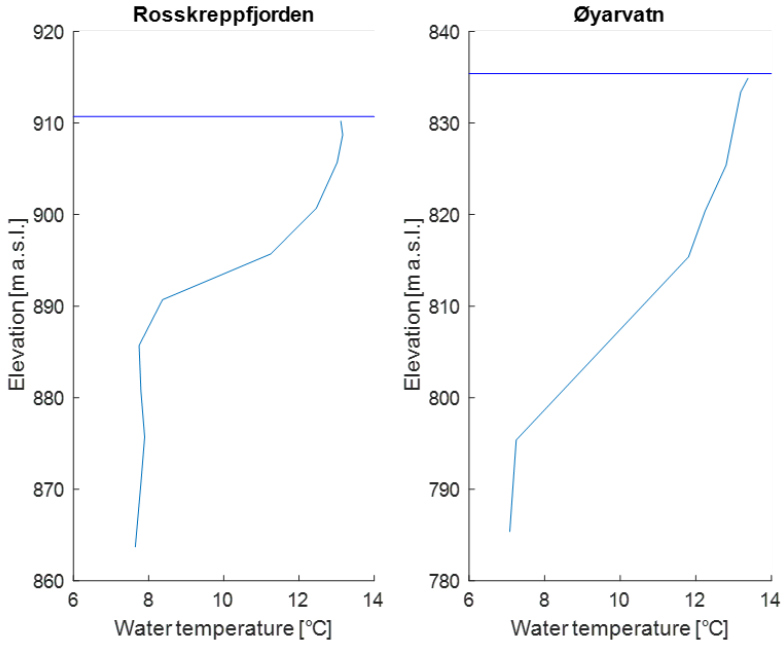

Figure 4.4.10: Water temperature vertical profile at time 09/09/2021 14:00:00

4.4.2 Parameters

The calibration process was focused mainly on light penetration coefficients and ice parameters. The most important are reported and explained below.

Ice albedo

Surface albedo has a key role on the lake heat budget. In fact, its decrease increases the energy absorbed by the lake. During winter period, albedo has a large variability related to the evolution of the ice cover, also ice thickness is significant during the initial stages of ice growth (Perovich, 1996). In particular, the albedo of snow-covered ice can reach 0.82-0.88 (snow dry), for melting snow 07-0.75, for bare, white ice 0.65, for ponds 0.3 and for deep, dark melt ponds 0.1 (Perovich *et al.*, 2002).

The default value in the model is 0.25. According to what can be seen from the camera, $Figure\ 4.4.11$, and the few data available, the ice cover consists of snow-ice in the upper layer. Note that snow and snow-ice are not included in the model. However, in the calibration, in order to better reproduce temperature data, a high value of albedo is considered. In particular the value used in Rosskreppfjorden is 0.65 while in Øyarvatn is 0.55.

Figure 4.4.11: Winter landscape in Øyarvatn - *Mid-lake camera*

Coefficient of water-ice heat exchange

This coefficient determines the rate of heat exchange between water and ice and it is expressed in $W/(m^2\ °C)$. In a free convection its value is in the range 0.3 - 175 $W/(m^2\ °C)$ and increases exponentially with temperature difference between surface and deeper water (Chen *et al.*, 2016). In condition of low velocity, LI *et al.* (2016) find out a linear

correlation between ice-water heat transfer coefficient, h_{wi}, and depth-averaged velocity, u_w: $h_{wi} = 4594.8 \cdot u_w$.

The default value is 10 $W/(m^2\ °C)$, for rivers it is computed in the model as a function of water velocity but for reservoirs it must be empirically adjusted. The value used is 40 $W/(m^2\ °C)$. This value refers to an average-depth velocity of 0.0087 m/s considering the empirical relationship. Although the velocity field has a wide variability, this value seems realistic in representing the winter period.

Fraction of solar radiation absorbed in the ice surface

The absorbed radiation flux in the surface layer depends on the wavelength. Near infrared light is mainly absorbed in the surface layer while a smaller amount in the visible waveband equal to even only a fraction of 0.06 of the total energy (Light *et al.*, 2008). The default value is set equal to 0.6, the calibrated value is reduced to 0.2. By doing this the 20 % of the incident radiation is absorbed in the ice surface.

Solar radiation extinction coefficient through ice

This coefficient determines the attenuation of light trough ice cover. Consequently, it affects the amount of light available for under-ice heating and ecosystem (Castellani *et al.*, 2022).

The attenuation varies with different snow and ice types, it depends on the internal structure and sky conditions. The extinction coefficient of bare ice is usually taken in the range 1.1-1.6 1/m, and for snow the attenuation is higher 4.3-40 1/m (Perovich, 1996). More recent studies find out that the extinction coefficient for bare ice is smaller and in the range 0.65-0.95 1/m (Light *et al.*, 2008).

The default value is 0.07 1/m and the selected one is set to 5 1/m in order to consider indirectly the snow cover.

In order to show the impact of each parameter on the temperature profile, for both Rosskreppfjorden and Øyarvatn, all the parameters explained above are set one at a time to the default value and the result is compared to the reference solution ($Figure\ 4.4.12$). The latter refers to the final selected values: $\beta_i = 0.2,\ \gamma_i = 5\ 1/m,\ h_{wi} = 40\ W/(m^2\ °C)$, ice albedo $= 0.65$ in Rosskreppfjorden and 0.45 in Øyarvatn.

The extinction coefficient and ice albedo result to be the factors that most influence the ice duration and, to a minor extent, also the fraction of solar radiation absorbed in the surface layer. As a consequence, the effect of a faster ice melting is reflected in higher temperature during spring and summer period. A lower value of the coefficient of water-ice heat exchange generate higher temperature in the water below ice cover.

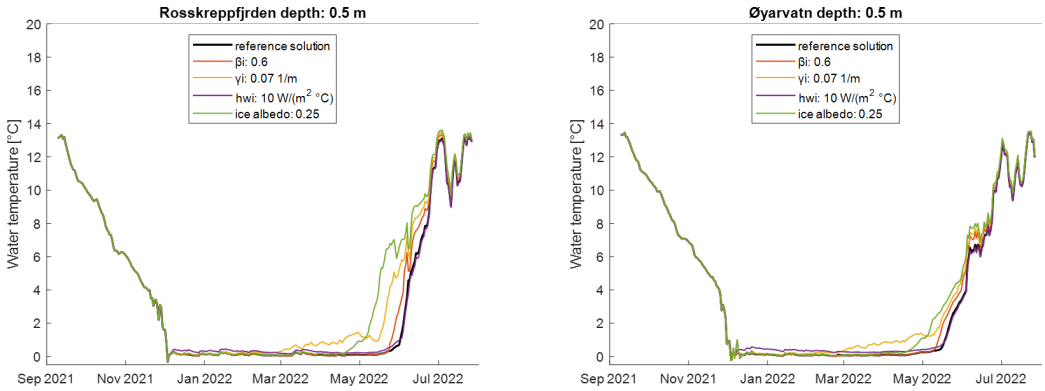

(a) (b)

Figure 4.4.12: Water temperature at a depth of 0.5 m in Rosskreppfjorden (a) and Øyarvatn (b) obtained by varying ice parameters: fraction of solar radiation absorbed in the ice surface, β_i, the extinction coefficient through ice, γ_i, the coefficient of water-ice heat exchange, h_{wi} and the ice albedo

Extinction coefficient

As with ice, light is also attenuated in water. In particular, the net extinction coefficient, λ, is computed as:

$$\lambda = \lambda_{H2O} + \lambda_{ISS} + \lambda_{POM} + \lambda_a + \lambda_{macro} + \lambda_{zoo} \tag{4.4.1}$$

In which:

- λ_{H2O} is the extinction for pure water $[1/m]$;
- λ_{ISS} is the extinction due to inorganic suspended solids $[1/m]$;
- λ_{POM} is the extinction due to organic suspended solids $[1/m]$;
- λ_a is the algae extinction coefficient $[1/m]$;
- λ_{macro} is the macrophyte extinction coefficient $[1/m]$;
- λ_{zoo} is the zooplankton extinction coefficient $[1/m]$.

All the components, except λ_{H2O} which is defined by the user, are obtained by multiplying the reference concentration by a parameter defined in input. In this specific case constituents are not simulated. As a result, the only important parameter is the extinction coefficient for pure water. The recommended value is 0.45 when only temperature, and no constituents, is simulated.

As reported by the *Sterkt Modifiserte VannForekomster* (SMVF, 2022), both Rosskreppfjorden and Øyarvatn are defined as "very clear" with a concentration of total suspended solid $TSS < 10mg/L$ and total organic carbon $TOC < 2mg/L$. Consequently, the value selected for both lakes is 0.2.

During fieldworks a Secchi disk with a diameter of 9" (22.96 cm) was tested, $Figure\ 4.4.13$. In both lakes the Secchi depth reached 7.5-8 meters. The Secchi depth, Z_{SD}, and the extinction coefficient, k_T, are related by the equation $h_T \cdot Z_{SD}$ = 1.7 (Poole and Atkins, 1929). Armengol *et al.* (2003) find out that the constant coefficient was in the range 1.49 and 1.99 using a Secchi disk with diameter 30 cm.

Considering the extinction coefficient used, 0.2 1/m, and the Secchi depth measured, the product obtained is between 1.5 and 1.6. Although the uncertainties related to the correlation between the diameter used and the constant coefficient, the result obtained is in accordance with the value used in the model.

Figure 4.4.13: Secchi disk

Fraction of incident solar radiation absorbed at the water surface

This coefficient represents the amount of solar radiation absorbed in the surface layer. The default value is 0.45, therefore the 45 % of the incident radiation is absorbed in the upper layer of the reservoir. In order to allow an higher amount of light penetration the value selected is equal to 0.1 in both reservoirs.

4.4.3 Calibration result

Once all the parameters were defined, the final result of the calibration phase shows good correlation between measured and simulated data, with a RMSE less than 1 °C in Rosskreppfjorden and Øyarvatn deep. The root mean square error is computed by referring to the temperature measured by the first sensor close to the buoy at a depth of 0.5 meters in order to reduce the uncertainties related to depth. The RMSE of Øyarvatn

shallow is much higher due to the rope breakage that cause the sensors to float on the surface, this is evident in $Figure\ 4.4.14(b)$.

Buoy	**RMSE**
Rosskreppfjorden	0.699 °C
Øyarvatn shallow	6.493 °C
Øyarvatn deep	0.572 °C

Table 4.1: Root mean square error between the temperature measured by the sensors of the three buoys at a depth of 0.5 meters and the simulated temperature at the same depth

It is important to note that all the buoys report some uncertainties due to the different location, rope breakage and mid-rope weight lost. However, the trend observed is similar. Rosskreppfjorden has sensors until a depth of 47 meters, however, in the period analysed the water level never reached high elevation, hence, the sensor placed at 47 meters is compared to the temperature simulated at a depth of 30 meters. Consequently, sensors at middle depth exhibit ambiguity on their measuring depth.

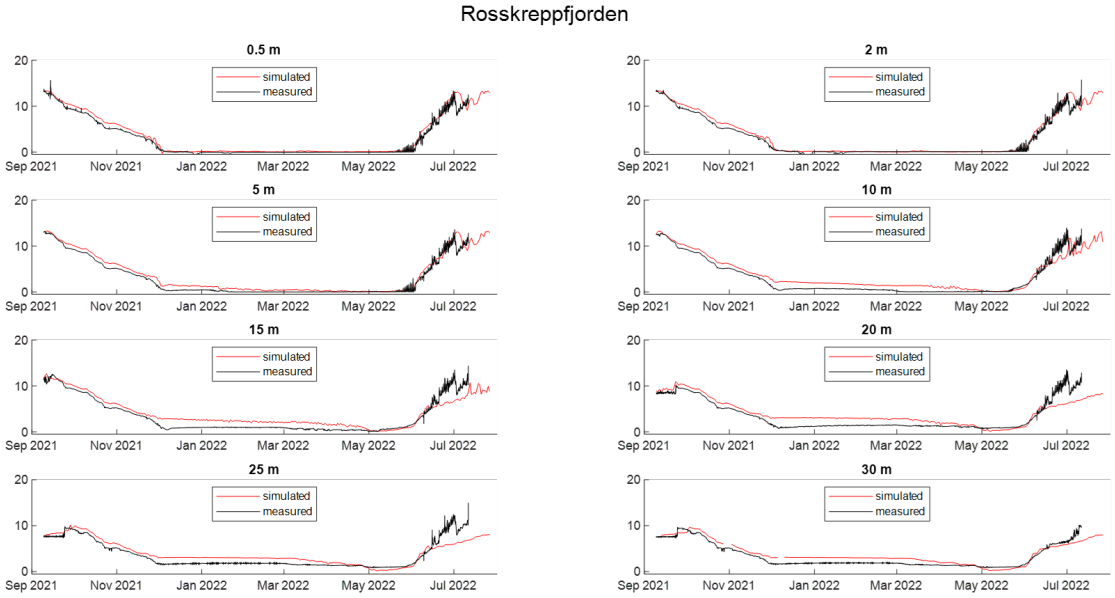

(a)

Øyarvatn shallow became useless after the rope broke, which probably occurred before the ice formation, considering the high temperature peaks. However, both simulated and measured water temperature show a fluctuating trend. Finally, Øyarvatn deep that moved largely away from its original location, seems to maintain its vertical profile correctly, and the water temperature is well reproduced.

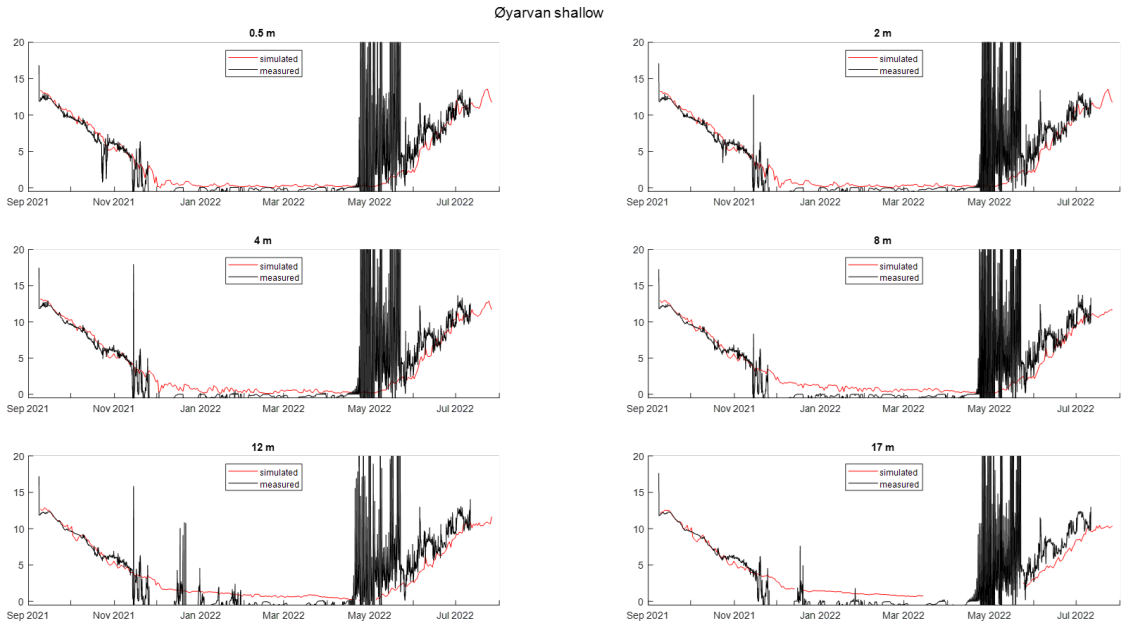

(b)

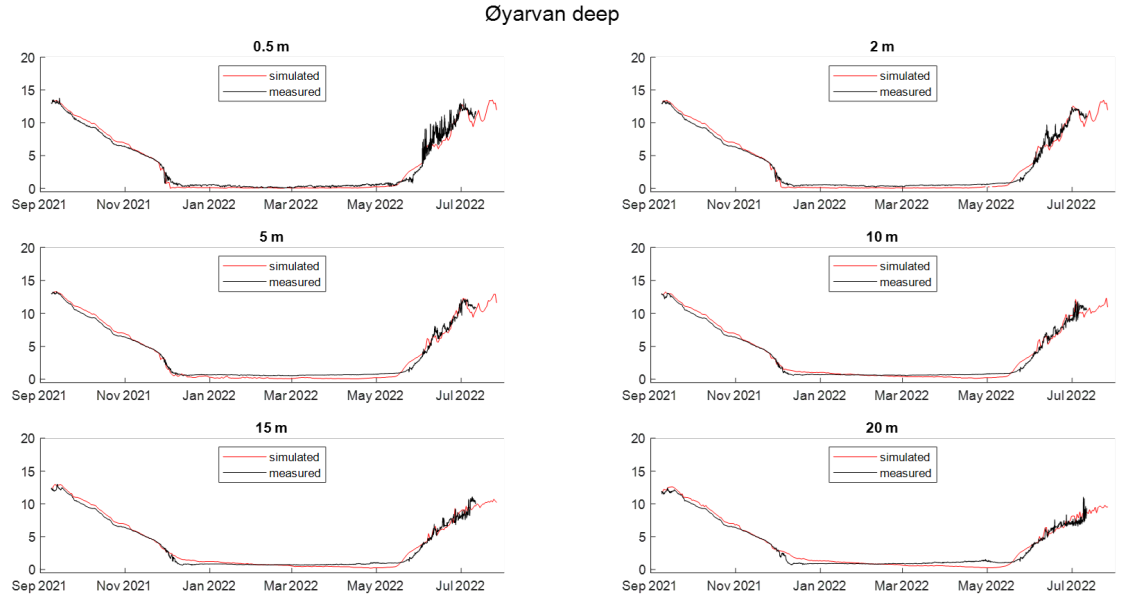

(c)

Figure 4.4.14: Comparison between water levels measured and simulated for Rosskreppfjorden (a) and Øyarvatn (b) for the calibration period in Julian Day

In addition, some CTD (*Conductivity, Temperature, and Depth*) measurements taken on the 11^{th} of July 2022, when the second fieldwork took place, are available. In particular, three vertical profiles were acquired in each lake. Their location in the CE-QUAL-W2 bathymetry is reported in $Table$ 4.2.

CTD number	segment
400	24
396-399	26
408	53
405-406	54

Table 4.2: Reference bathymetry segments of CTD measurements

Rosskreppfjorden measured and simulated temperature show a complete mixing along the vertical profile. However, the simulated profile has a lower water temperature. In addition, at the bottom there is a colder area, it can be explained by looking at the bathymetry, *Figure* 4.4.16. In fact, at the bottom the width is very low, around 5 meters, and mixing is probably not favoured there.

In Øyarvatn the simulated temperature profile follows quite well the measured one except at the bottom for CTD 405-406. These measurements refer to segment 54, *Figure* 4.4.17, where the nearest segments have a minor depth. Consequently, mixing is less effective in that area.

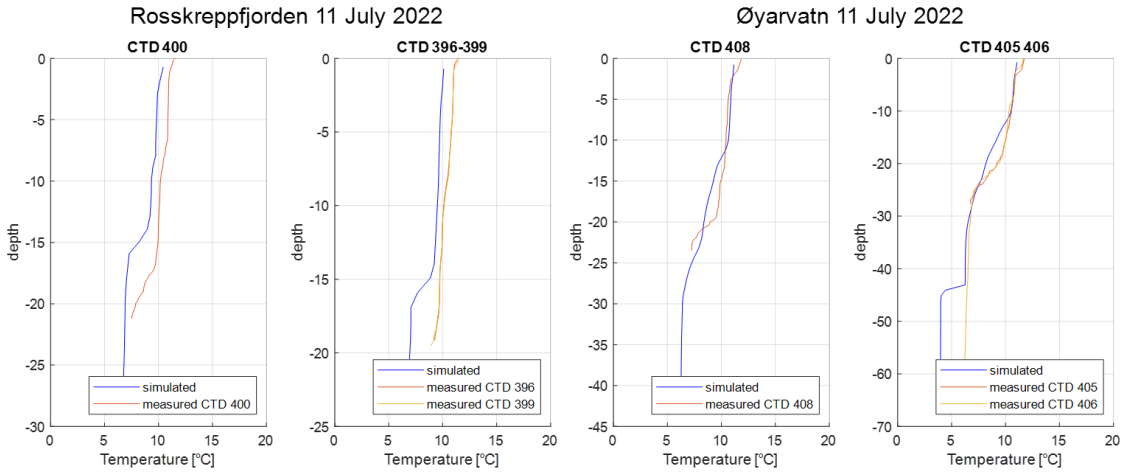

(a) (b)

Figure 4.4.15: CTD measurements in Rosskreppfjorden (a) and Øyarvatn (b) on 11/07/2022

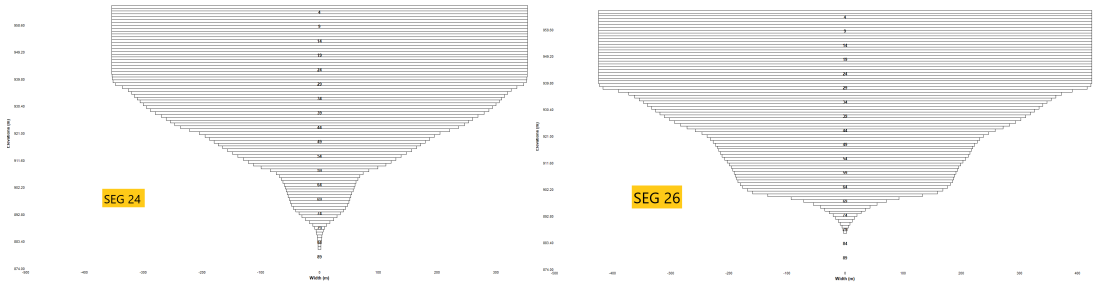

(a) (b)

Figure 4.4.16: Sections of segments 24 and 26 where CTM measurements were taken in Rosskreppfjorden

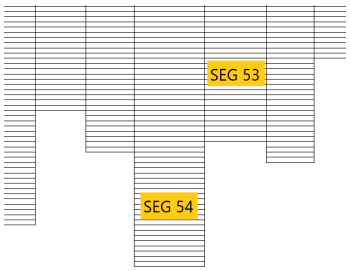

Figure 4.4.17: Zoom on the bottom of segments 53 and 54 where CTD measurements were taken in Øyarvatn

Finally, the presence or absence of the simulated ice is compared with what was recorded by the two cameras in Øyarvatn. In particular, in $Figure$ 4.4.18 the presence of ice is indicated by the number 1 while its absence is indicated by the number 0.

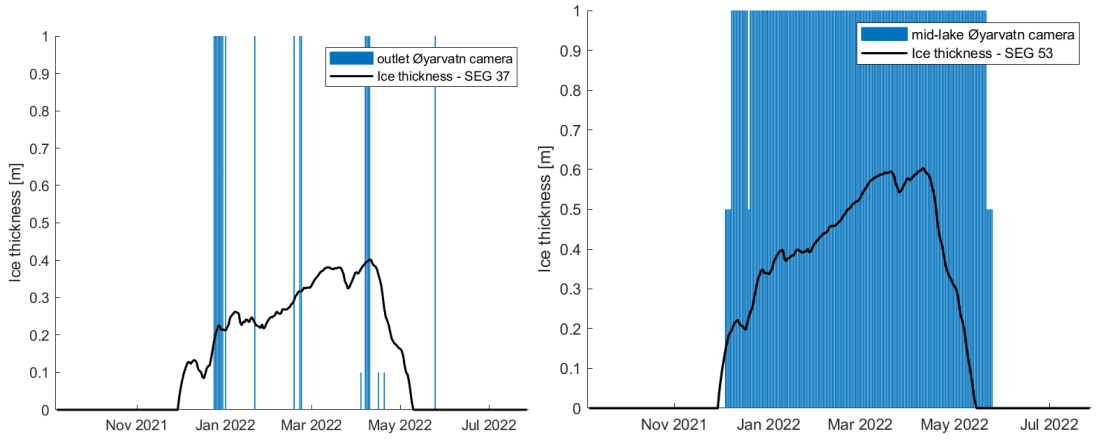

(a) (b)

Figure 4.4.18: Ice thickness simulated comparing the presence (1) or absence (0) of ice recorded by the two cameras in Øyarvatn

The comparison shows a little anticipation in the simulated ice duration for the camera located in the middle of Øyarvatn while the one nearest to the outlet shows a different trend. In fact, there the simulated ice seems more stable. However, the trend reported by the camera refers mainly to the outlet and not to the entire segment. It is interesting to note also that the closest segment to the one considered does not record ice formation for the entire period.

Although it is difficult to compare pictures to simulated values, it is clear that closer to the outlet the maximum ice thickness is much lower than in a further place. The results in $Figure$ 4.4.18 report a reduction of the maximum ice thickness of one-third, from 0.6 m in the middle to 0.4 m closer to the outlet.

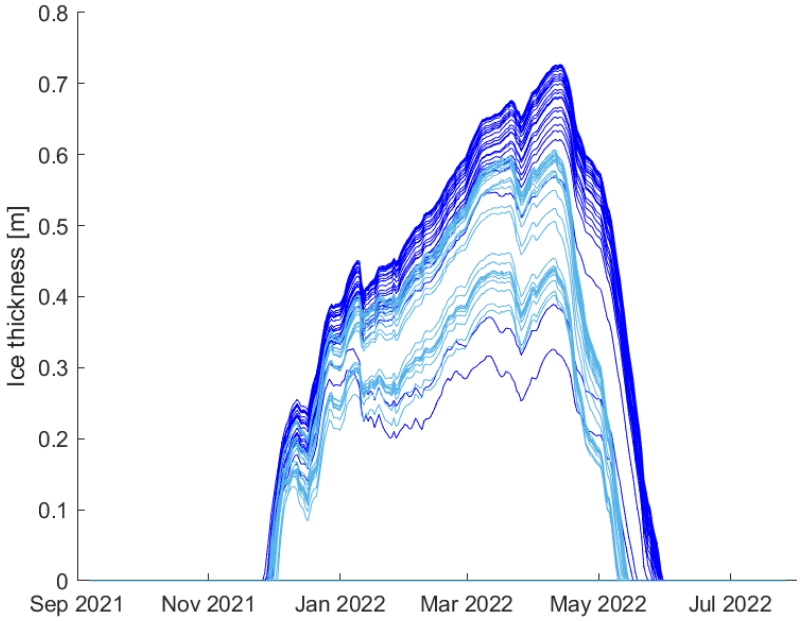

Figure 4.4.19: In blu the ice thickness in the segments of Rosskreppfjorden and in light blue the ice thickness in Øyarvatn

In $Figure$ 4.4.19 are reported the ice thicknesses in all the segments for both lakes. In Rosskreppfjorden, blue in figure, the ice cover period is longer with higher ice thickness. Instead, in Øyarvatn, light-blue in figure, ice cover period is shorter with thinner ice thickness. This result is compatible with what expected.

5 RESULTS

5.1 Scenarios of an optimal price-based scheduling

The discharges exchanged in the pumped-storage system are obtained from a medium-term optimal stochastic scheduling model (Schäffer *et al.*, 2022), initially used for conventional hydropower plants and recently extended to include pumping operation. The scheduling model aims to maximize production based on inflow and price according to an optimization problem. Therefore, by giving in input prices and inflows the model returns in output several possible scenarios.

In addition, it is necessary to provide the volume - water level curve for both the lakes in order to correlate a variation of the water volume to a water level, the latter being the constraining term. This has been done starting from the CE-QUAL-W2 bathymetry and considering a water level variation between the lowest and the highest regulated water level. In order to overcome compatibility issues between the two models, the lowest regulated water level is increased of 5 meters. In the scheduling model this curve has been provided selecting 10 points from the curve obtained from the CE-QUAL-W2 bathymetry, *Figure* 5.1.1.

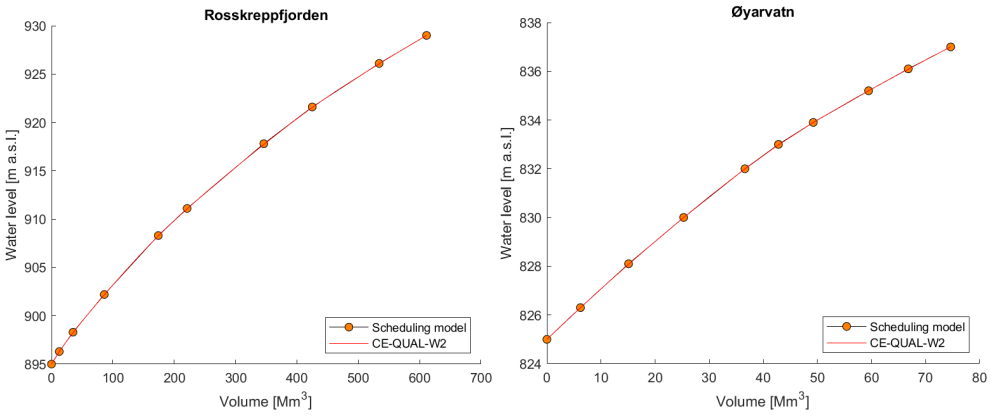

(a) (b)

Figure 5.1.1: Comparison between the curves volume - water level for the two reservoirs in CE-QUAL-W2 model and in the scheduling model

The inputs of the scheduling model, inflows and prices, have a weekly resolution. Instead, the output returns discharges and water levels with a three-hours resolution. In particular, the model simulates years consisting of 52 weeks, each with 56 three-hours steps.

In order to correlate the output of the stochastic model to specific water inflows, the model was adapted to simulate historical scenarios. This enables the generation of all the discharges that influence the water balance of the two lakes and simulates real years with their reference meteorological forcing. As a consequence, the inflows provided to the model are the one computed performing the water balance mentioned in *Chapter* 3. It is important to note that the inflows are provided as a volume to the model, expressed in Mm^3, with a weekly resolution (*Figure* 5.1.2).

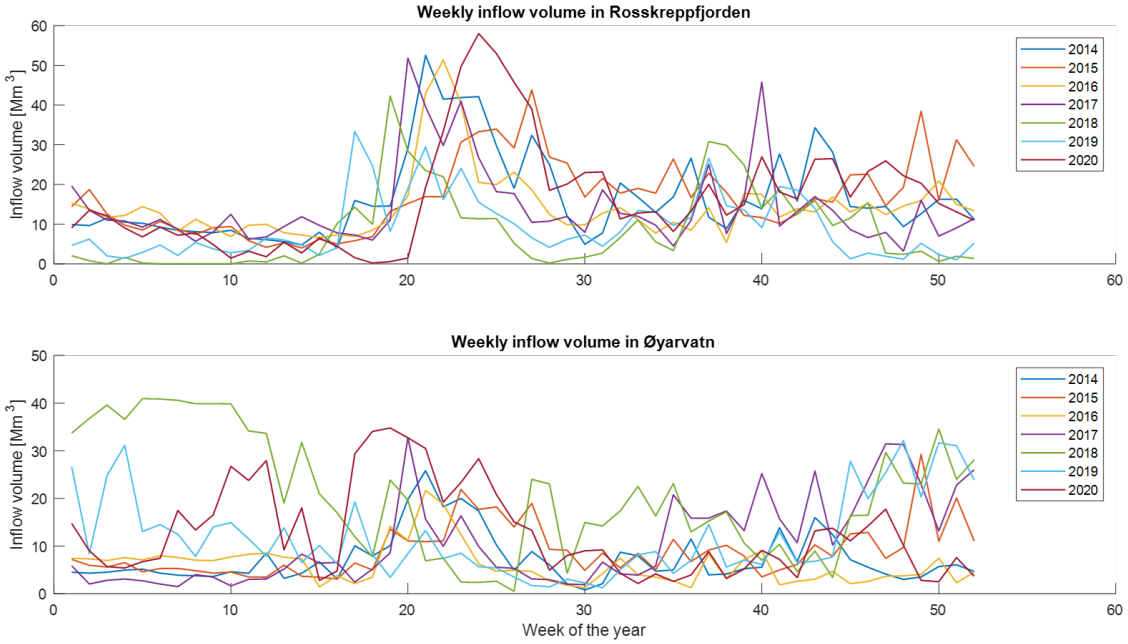

Figure 5.1.2: Weekly inflow volumes in Mm^3 in Rosskreppfjorden and Øyarvatn

Regarding electricity prices, the data considered are provided by a SINTEF project called *New environmental restrictions - overall impact on the power system* (SINTEF, 2022). The prices refer to a forecast of energy price in 2030 based on historical meteorological conditions from 1981 to 2010. In particular, in the model are used weekly average prices, expressed in €/MWh. Since the energy price is the governing factor in determining the pump or turbine mode, it has been decided to select a reference year for price between those available and keep it fixed for all the years simulated.

In this case, two different price years are selected: 1998 and 2000 (*Figure* 5.1.3). This choice allows to detect the effects of a greater price fluctuation on the different discharges involved.

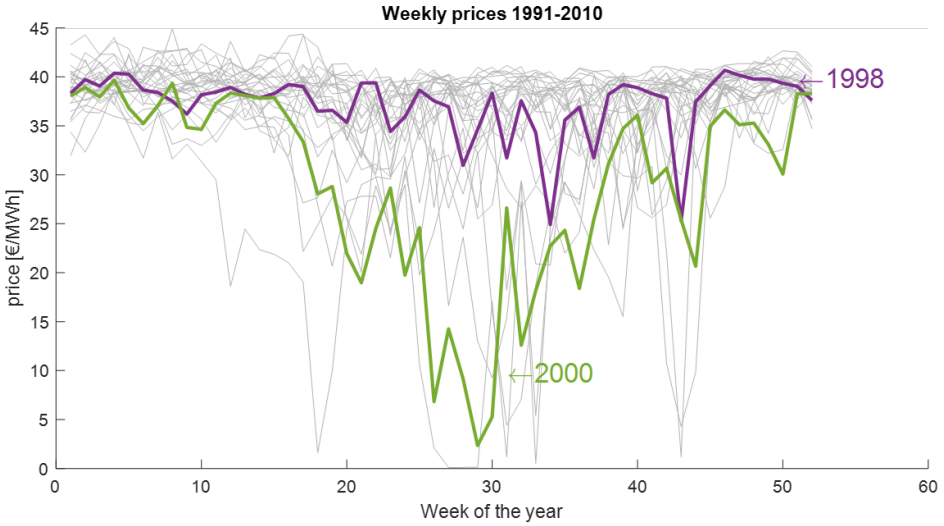

Figure 5.1.3: historical weekly prices from 1981 to 2010, highlighted in green (year200) and in purple (year 1998) the two years selected as reference years

Inflows, especially in Rosskreppfjorden, and the prices show an opposite trend. In fact, the peak of the inflows occur during the snow and ice melt period while prices decrease. During the winter period, on the other hand, prices are higher due to increased energy demand and lower water availability.

The scheduling model allows to simulate both traditional, one-way hydropower plant, and pumping. Therefore, for each of the two price years selected, two simulations, with and without the pump, are performed.

Before analyzing the simulations is important to discuss the limitations of the model used to generate the discharges.

5.1.1 Limitations of the scheduling model

As already mentioned, the input data have a weekly resolution. Consequently, the initial hourly data trend is lost. In addition, there is not a perfect correlation between water levels predicted by the scheduling model and those obtained from the simulation in CE-QUAL-W2. In *Figure* 5.1.4 is illustrated an example obtained for price-year 2000 and with pumping mode. It is evident that the scheduling model seems to overestimate the water level, and this difference increases with time. It may result from the different water balance computation due to bathymetry, but mainly from the time step used. Consequently, the range of possible water level variations, between LRV and HRV, was reduced increasing the lowest regulated water volume.

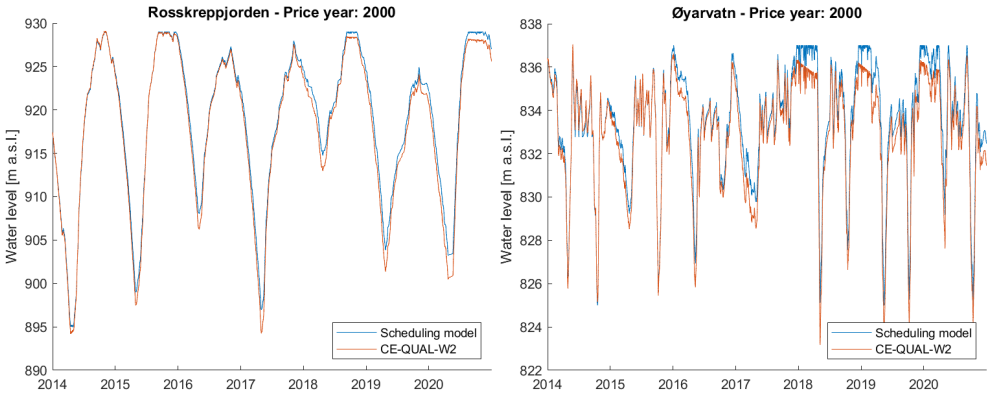

(a) (b)

Figure 5.1.4: Water level predict by the scheduling model and obtained by the simulation for price-year 2000 and simulation with pumping

Moreover, the scheduling model has a year of 52 weeks corresponding to 364 days. However, in CE-QUAL-W2 real years, of 365-366 days, are considered. In order to cope with this issue during the one/two last days of the years zero discharges are simulated.

5.2 Simulation setup

The simulations analysed examine two selected price-year: 1998 and 2000. In particular, two simulations are performed for each price-year, one with and one without the pump. In all the cases the period refer to the years 2014-2020. Specifically, the analysis is focused on detecting the effects on temperature profile and ice cover by comparing two segments for each reservoir, one close to the inlet/outlet and the other one in the middle of the lake (*Figure* 5.2.1).

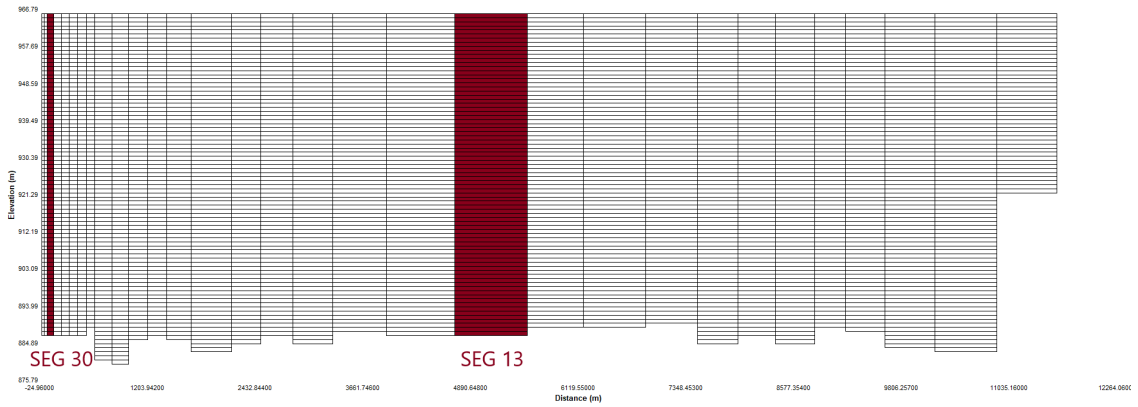

(a) Rosskreppfjorden

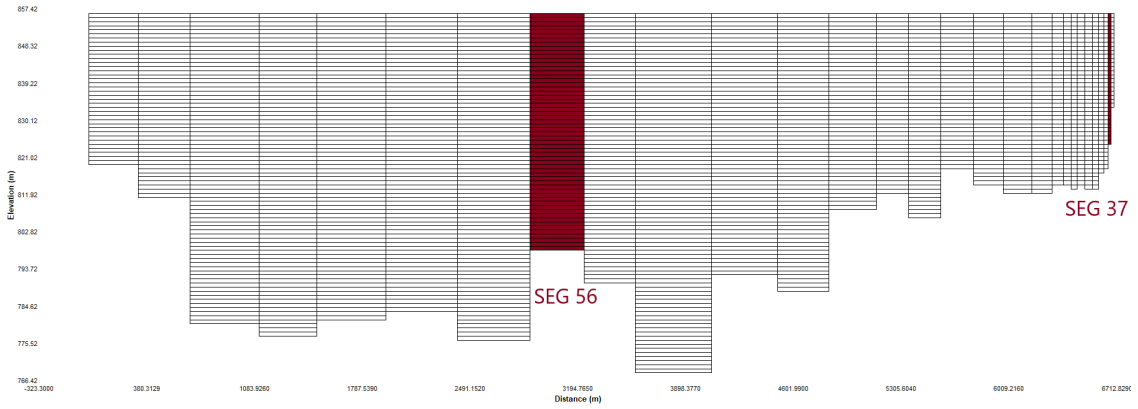

(b) Øyarvatn

Figure 5.2.1: Selected segments for the analysis

The meteorological data are those reported by OpenWeather and the inflow temperature is the one obtained from air2water.

The initial conditions of all the simulations are the same. The water level is that reported by the power plant on January 1^{st} 2014, corresponding to 917.41 m a.s.l. in Rosskreppfjorden and 836.42 m a.s.l. in Øyarvatn. Regarding the initial water temperature vertical profile, it is considered constant and equal to 2 °C. Finally, the initial ice cover is set at 0.25 meters.

5.3 Price-year: 1998

The prices for year 1998 are within the range 25-40 €/MWh (*Figure* 5.1.3) with higher fluctuations during fall period. In *Figure* 5.3.1 are reported the annual cumulative water volume curves for each component of the water balance. In both traditional and pumped-storage modes the turbinate volumes are similar, and comparable with the inflow volume to Rosskreppfjorden. The amount of volume pumped is much less than that turbined, and equal to zero in the first half of the year in accordance with the higher energy prices.

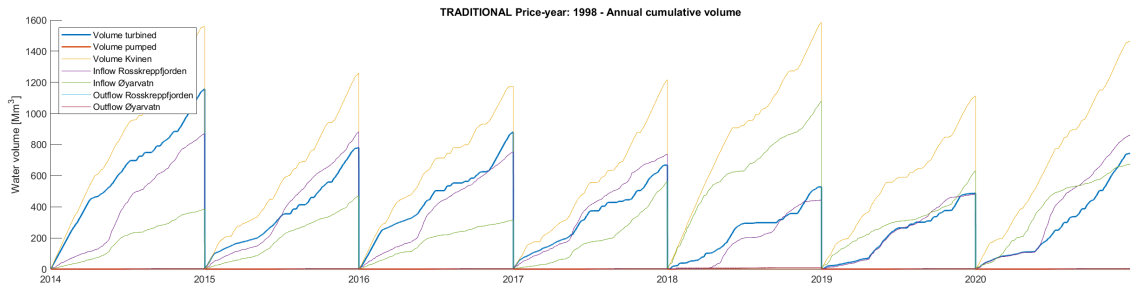

(a)

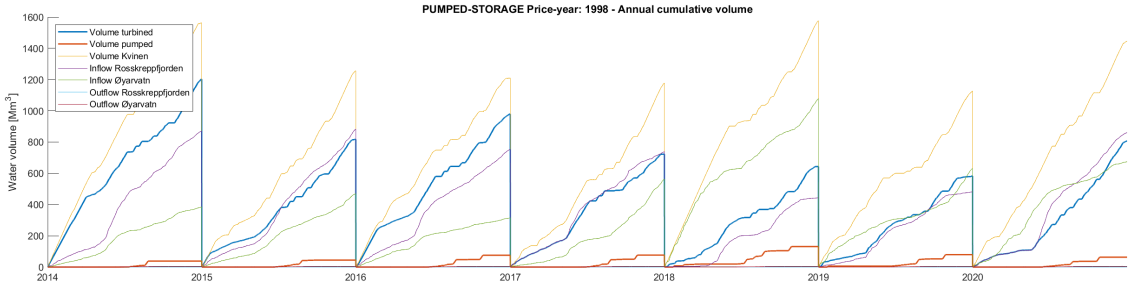

(b)

Figure 5.3.1: Annual cumulative water volume obtained by the scheduling model for price-year 1998 with (a) and without (b) the pump

In particular, in 2018 the pump works more due to the increased inflows into Øyarvatn. Moreover, it is important to note that the highest volume is for the Kvinen power plant.

In order to focus the attention on ice cover, the cumulative water volumes involved in the water balance are performed referring to only the period from November 1^{st} to June 1^{st}, $Figure$ 5.3.2. The result shows that pumping operations are negligible if not absent during the years analysed.

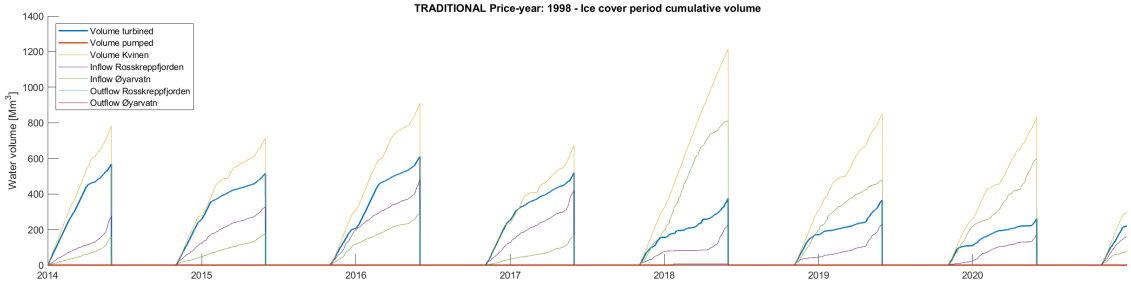

(a)

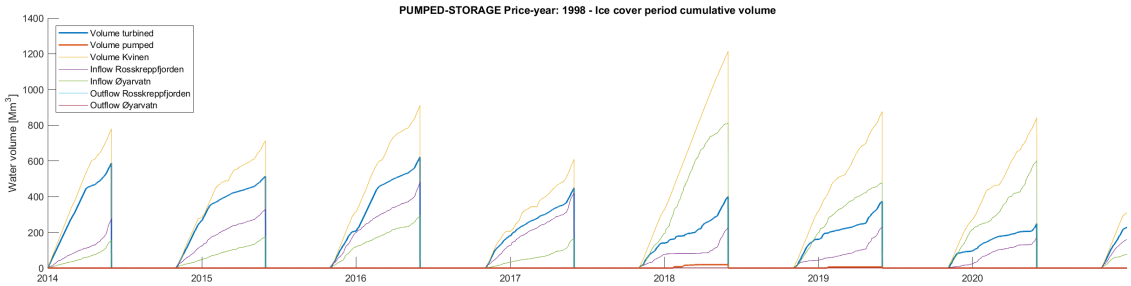

(b)

Figure 5.3.2: Cumulative water volume during ice cover period 01/11 - 01/06 with (a) and without (b) the pump

The water levels predicted by the model, $Figure$ 5.3.3, show different trend in the two reservoirs. In Rosskreppfjorden it is kept at the minimum until the end of the winter period before being filled up with increased inflow at the beginning of summer. On the

other hand, in Øyarvatn the water level shows frequent oscillations during all the period analysed. In particular, with the pump Øyarvatn reaches higher water level.

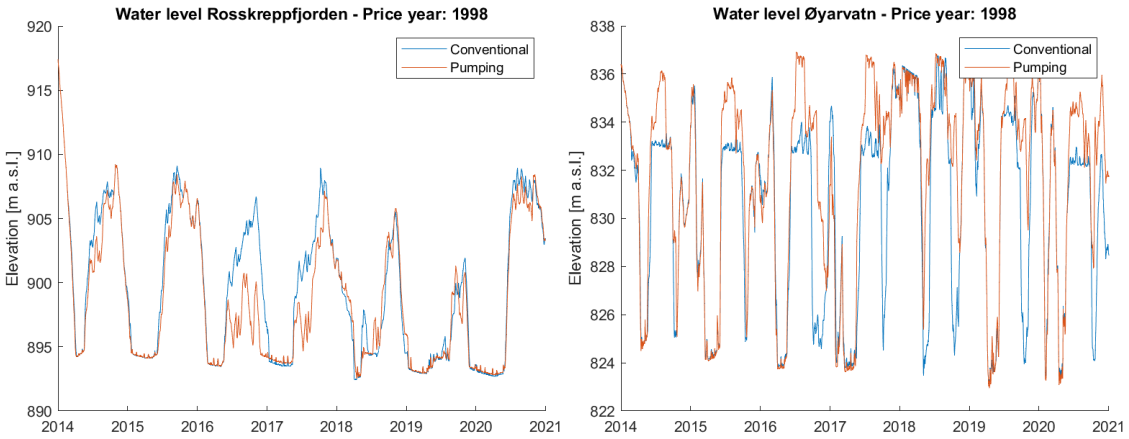

(a) (b)

Figure 5.3.3: Comparison between water levels with and without the pump in Rosskreppfjorden (a) and Øyarvatn (b) for price-year 1998

Below are analysed in more detail the two segments selected for Rosskreppfjorden, segments 30 and 13, and for Øyarvatn, segments 37 and 56.

5.3.1 Rosskreppfjorden

In *Figure* 5.3.4 and *Figure* 5.3.5 are illustrated the evolution of the water temperature profiles over time with and without the pump. In both segments and for both the operational modes, a period with a strong stratification is not visible. In order to quantify this latter, in *Figure* 5.3.6 is reported the evolution of the difference between the temperature at the top and at the bottom of the water column for each time step. Two recirculations periods are easily identifiable in spring and fall when the temperature difference is zero. In contrast, during winter, it is possible to recognize a stable stratification only in the segment 13, further away from the Rosskrepp power plant inlet. Moreover, in summer the stratification is not stable for all the cases analysed. Finally, the difference between the two traditional and pumped-storage scenarios is not appreciable. However, the amount of discharge pumped is negligible respect to that turbined.

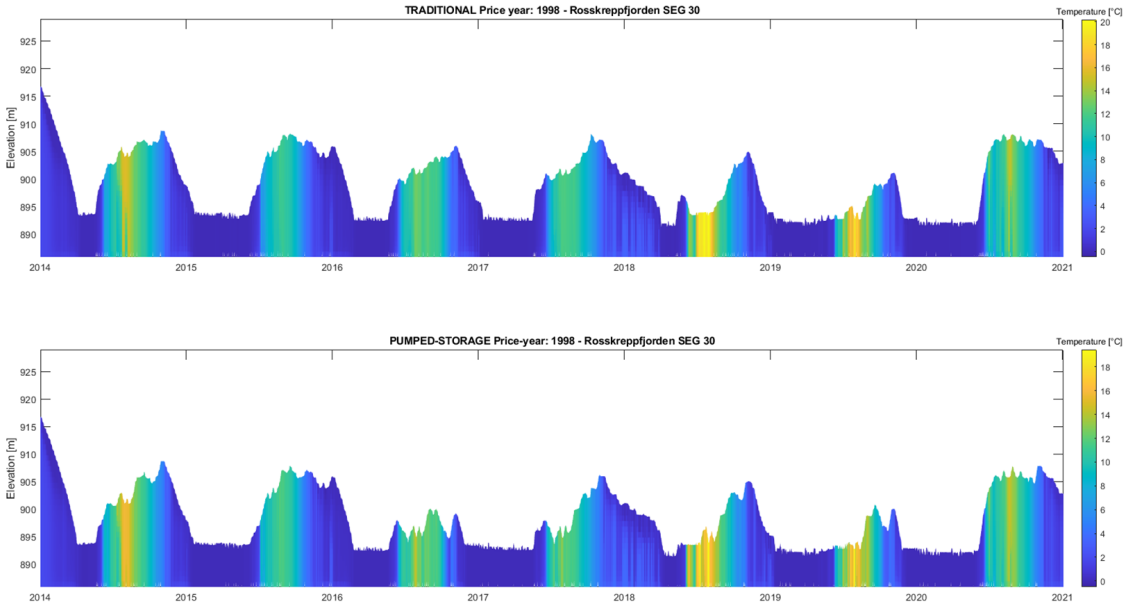

Figure 5.3.4: Evolution of the temperature vertical profile in segment 30 for price-year 1998

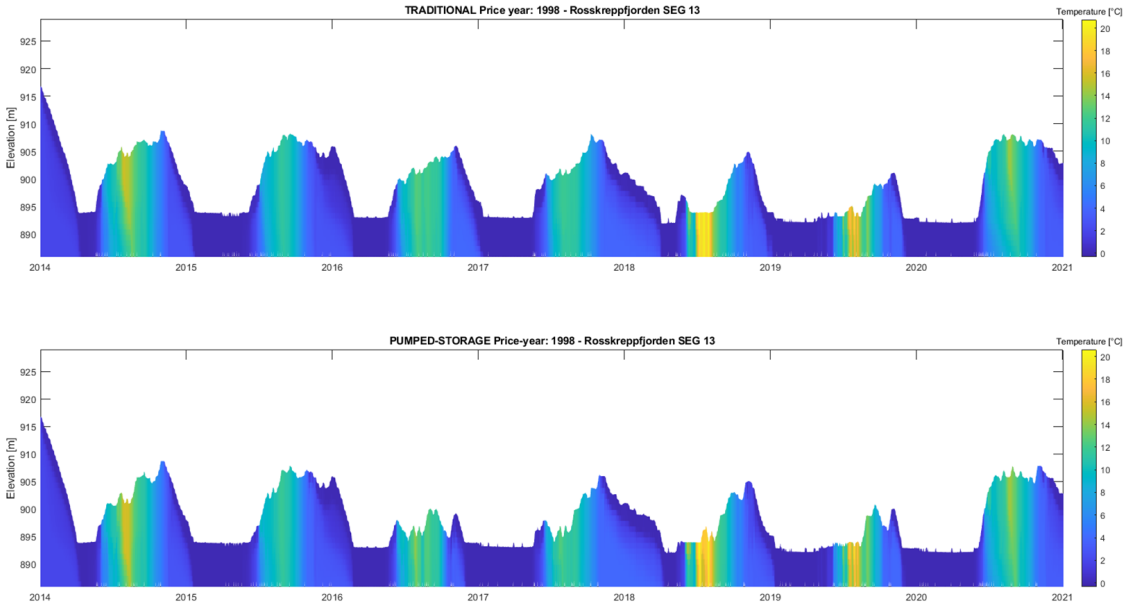

Figure 5.3.5: Evolution of the temperature vertical profile in segment 13 for price-year 1998

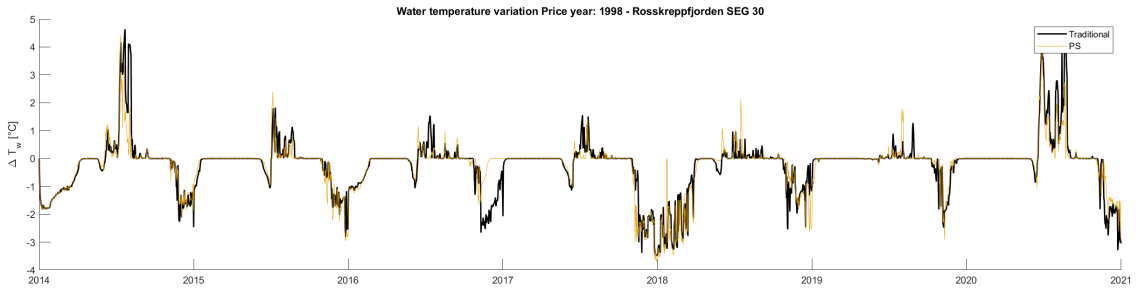

(a)

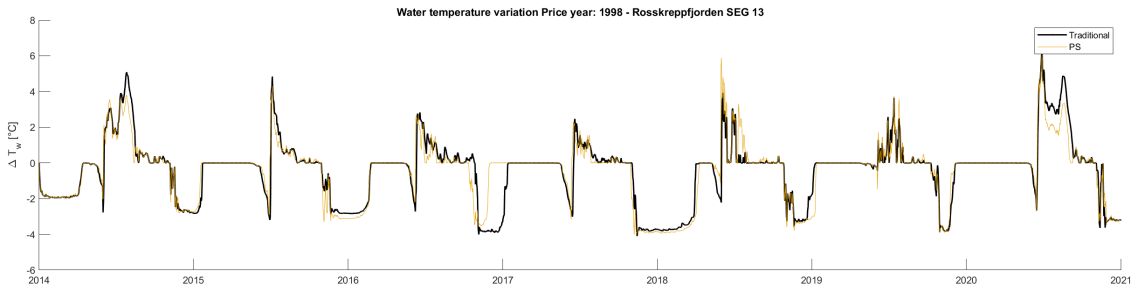

(b)

Figure 5.3.6: Evolution of the temperature difference between the top and the bottom of the water column in segment 30 (a) and 13 (b) for price-year 1998

Regaring ice cover, it is evident from $Figure$ 5.3.7 that in the middle of the lake the ice thickness and duration in the two configurations is the same.

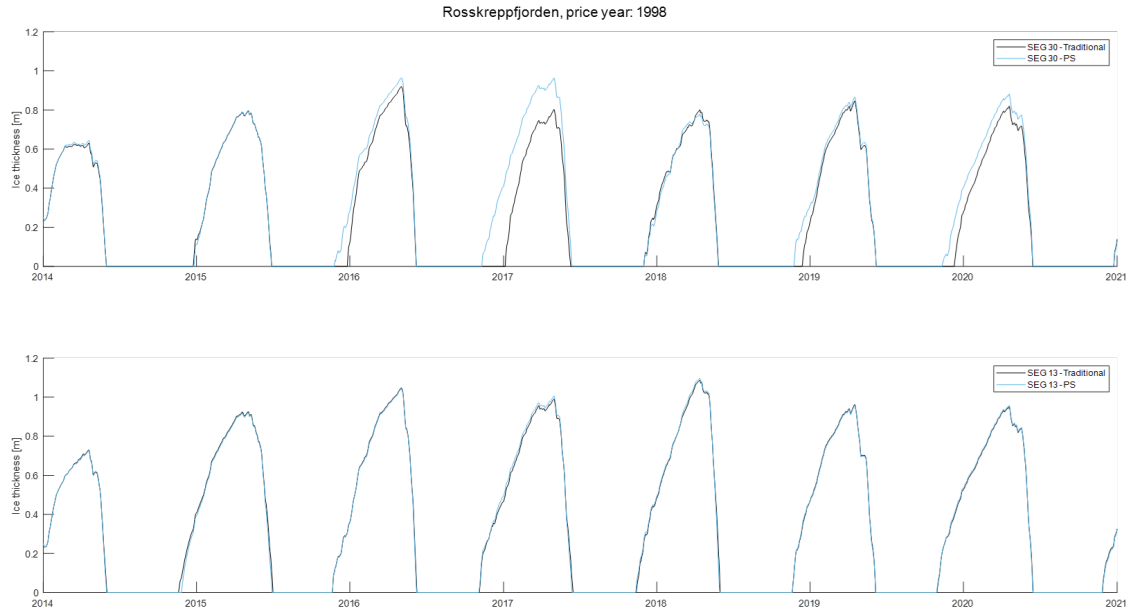

Figure 5.3.7: Ice thickness in Rosskreppfjorden for price-year 1998

Instead, in segment 30 are visible a few differences, the most evident occurs in winter 2017. In particular, in that year ice duration is longer and ice thickness higher for the

scenario with the pump. As discussed previously, during ice cover period the pumping operation is negligible, therefore the impact is due to the turbined discharge. In fact, according to $Figure$ 5.3.2 in that winter for the pumped-storage scenario the amount of water volume turbined is less. Consequently, the ice cover is less affected.

Moreover, comparing the two segments, ice formation closer to the intake is postponed due to the effect of the withdrawal.

5.3.2 Øyarvatn

In contrast with what observed in Rosskreppfjorden, in Øyarvatn there is a visible difference between the segment closer to the outlet, $Figure$ 5.3.8, respect to that in the middle of the lake, $Figure$ 5.3.9. In fact, the latter shows a clear stratification in both summer and winter period while in segment 37 the profile is almost always mixed.

This is more evident comparing the trend of the differences in top-bottom water temperatures in the two segments, $Figure$ 5.3.10. Specifically, in summer this difference is about three times greater in segment 56 respect to segment 37, hence the stratification is much more stable in the middle of the lake.

As for Rosskreppfjorden, it is significant to point out that traditional and pumped-storage show similar trend.

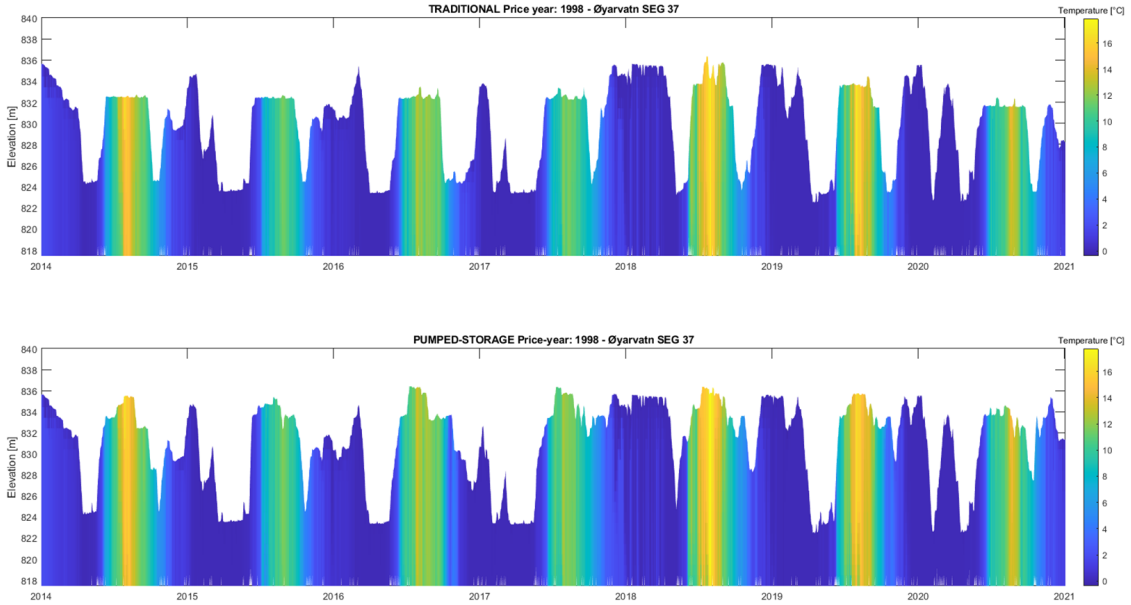

Figure 5.3.8: Evolution of the temperature vertical profile in segment 37 for price-year 1998

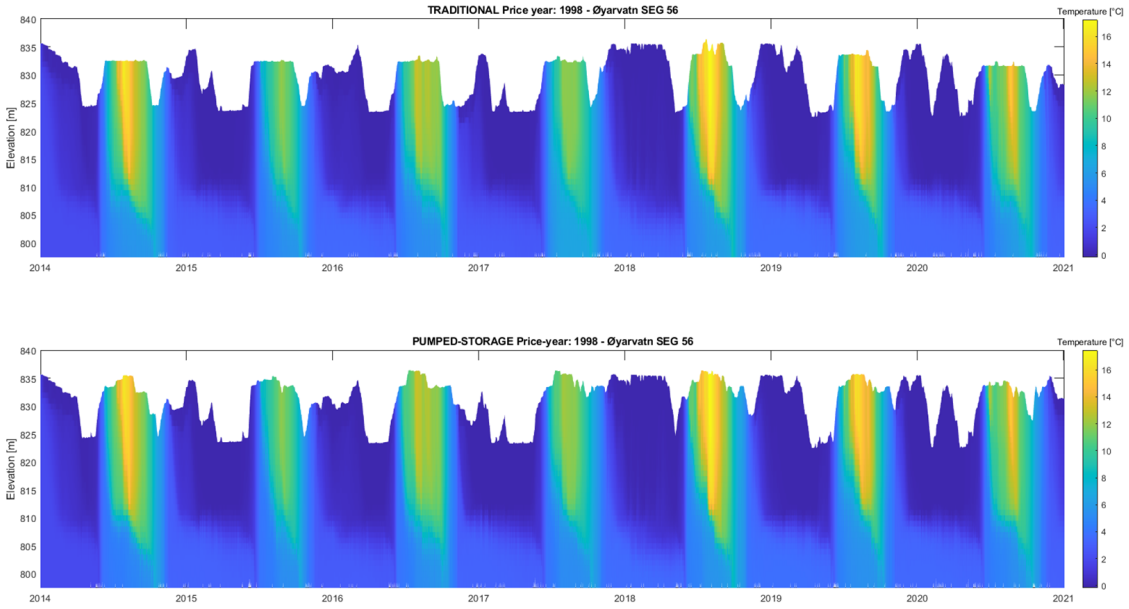

Figure 5.3.9: Evolution of the temperature vertical profile in segment 56 for price-year 1998

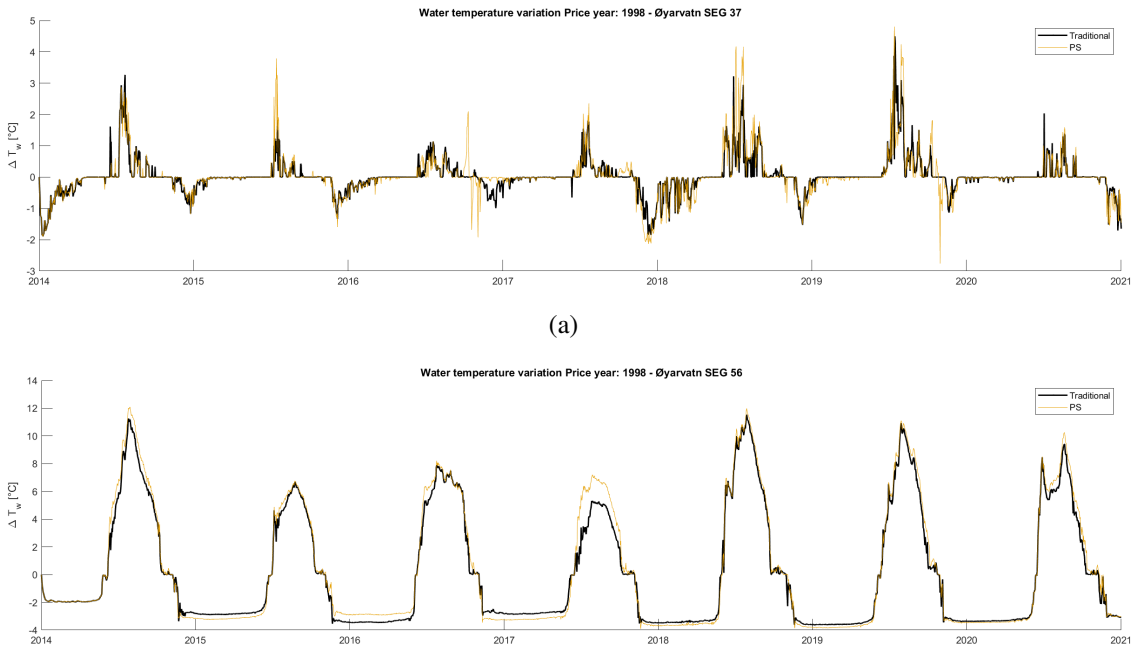

(a)

(b)

Figure 5.3.10: Evolution of the temperature difference between the top and the bottom of the water column in segment 37 (a) and 56 (b) for price-year 1998

Although the ice cover is not affected in the middle of the lake, as for Rosskreppfjorden, at the outlet in segment 37 the impact is severe: not all the years record ice formation.

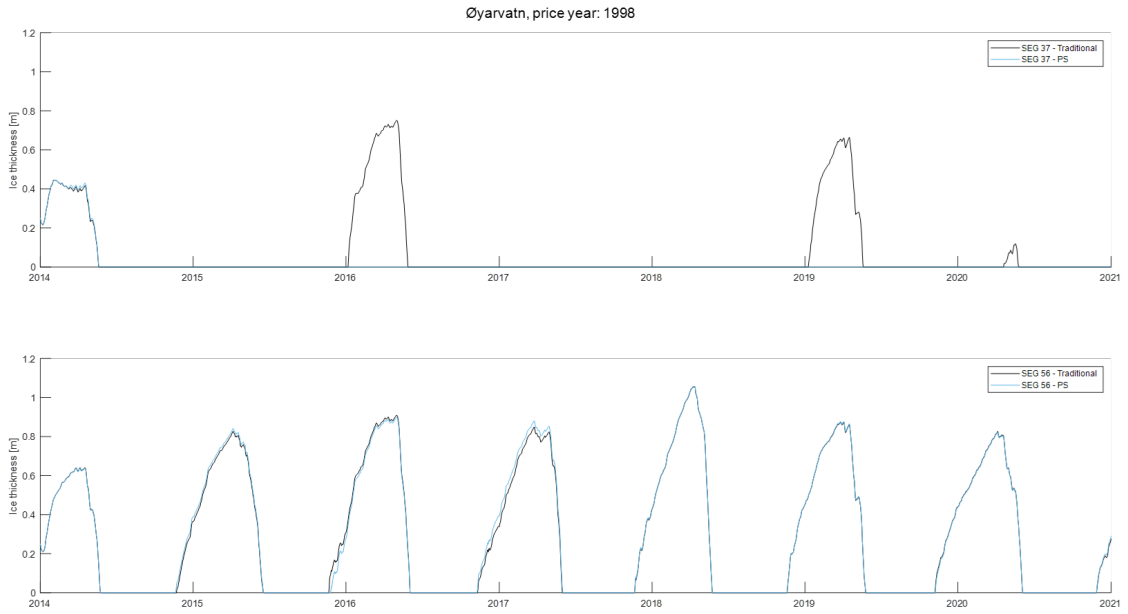

Figure 5.3.11: Ice thickness in Øyarvatn for price-year 1998

5.4 Price-year: 2000

In 2000 the prices report higher variability respect to year 1998, from less than 5 €/MWh in summer to 40 €/MWh during winter (*Figure* 5.1.3). As a consequence, in this case the amount of pumped discharge is higher than in the previews one. In addition, it is interesting to report that in 2018 the volumes pumped and turbined are comparable.

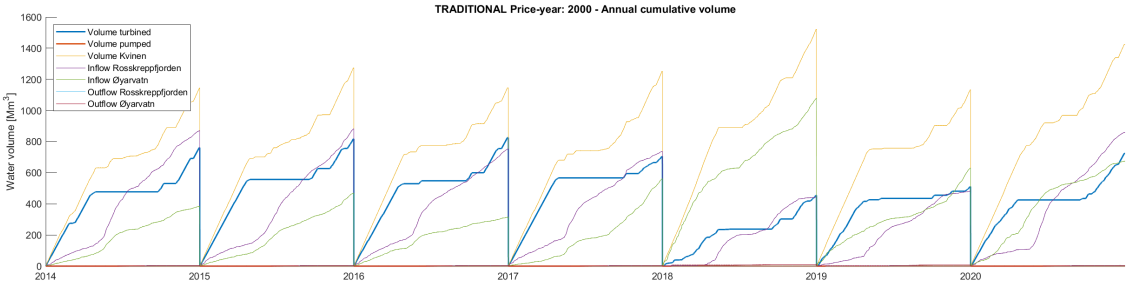

(a)

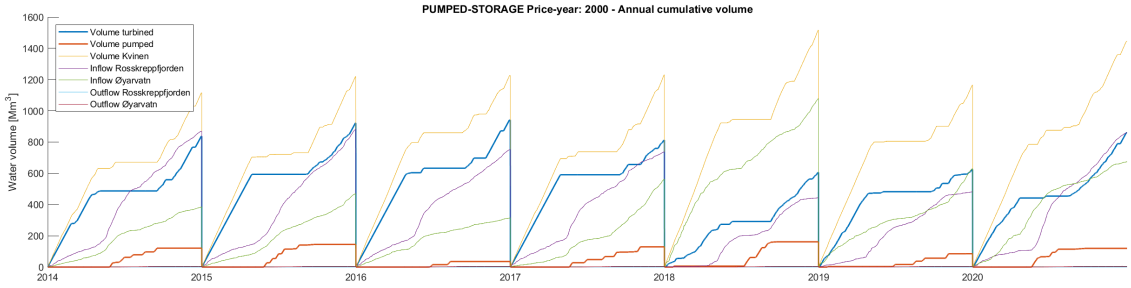

(b)

Figure 5.4.1: Annual cumulative water volume obtained by the scheduling model for price-year 2000 with (a) and without (b) the pump

Regarding the amount of water volumes exchanged during ice cover period, $Figure$ 5.4.2 shows that pumping operations are negligible if not absent during the years analysed, as for the previous case.

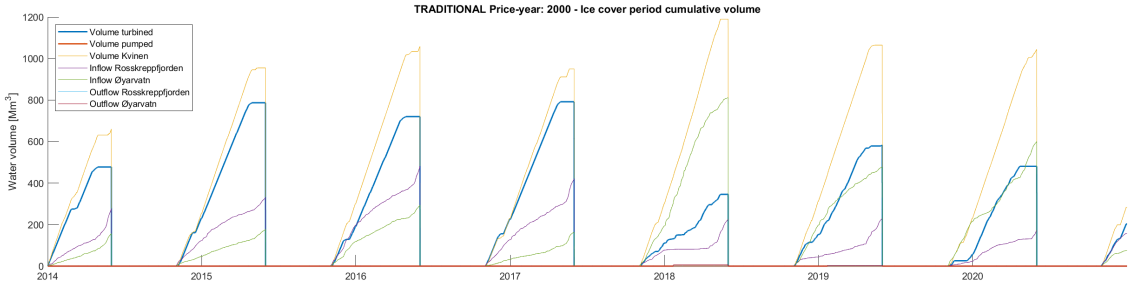

(a)

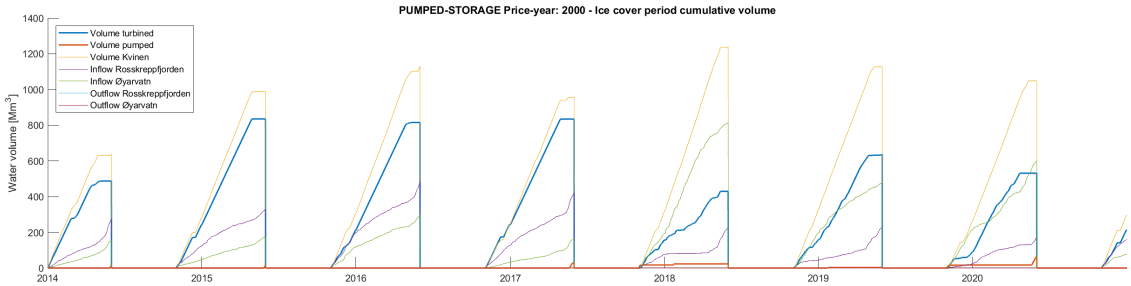

(b)

Figure 5.4.2: Cumulative water volume during ice cover period 01/11 - 01/06 with (a) and without (b) the pump for price-year 2000

In contrast with what obtained with price-year 1998, Rosskreppfjorden reaches the highest regulated water volume in most of the years during fall considering the simulation with the pump ($Figure$ 5.4.3). Instead, Øyarvatn has a water level with frequent fluctuations. In particular, the highest water level refers to the conventional power plant.

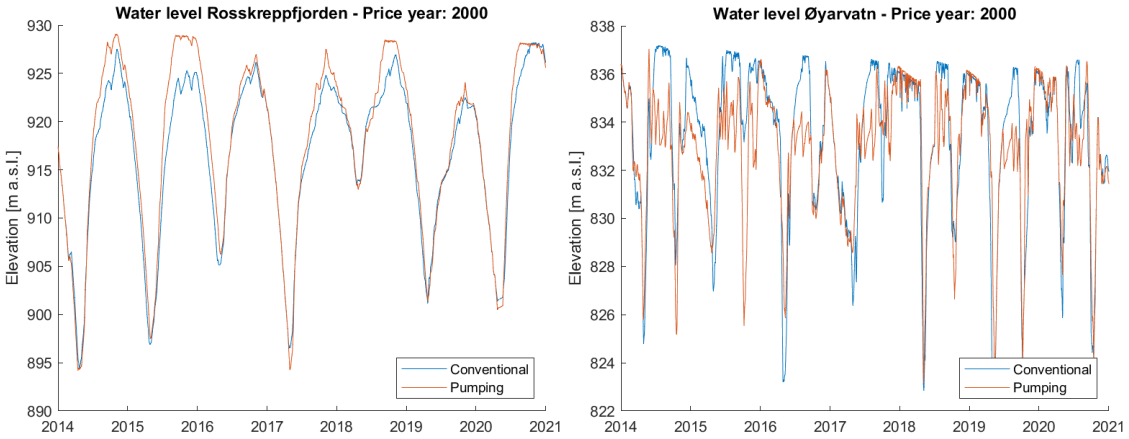

(a) (b)

Figure 5.4.3: Comparison between water levels with and without the pump in Rosskreppfjorden (a) and Øyarvatn (b) for price-year 2000

5.4.1 Rosskreppfjorden

Figure 5.4.4 and *Figure* 5.4.5 show the evolution of the water temperature vertical profile over time in the two segments analysed in Rosskreppfjorden. Although the pattern is similar, in segment 30 it is possible to identify short mixing periods which interrupt stratification especially during summer. In particular, this segment appears much more affected when pumped-storage is considered. It is very visible in 2018 especially comparing the difference in water temperature between top and bottom, *Figure* 5.4.6. In fact, the latter in that year shows frequent oscillations during summer.

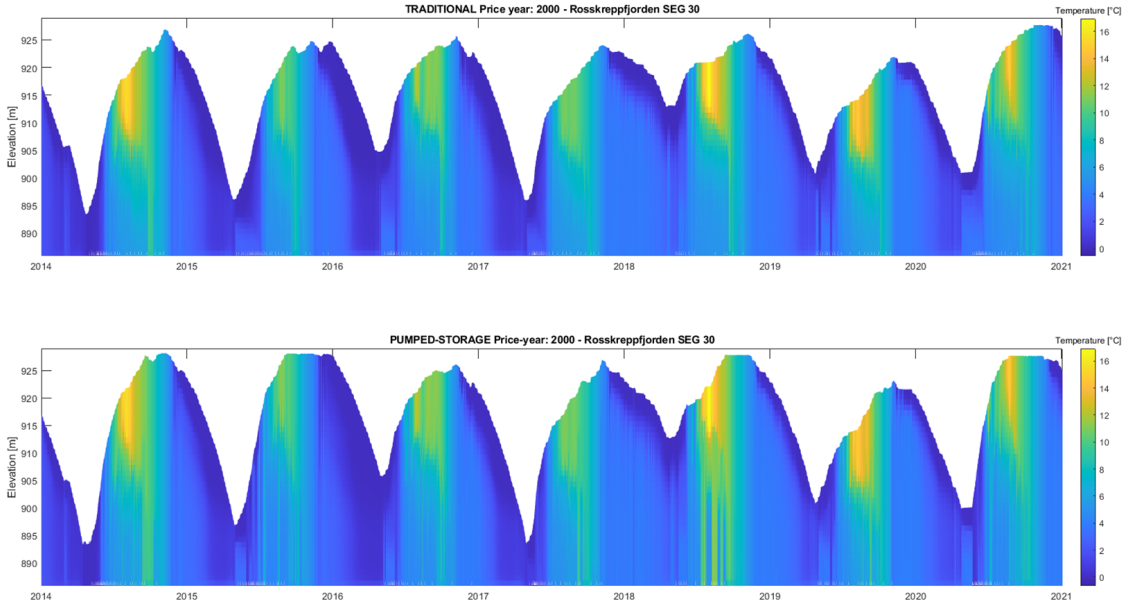

Figure 5.4.4: Evolution of the temperature vertical profile in segment 30 for price-year 2000

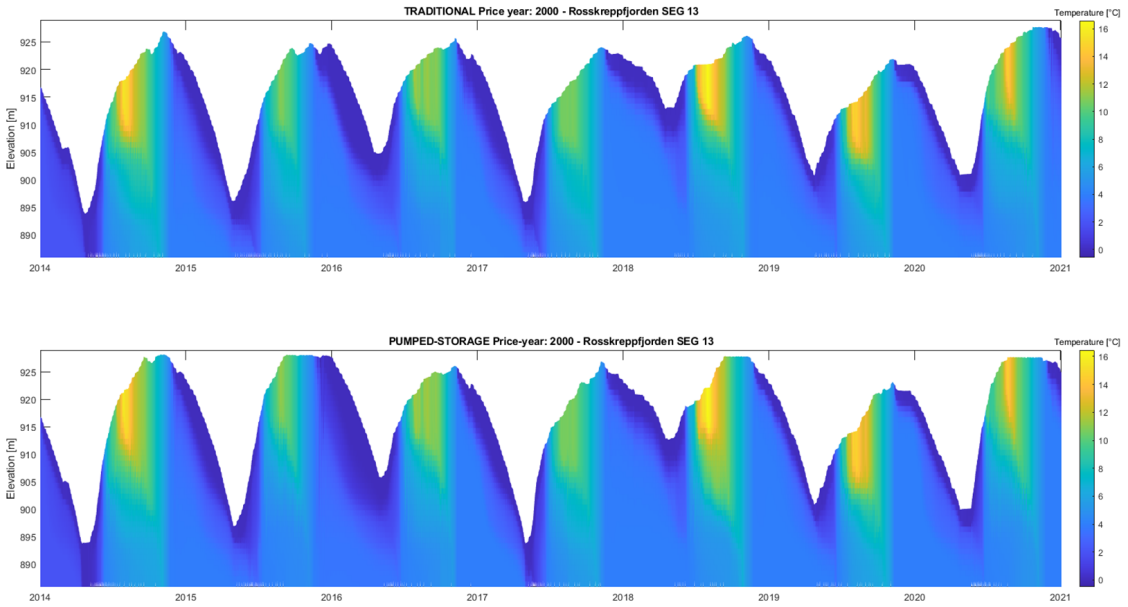

Figure 5.4.5: Evolution of the temperature vertical profile in segment 13 for price-year 2000

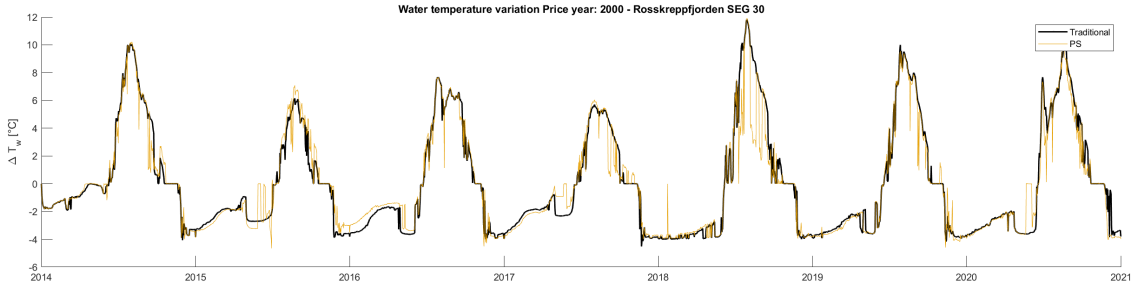

(a)

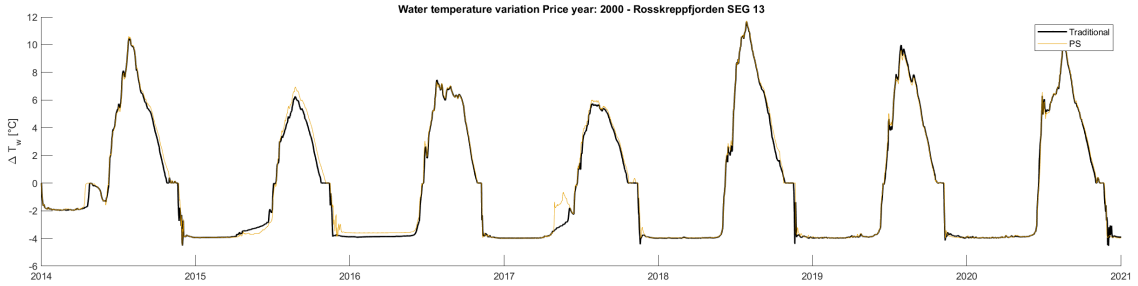

(b)

Figure 5.4.6: Evolution of the temperature difference between the top and the bottom of the water column in segment 30 (a) and 13 (b) for price-year 2000

The ice cover in Rosskreppfjorden is not highly affected in both the scenarios. Furthermore, the two segments do not show great differences.

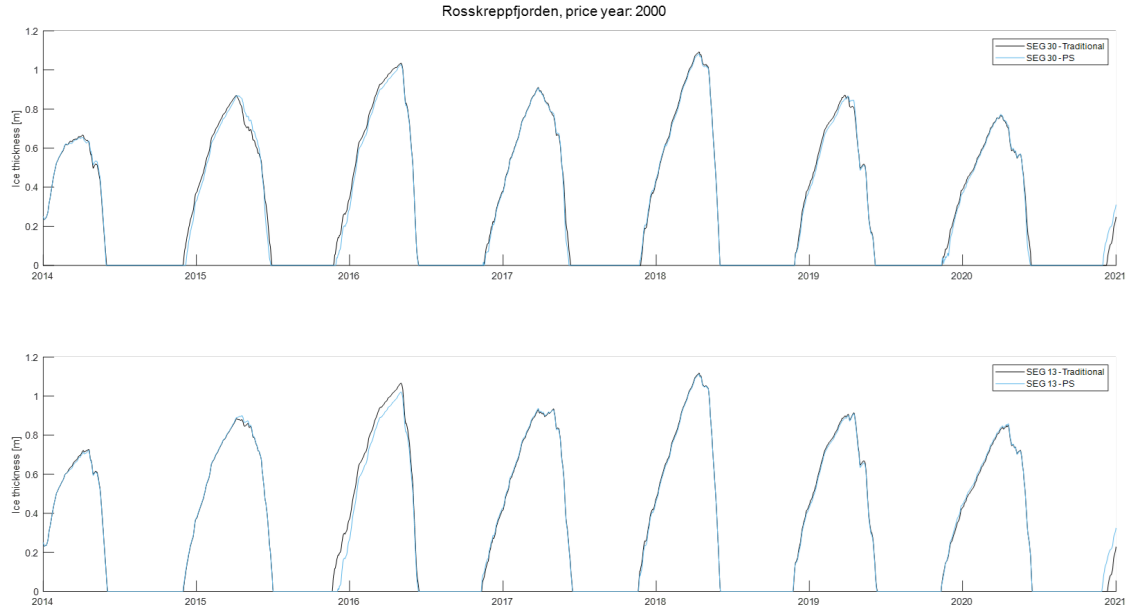

Figure 5.4.7: Ice thickness in Rosskreppfjorden for price-year 2000

5.4.2 Øyarvatn

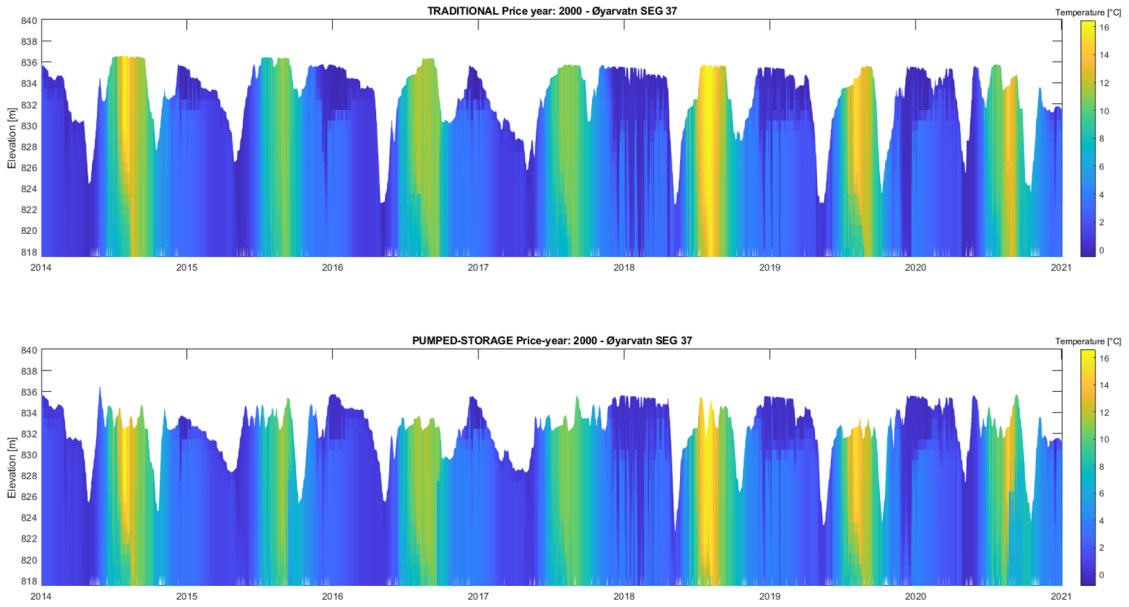

Figure 5.4.8: Evolution of the temperature vertical profile in segment 37 for price-year 2000

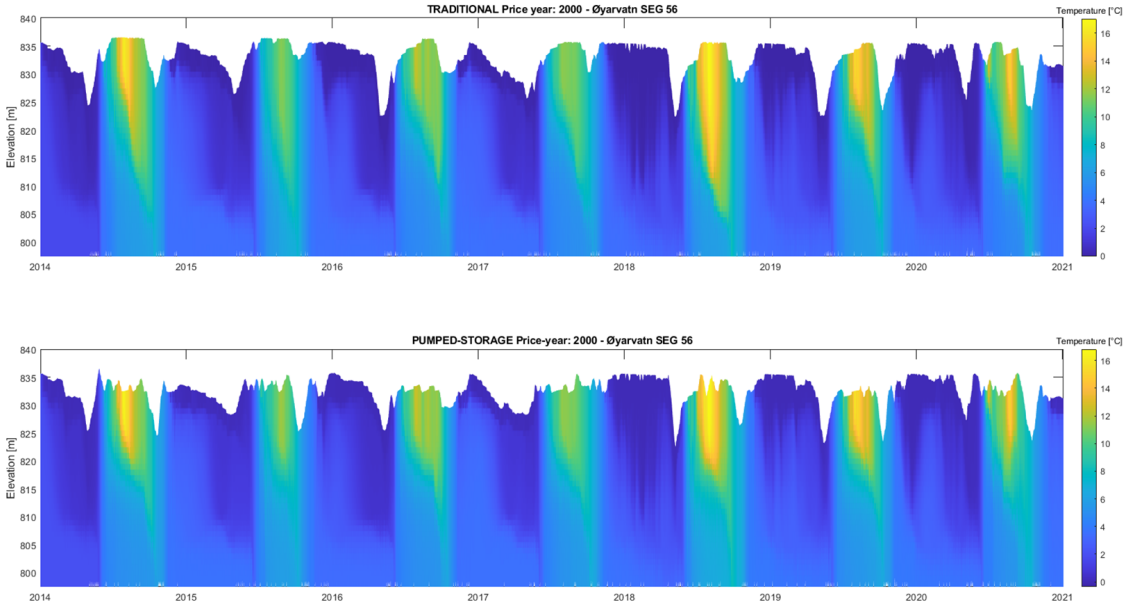

Figure 5.4.9: Evolution of the temperature vertical profile in segment 56 for price-year 2000

In Øyarvatn the segment 37 (*Figure* 5.4.8), closer to the inlet/outlet, reports a light unstable stratification during winter and summer. In particular, the vertical profile is much

more mixed than in segment 56 (*Figure* 5.4.9). The water temperature difference between top and bottom shows a very similar trend comparing the conventional and the pumped-storage system, *Figure* 5.4.10.

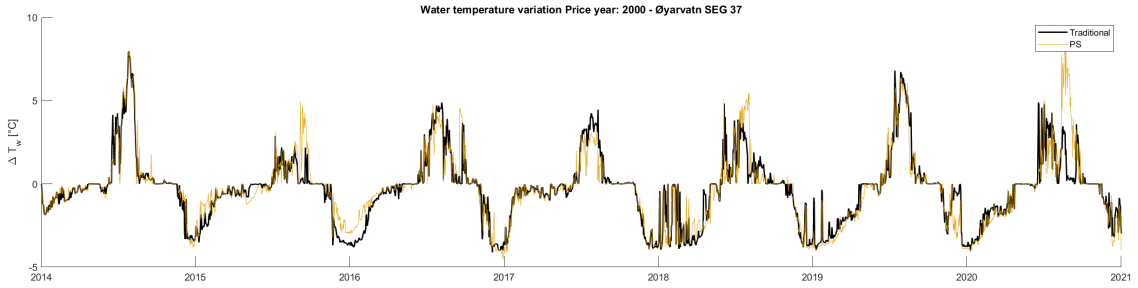

(a)

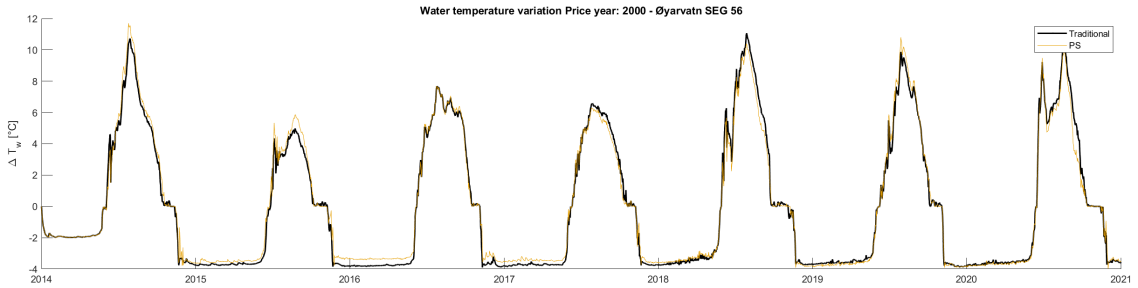

(b)

Figure 5.4.10: Evolution of the temperature difference between the top and the bottom of the water column in segment 37 (a) and 56 (b) for price-year 2000

In *Figure* 5.4.11 is illustrated the evolution of ice thickness over time. Only segment 37 is particularly affected in both scenarios. It is interesting to note that ice thickness is much more influenced than ice duration, especially in winter 2015.

In addition, comparing the two segments, the ice formation closer to the outlet of Rosskrepp power plant is postponed.

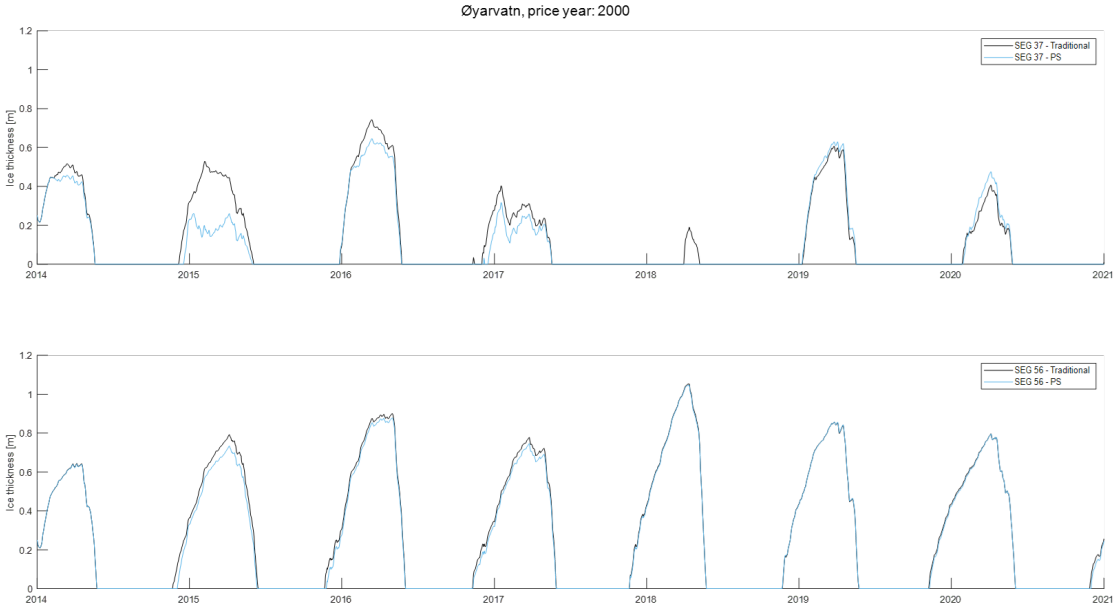

Figure 5.4.11: Ice thickness in Øyarvatn for price-year 2000

6 CONCLUSIONS

6.1 The impact of the energy price on pumping and its hydro-thermodynamic effects

The price of energy is the main factor determining the amount of discharges exchanged between the two lakes. Specifically, when prices are consistently high, the pump is minimally utilized. On the other hand, a decreasing in energy price promotes its operation. However, according to what obtained, the amount of water pumped is not comparable to the amount of water turbined, the latter being much greater.

Consequently, with high prices, as in year 1998, the impacts of a conventional or pumped-storage hydropower plant are similar. Although the two operational modes show the same trend, it is significant to point out that the area closest to the inlet/outlet is the most affected. There, the temperature vertical profile is mostly mixed throughout the year and only unstable and discontinuous stratification occurs.

On the other hand, when prices are more variable, as in year 2000, the pumping plays a major role. In this case, the impacts in the segment close to the inlet/outlet are different if the pump is present or not, especially for the upper reservoir. In fact, the results obtained show that in Rosskreppfjorden the stratification in much more unstable with a pumped-storage system than considering the conventional hydropower plant.

Another factor to take into account are the water level fluctuations. The latter, are more frequent in the lower reservoir, Øyarvatn. Moreover, the implementation of the pumped-storage system further increases their frequency.

In addition, due to the high energy price during the winter period, pumping is not cost-effective. Consequently, the hydroelectric power plant operates mainly as a conventional power plant, even though the pump is implemented in the system. Therefore, the impacts observed on ice cover refer to a conventional power plant. Specifically, the area closer to the outlet of the lower reservoir shows higher changes on the temperature stratification profile. In some years, ice formation does not occur because of the turbined discharge. However, when ice formation occurs, it is postponed in both reservoirs.

In the end, according to the results obtained, both reservoirs are more affected if a pumped-storage system is implemented. In particular, the area nearest to the inlet/outlet is the most impacted. In the upper reservoir, Rosskreppfjorden, stratification becomes less stable with short mixing periods due to the discharges pumped. In contrast, the lower reservoir, Øyarvatn, experiences greater water level fluctuations.

6.2 Future perspective

The results of this work will provide a first evaluation of the impact of a pumped-storage system on the two connected reservoirs, with a particular focus on the temperature and its repercussion on ice. In order to obtain a more realistic analysis of the effects of the pump in the system, further investigation is required.

The availability of more data from the ongoing fieldwork is needed in order to improve the model and obtain a better calibration.

Furthermore, it will be relevant to investigate how the pumping during winter period may impact the ice cover, both in terms of duration and extension.

In addition, the study case refers to only a first small part of a bigger system of connected lakes, called Sira-Kvina, used for hydropower production. It will be interesting to detect if more connections will noticeably affect all the reservoirs chain.

REFERENCES

Armengol J, Caputo L, Comerma M, Feijoó C, Garcia J, Marcé R, Navarro E, Ordóñez J (2003). "Sau reservoir's light climate: Relationships between Secchi depth and light extinctin coefficient." *Limetica*, **22**, 195–210. doi:https://doi.org/10.23818/limn.22.13.

Bermudez M, Cea L, Puertas J, Rodriguez N, Baztan J (2018). "Numerical Modeling of the Impact of a Pumped-Storage Hydroelectric Power Plant on the Reservoirs'Thermal Stratification Structure: a case in NW Spain." *Environmental Modeling & Assessment*, **23**(1), 71–85. doi:10.1007/s10666-017-9557-3.

Bonalumi M, Anselmetti F, Wuest A, Schmid M (2012). "Modeling of temperature and turbidity in a natural lake and a reservoir connected by pumped-storage operations." *Water Resources Research*, **48**(8). doi:10.1029/2012WR011844.

Burt WV (1954). "Albedo over wind-roughened water." *Journal of the Atmospheric Sciences*, **11**, 283–290. doi:https://doi.org/10.1175/1520-0469(1954)011<0283:AOWRW>2.0.CO;2.

Castellani G, Veyssière G, Karcher M, Stroeve J, Banas SN, Bouman AH, Brierley SA, Connan S, Cottier F, Große F, Hobbs L, Katlein C, Light B, McKee D, Orkney A, Proud R, Schourup-Kristensen V (2022). "Shine a light: Under-ice light and its ecological implications in a changing Arctic Ocean." *Ambio*, **51**, 307–317. doi:10.1007/s13280-021-01662-3.

Chen X, Høyland KV, Ji S (2016). "The Determination of Heat Transfer Coefficient n Water-ice Surface in a Free Convection." *Port and Ocean Engineering under Arctic Conditions*.

Cogley JG (1979). "Albedo over wind-roughened water." *Monthly Weather Review*, **107**, 775–781. doi:https://doi.org/10.1175/1520-0493(1979)107<0775:TAOWAA>2.0.CO;2.

Davies JA, Robinson PJ, Nunez M (1971). "Field Determinations of Surface Emissivity and Temperature for Lake Ontario." *Journal of Applied Meteorology and Climatology*,

10, 811–819. doi:https://doi.org/10.1175/1520-0450(1971)010<0811:FDOSEA>2.0.CO;2.

EPA (1971). "Effect of Geographical Location on Cooling Pond Requirements and Performance." *Water Pollution COntrol Research SEries, Report No.16130 FDQ, Environmental Protection Agency, Water Quality Office, Washington, District of Columbia*, p. 160.

Erdede SB, Bektas S (2020). "Examining the Interpolation Methods Used in Forming the Digital Elevation Models." *Celal Bayar Universitesi Fen Bilimleri Dergisi*, **16**, 207–214. doi:10.18466/cbayarfbe.678176.

Fink G, Schmid M, Wahl B, Wolf T, Wüest A (2014). "Heat flux modifications related to climate-induced warming of large European lakes." *Water Resources Research*, **50**, 2072–2085. doi:https://doi.org/10.1002/2013WR014448.

Franssen HJ, Scherrer S (2008). "Freezing of lakes on the Swiss plateau in the period 1901-2006." *International Journal of Climatology*, **28**(4), 421–433. doi:10.1002/joc.1553.

Kartverkets (2022). "Hoydedata, DTM 1m resolution." `https://hoydedata.no/LaserInnsyn/`. Accessed: 03/05/2022.

Klima (2022). "Norsk Klimaservicesenter." `https://seklima.met.no/stations/`. Accessed: 13/09/2022.

Kobler UG, Martin S (2019). "Ensemble modelling of ice cover for a reservoir affected by pumed-storage operation and climate change." *Hydrological Precesses*, **33**(20), 2676–2690. doi:10.1002/hyp.13519.

Kobler UG, Wüest A, Schmid M (2018). "Effects of Lake-Reservoir Pumped-Storage Operations on Temperature and Water Quality." *Sustainability*, **10**(6), 1968. doi:10.3390/su10061968.

Leppäranta M (1993). "A review of analytical models of sea-ice growth." *Atmosphere-Ocean*, **31**(1), 123–138. doi:10.1080/07055900.1993.9649465.

Leppäranta M (2014). "Interpretation of statistics of lake ice time series for climate variability." *Hydrology Research*, **45**(4-5), 673–683. doi:10.2166/nh.2013.246.

LI N, Tuo Y, Deng Y, LI J, Liang R, An R (2016). "Heat transfer at ice-water interface under conditions of low flow velocities." *Journal of Hydrodynamics, Ser. B*, **28**, 603–609. doi:10.1016/S1001-6058(16)60664-9.

Light B, Grenfell T, Perovich D (2008). "Transmission and absorption of solar radiation by Arctic sea ice during the melt season." *Journal of Geophysical Research*, **113**. doi: 10.1029/2006JC003977.

Livingstone DM, Imboden DM (1989). "Annual heat balance and equilibrium temperature of Lake Aegeri, Switzerland." *Aquatic Sciences*, **51**, 351–369. doi:https://doi.org/10.1007/BF00877177.

Meng Q, Liu Z, Borders BE (2013). "Assesment of regression kriging for spatial interpolation - comarisons of seven GIS interpolation methods." *Cartography and Geographic Information Science*, **40**(1), 28–39. doi:10.1080/15230406.2013.762138.

MET (2022). "Meteorologisk Institutt." `https://www.met.no/`. Accessed: 15/07/2022.

Müller M, Cesare GD, Schleiss AJ (2018). "Flow field in a reservoir subject to pumped-storage operation - in situ measurement and numerical modeling." *Journal of Applied Water Engineering and Research*, **6**(2), 109–124. doi:10.1080/23249676.2016.1224692.

NEVINA (2022). "NEVINA Nedbørfelt-Vannføring-INdeks-Analyse." `https://nevina.nve.no/`. Accessed: 08/09/2022.

NiB (2022). "Norge i bilder." `https://www.norgeibilder.no/`. Accessed: 03/07/2022.

OpenWeather (2022). "OpenWeather Forecasting model." `https://openweather.co.uk/`. Accessed: 13/09/2022.

Perovich D, Grenfell T, Light B, Hobbs P (2002). "Seasonal evolution of the albedo of multiyear Arctic sea ice." *Journal of Geophysical Research*, **107**, SHE 20–1–SHE 20–13. doi:10.1029/2000JC000438.

Perovich DK (1996). "The optical properties of sea ice." *Monograph 96-1*.

Piccolroaz S, Toffolon M, Majone B (2013). "A simple lumped model to convert air temperature into surface water temperature in lakes." *Hydrology and Earth System Sciences*, **17**, 3323–3338. doi:https://doi.org/10.5194/hess-17-3323-2013.

Poole HH, Atkins WRG (1929). "Photo-electric Measurements of Submarine Illumination throughout the Year." *Journal of the Marine Biological Association of the United Kingdom*, **16**, 297 – 324. doi:https://doi.org/10.1017/S0025315400029829.

Raphael JM (1962). "Prediction of Temperature in Rivers and Reservoirs." *Journal of the Power Division*, **88**, 157–182. doi:https://doi.org/10.1061/JPWEAM.0000338.

Sadeghian A, de Boer D, Hudson JJ, Wheater H, Lindenschmidt KE (2015). "Lake Diefenbaker temperature model." *Journal of Great Lakes Research*, **41**, 8–21. doi:https://doi.org/10.1016/j.jglr.2015.10.002.

Schmid M, Hunziker S, Wüest A (2014). "Lake surface temperatures in a changing climate: a global sensitivity analysis." *Climatic Change*, **124**, 301–315. doi:https://doi.org/10.1007/s10584-014-1087-2.

Schmid M, Read J (2022). "Heat Budget of Lakes." In "Encyclopedia of Inland Waters (Second Edition)," pp. 467–473. Elsevier. doi:https://doi.org/10.1016/B978-0-12-819166-8.00011-6.

Schäffer LE, Helseth A, Korpås M (2022). "A stochastic dynamic programming model for hydropower scheduling with state-dependent maximum discharge constraints." *Renewable Energy*, **194**, 571–581. doi:10.1016/j.renene.2022.05.106.

SINTEF (2022). "SINTEF project: New environmental restrictions - overall impact on the power system." `https://www.sintef.no/prosjekter/2020/nye-miljorestriksjoner-samlet-innvirkning-pa-kraftsystemet/`. Accessed: 07/08/2022.

Sira-Kvina (2022). "Sira-Kvina Rosskrepp kraftverk." `https://www.sirakvina.no/roskrepp-kraftverk/roskrepp-kraftverk-article257-921.html`. Accessed: 30/09/2022.

SMVF (2022). "Vann-Nett Portal." `https://vann-nett.no/portal/#/`. Accessed: 13/09/2022.

Toffolon M, Cortese L, Bouffard D (2021). "SELF v1.0:a minimal physicaò model for predicting time of freese-up in lakes." *Geoscientific Model Development*, **14**, 7527–7543. doi:10.5194/gmd-14-7527-2021.

Toffolon M, Piccolroaz S, Majone B, Soja AM, Peeters F, Schmid M, Wuest A (2014). "Prediction of surface temperature in lakes with different morphology using air temperature." *Limnology and Oceanography*, **59**, 2185–2202. doi:https://doi.org/10.4319/lo.2014.59.6.2185.

Wells S (2021). "CE-QUAL-W2: A Two-Dimensional, Laterally Averages, Hydrodynamic and Water Quality Model, Version 4.5." *User Manual. Department of Civil and Environmental Engineering, Portland State University*.

WMO (2008). "Guide to meteorological instruments and methods of observation." *WMO No.8, Geneva, Switzerland*.

AKNOWLEDGMENTS

First and foremost, I would like to express my sincere gratitude to Prof. Marco Toffolon for letting me join in the HydroConnect project. I thank him for the continuous support, his patience, motivation, and knowledge he shared with me. He guided me in all the phases of my thesis.

I am deeply grateful to Ana Adeva Bustos for sharing with me her great passion for this work and her experience. She always provides me her support with her precious advice. I also thank her for the good and instructive time spent on the fieldwork.

I would like to extend my sincere thanks to Atle Harby, whose valuable knowledge guided me towards a great improvement in the model's results.

Thanks to the entire SINTEF Energy for providing me the economic and technical support during these three months in Trondheim.

A big thank you goes to all the people I met during these years, for experiences we shared and the support I felt. A special thought goes to my 'old' friends, for always being present in my life. Last but not least, I would like to thank my family, for all the support throughout my life.